university of groningen

faculty of science and engineering

Average Surface Roughness for 2-Dimensional Atmospheric flow

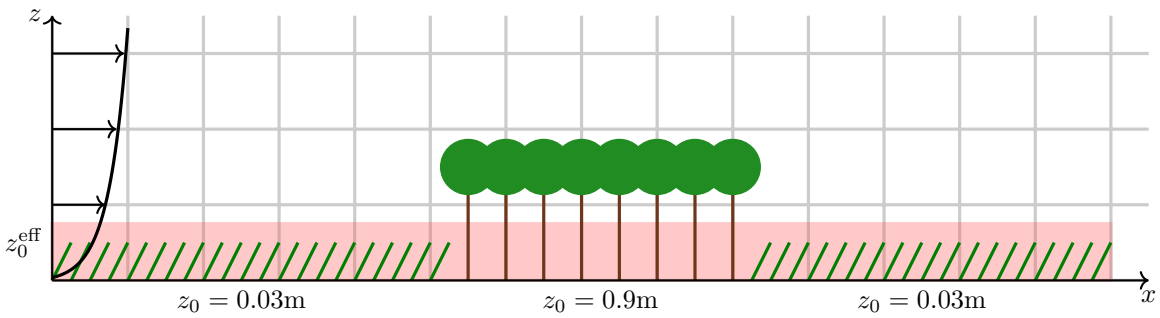

Bachelor's Project Applied Mathematics

July 12, 2023

Student: M. A. Mandeville

First supervisor: dr. ir. R. Luppes

Second supervisor: dr. A.E. Sterk

Abstract

Roughness length represents the height at which the wind flow becomes zero, under neutral atmospheric conditions and in the absence of any obstacles. It is strongly related to the height of the different elements in a heterogeneous terrain. In this thesis, we consider two homogeneous regions, grassland and forest, under either a single- or multi-layer model, following Klaassen (1992) and Luppes (1993). We interest ourselves in finding an average roughness length to represent the entire heterogeneous terrain when considering larger scale meteorological simulations. Such an average length, also called the 'effective roughness length' (ERL) is computed in four manners, as detailed by André and Blondin (1986), Taylor (1989), de Vries et. al. (2003), and finally by simply averaging the logarithmic law. We compare the four methods and relate these to the output wind profile for different terrains, and conclude that de Vries et al.'s effective roughness length is the most accurate.

Keywords Surface roughness length, Effective roughness length (ERL), Two dimensional atmospheric flow, Single and multi layer surface types.

Mathematics subject classification (2020) 76-10, 76D05, 76D10

Contents

1 Introduction

Meteorology is a part of everyone's daily life; we check the weather before leaving our house as to not get surprised by rain. To this end, we would like meteorological calculations to be as precise as possible. These models use atmospheric flow in their calculations, and such a flow depends on the surface type considered. For instance, the temperature and the wind velocity are different through a forest or over grassland. These two surfaces are the ones considered here, in three different dispositions. We refer to the upper layer of a forest as the *canopy height* h_c, where we assume $h_c = 10\text{m}$ in this study.

Roughness length, denoted by z_0, corresponds to the height at which wind flow becomes zero, under neutral atmospheric conditions and in the absence of any obstacles. An atmospheric layer is called *neutral* if it is not saturated, and if the rate at which the temperature changes is the same as the dry-adiabatic rate. Saturation occurs when the atmosphere contains the maximum quantity of water vapour possible at its given temperature. A process is called *adiabatic* if no heat is transferred with the surrounding air. The dry adiabatic rate corresponds to the rate at which air cools down, and is given by 9.8°C per kilometer for the Earth's atmosphere.

For simplicity, we here only consider a two dimensional plane, and assume that the atmosphere does not change over the different surfaces of a heterogeneous terrain, allowing for the wind velocity, the temperature, and the humidity to change as the air moves over each surface. We consider the upper right quadrant of the real plane $\mathbb{R}^2$, where we suppose that atmospheric flow moves from left to right.

Wind velocity, denoted by u is commonly given by:

$$u(z) = \frac{u_*(z)}{\kappa} \ln\left(\frac{z}{z_0}\right), \tag{1.1.1}$$

where u_* is the friction velocity, which corresponds to the shear stress rewritten in velocity units, and $\kappa \approx 0.4$ is the von Kármán constant. Shear stress is the force per unit area acting parallel to an infinitesimal surface element. Note that equation (1.1.1) is the most simple and basic formula for atmospheric flow there is. Some authors may add a stability function, like Garratt & Pielke (1989), or a displacement term as de Vries et al. (2003). Regardless, this equation is referred to as the *logarithmic law*.

From the logarithmic law (1.1.1), one can see that roughness length z_0 is a local value. In fact, it is a constant value for a single homogeneous terrain. For instance, grassland typically has roughness length of 0.03m, while for forest it is roughly 0.9m. When looking at larger scale meteorological phenomena, one may not have interest for the local behaviour of the atmospheric surface flow, but would rather study the global one. To this end, it is useful to define an *effective roughness length* (ERL) z_0^{eff}, which thus corresponds to the roughness length of an entire heterogeneous terrain. In this paper, we study four methods for computing an ERL, as detailed by André & Blondin (1986), Taylor (1987), de Vries et al. (2003), and finally by simply averaging the logarithmic law.

In order to determine which method yields the most accurate effective roughness length, we must compare the output wind profile of the effective model, with some other heterogeneous model. In this thesis, we consider two homogeneous regions, grassland and forest, under either a single- or a multi-layer approach, following Klaassen (1992) and Luppes (1993).

We begin the paper by providing a description as well as the derivation for the various equations which make up the models given by Klaassen and Luppes. Then, we look into three of the methods used to compute the effective roughness lengths, following the papers by André and Blondin, Taylor, and de Vries et al. After this, we run simulations for various disposition of the regions we consider (grass and forest), and compare them to analyse the effect of vortices

appearing after the rougher regions. Finally, we compare the four methods for the effective roughness lengths, in order to conclude on the most effective and accurate one.

All simulations are done using the code written by Luppes (1993), under the grid-refinement done by Slump (2021). Some background on fluid mechanics is provided in Appendix A, to allow the reader a full understanding on the derivation of the equations which model atmospheric flow. A table of notation is provided after the appendices, to which the reader is encouraged to refer back to if needed.

Acknowledgements

I would like to thank my supervisor, Roel Luppes, for his advice and help in writing this thesis. Further thanks go to Laurens, Remco, Stef, and Tijmen for their daily presence and support. Finally, I would like to thank my parents for always encouraging me and listening to me ramble about mathematics, and for supporting me in my studies.

I dedicate this thesis to my grandfather, Papi Jo.

2 Theory of the models

In this section, we look at the theory behind two different surface layer models: single-layer and multi-layer (Klaassen, 1992, Section 2). These models are described in general in the first subsection, and in further detail in the second and third, respectively. The equations modelling the atmospheric flow are given in the first subsection, and the boundary conditions are detailed in the fourth. All variables used in this section are assumed to be Reynolds averaged, which is explained in Appendix A.3.

2.1 General description of the surface-layer model

We look at the equations governing the two different surface models proposed by Klaassen (1992), and used by Luppes (1993). We recall that we study regions of infinite length in the direction perpendicular to the wind flow (here: y-axis), which leads us to only having a two-dimensional model in x and z, where z represents the height. We also assume that the atmospheric flow is incompressible and stationary, as we consider a small scale model and atmospheric properties do not change over a sufficiently short time.

2.1.1 Equations for atmospheric flow

The Navier-Stokes equations together with the equation of continuity and the energy equation completely model Newtonian fluid flow in hydro- and aerodynamics. The derivation and the physical properties underlining these equations are given in Appendix A.1. Some terms can be neglected in some parts of the domain, which allows us to simplify these equations (Veldman, 2009). For instance, the viscosity term is only of interest when considering the boundary layer. In what follows, we look at the Navier-Stokes equations for steady, two-dimensional, incompressible flow. We consider a Cartesian coordinate system (x, z), with respective velocity components (u, w).

Steady, or stationary, flow means that the velocity does not change over time. In other words, $\partial_t \mathbf{u} = 0$, where $\mathbf{u} = (u, w)$ is the velocity vector. Then, for a two-dimensional, stationary, incompressible flow, we have,

$$\begin{aligned} \frac{\partial u}{\partial x} + \frac{\partial w}{\partial z} &= 0, \\ u\frac{\partial u}{\partial x} + w\frac{\partial u}{\partial z} &= F_x - \frac{1}{\varrho}\frac{\partial p}{\partial x} + \nu\left(\frac{\partial^2 u}{\partial x^2} + \frac{\partial^2 u}{\partial z^2}\right), \\ u\frac{\partial w}{\partial x} + w\frac{\partial w}{\partial z} &= F_z - \frac{1}{\varrho}\frac{\partial p}{\partial z} + \nu\left(\frac{\partial^2 w}{\partial x^2} + \frac{\partial^2 w}{\partial z^2}\right), \end{aligned} \tag{2.1.1}$$

where $\nu = \mu/\varrho$ is the *kinematic viscosity*, p is the pressure, μ is the viscosity, ϱ is the density, and F_x, F_z denote the x and z components of the body force, respectively. We note that for this model $F_z = 0$, as the only vertical body force here is gravity, which one may combine with the pressure into a single force. Furthermore, the horizontal body force is given by $F_x = -F_d + F_{cg}$, where F_d is the *drag force* and F_{cg} is the *countergradient force*. These two forces are detailed in the next sections, for each of the two model types studied.

We want to simplify the above equations further, to make the solution process easier. We do this by looking at the boundary layer in greater detail. We can sketch it such as given in Figure 1. To estimate the thickness of the boundary layer, we consider it for simplicity as a straight boundary coinciding with the x-axis. We also require further assumptions, such as (Veldman, 2009, Section 1.2):

1. the velocity at the outer edge of the velocity layer is of the order U;

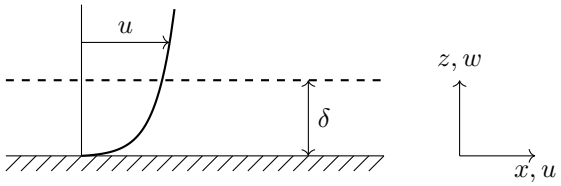

Figure 1. Sketch of the boundary layer.

2. the derivatives in the x direction can be estimated using a characteristic length L, independent from ν;

3. the thickness of the boundary layer has a characteristic size δ, with $\delta \ll L$, and derivative in the z direction can be based on this length scale;

4. there is no external influence (e.g. a shock wave) that would introduce a special scale for the pressure gradient. In other words, the pressure gradient adapts to the other terms in the equations.

Under these assumptions, we begin the estimation of the thickness of the boundary layer by using the continuity equation,

$$\frac{\partial u}{\partial x} + \frac{\partial w}{\partial z} = 0. \tag{2.1.2}$$

This implies that the partial derivative $\partial u/\partial x$ can be estimation such as:

$$\frac{\partial u}{\partial x} \sim \frac{U}{L}, \tag{2.1.3}$$

which should then also hold for the second term $\partial w/\partial z$. Since at the surface of the boundary layer the vertical component of the velocity is equal to zero, i.e. $w = 0$, and since the derivatives with regards to z can be estimated by δ, we obtain

$$w \sim \frac{\delta U}{L}, \tag{2.1.4}$$

inside the boundary layer. We then consider the x component of the momentum equation:

$$u\frac{\partial u}{\partial x} + w\frac{\partial u}{\partial z} = F_{cg} - F_d - \frac{1}{\varrho}\frac{\partial p}{\partial x} + \nu\frac{\partial^2 u}{\partial x^2} + \nu\frac{\partial^2 u}{\partial z^2}. \tag{2.1.5}$$

We have, since $\partial u/\partial x \sim U/L$, and $u \sim U$, that

$$u\frac{\partial u}{\partial x} \sim \frac{U^2}{L}. \tag{2.1.6}$$

Similarly,

$$w \sim \frac{\delta U}{L} \text{ and } \frac{\partial u}{\partial z} \sim \frac{U}{\delta} \implies w\frac{\partial u}{\partial z} \sim \frac{U^2}{L}. \tag{2.1.7}$$

And, $\partial^2 u/\partial x^2 \sim U/L^2$, $\partial^2 u/\partial z^2 \sim U/\delta^2$. Moreover, we note that the drag force and the countergradient force are either zero, or of the order U^2 and U respectively. These forces are detailed further in Sections 2.2 and 2.3 for both surface types. Combining these results yields

$$\underbrace{u\frac{\partial u}{\partial x} + w\frac{\partial u}{\partial z}}_{\sim U^2/L} = \underbrace{F_{cg}}_{\sim U} - \underbrace{F_d}_{\sim U^2} - \frac{1}{\varrho}\frac{\partial p}{\partial x} + \underbrace{\nu\frac{\partial^2 u}{\partial x^2}}_{\sim \nu U/L^2} + \underbrace{\nu\frac{\partial^2 u}{\partial z^2}}_{\sim \nu U/\delta^2}. \tag{2.1.8}$$

From this, we can conclude that

- both of the convective terms have the same order $\sim U^2/L$;

- the diffusive term containing the x derivatives is much smaller than the diffusive term with z derivatives, since $\delta \ll L$;

- the pressure is of the order $p \sim \varrho U^2$.

In a similar way, looking at the z component of the equations of momentum, we obtain

$$\underbrace{u\frac{\partial w}{\partial x} + w\frac{\partial w}{\partial z}}_{\sim U^2\delta/L^2} = -\frac{1}{\varrho}\frac{\partial p}{\partial z} + \underbrace{\nu\frac{\partial^2 w}{\partial x^2}}_{\sim \nu U\delta/L^3} + \underbrace{\nu\frac{\partial^2 w}{\partial z^2}}_{\sim \nu U/(\delta L)}. \tag{2.1.9}$$

We see that the convective term and the diffusive term are of the same order, $\sim U^2\delta/L^2$, which allows us to determine the order of magnitude of $\partial p/\partial z$, which is $\sim \varrho U^2\delta^2/L^2$. This is much smaller than $\partial p/\partial x$ above. Therefore, we may assume that the pressure is constant in the z direction. Finally, this yields the following system of equations for a two dimensional boundary layer flow:

$$\begin{aligned} \frac{\partial u}{\partial x} + \frac{\partial w}{\partial z} &= 0, \\ u\frac{\partial u}{\partial x} + w\frac{\partial u}{\partial z} &= -F_d + F_{cg} - \frac{1}{\varrho}\frac{\partial p}{\partial x} + \nu\frac{\partial^2 u}{\partial z^2}, \\ 0 &= \frac{1}{\varrho}\frac{\partial p}{\partial z}. \end{aligned} \tag{2.1.10}$$

This can be rewritten in terms of the shear stress tensor, which is given by the following equation, for a 2-dimensional flow:

$$\tau_{ij} = 2\mu e_{ij}, \quad e_{ij} = \frac{1}{2}\left(\frac{\partial u_i}{\partial j} + \frac{\partial u_j}{\partial i}\right). \tag{2.1.11}$$

More details on the shear stress tensor are provided in Appendix A.1. We then see that

$$\frac{\partial}{\partial z}\tau_{xz} = \mu\left(\frac{\partial^2 u}{\partial z^2} + \frac{\partial^2 w}{\partial z \partial x}\right), \tag{2.1.12}$$

where $\partial^2 w/(\partial z\partial x) \sim U/(L\delta)$ and $\partial^2 u/\partial z^2 \sim U/\delta^2$. We note that $\delta^2 \ll \delta L$, so we can rewrite the above equation as

$$\frac{\partial}{\partial z}\tau_{xz} = \mu\frac{\partial^2 u}{\partial z^2} = \varrho\nu\frac{\partial^2 u}{\partial z^2}. \tag{2.1.13}$$

Substituting into the previous system of equations (2.1.10) yields:

$$\begin{aligned} \frac{\partial u}{\partial x} + \frac{\partial w}{\partial z} &= 0, \\ u\frac{\partial u}{\partial x} + w\frac{\partial u}{\partial z} + \frac{1}{\varrho}\frac{\partial p}{\partial x} &= \frac{1}{\varrho}\frac{\partial \tau}{\partial z} - F_d + F_{cg}, \\ \frac{\partial p}{\partial z} &= 0, \end{aligned} \tag{2.1.14}$$

where $\tau = \tau_{xz}$ is given as in equation (2.1.12). From this point onward, we refer to τ as the *shear stress*, and we ignore the subscripts.

This model (2.1.14) is still incomplete, as atmospheric flow depends on heat, which does not appear in the above system of equation. Namely, there is *sensible heat* H, which is the heat that causes an object to change temperature, and *latent heat* E, which is the heat added to an object in order for it to change state. These heats appear in the equations for potential temperature θ and specific humidity q respectively.

The potential temperature of a region of fluid at pressure p is defined to be the temperature that an unsaturated parcel of dry air would have if brought adiabatically, i.e. without heat

transfer, and reversibly from its initial state to a standard pressure p_0. In mathematical terms, this can be written as:

$$\theta = T\left(\frac{p_0}{p}\right)^{R/c_p}, \tag{2.1.15}$$

where T is the temperature, p is the pressure, p_0 is the standard pressure, R is the gas constant, and c_p is the specific heat at constant pressure. Using the equation for conservation of energy, and in particular for conservation of temperature (Veldman, 2009, Section 1.1):

$$\frac{\partial c_v T}{\partial t} + \frac{\partial c_v T u_i}{\partial j} = \frac{1}{\varrho}\frac{\partial k \partial_i T}{\partial i} + 2\mu e_{ij}\frac{\partial u_i}{\partial j}, \tag{2.1.16}$$

and the fact that c_v and c_p are related using the equations of state for ideal gases, we obtain the heat transport equations for the potential temperature and specific humidity:

$$\begin{aligned} u\frac{\partial \theta}{\partial x} + w\frac{\partial \theta}{\partial z} &= \frac{1}{\varrho c_p}\left(-\frac{\partial H}{\partial z} + H_s\right), \\ u\frac{\partial q}{\partial x} + w\frac{\partial q}{\partial z} &= \frac{1}{\varrho}\left(-\frac{\partial E}{\partial z} + E_s\right). \end{aligned} \tag{2.1.17}$$

Ideal gases and the gas law are given in greater detail in Appendix A.2. A more complete derivation of the equations for potential temperature and specific humidity can be found in Chapter 3 of the book by Stull (2013). This then leads to the complete model of a two dimensional atmospheric boundary layer flow:

$$\begin{aligned} u\frac{\partial u}{\partial x} + w\frac{\partial u}{\partial z} + \frac{1}{\varrho}\frac{\partial p}{\partial x} &= \frac{1}{\varrho}\frac{\partial \tau}{\partial z} - F_d + F_{cg}, \\ \frac{\partial p}{\partial z} &= 0, \\ \frac{\partial u}{\partial x} + \frac{\partial w}{\partial z} &= 0 \\ u\frac{\partial \theta}{\partial x} + w\frac{\partial \theta}{\partial z} &= \frac{1}{\varrho c_p}\left(-\frac{\partial H}{\partial z} + H_s\right), \\ u\frac{\partial q}{\partial x} + w\frac{\partial q}{\partial z} &= \frac{1}{\varrho}\left(-\frac{\partial E}{\partial z} + E_s\right), \end{aligned} \tag{2.1.18}$$

where F_d is the drag force, F_{cg} is the countergradient force, H_s and E_s are the sensible and latent heat at the surface, respectively. These equations are underlining to both models describing atmospheric flow in heterogeneous vegetated terrains; single-layer and multi-layer, which are studied in the later sections.

After having given the system of equations for the model, we need to detail a few more terms, in order to have a precise description. Namely, to compute the pressure, we can use the first two equations of (2.1.18), together with some boundary conditions. The boundary condition is given when considering the upper edge of the boundary layer, for which u_e and p_e denote the horizontal velocity component and pressure on that edge. Thus, since we are at the edge of the boundary layer, we have $\partial_z u_e = 0$, and no force is being applied to it.

This then leads, using the first equation of the above model (2.1.18), to

$$u_e\frac{du_e}{dx} + \frac{1}{\varrho}\frac{dp_e}{dz} = 0. \tag{2.1.19}$$

Furthermore, we can compute the density ϱ of the air using the equations of state for ideal gases. Rewriting, this yields the density in terms of the measured initial values:

$$\varrho = \frac{p_0 M}{RT_0}, \tag{2.1.20}$$

where p_0 and T_0 are the pressure and absolute temperature used in the calculations of the initial profiles. To compute the momentum flux, we use the same reasoning as in Appendix B on the derivation of the Obukhov length, together with the formula given by Garratt and Pielke (Garratt & Pielke, 1989, Sections 3.1 and 3.2):

$$u_* = \frac{\kappa u}{\ln(z/z_0) - \psi_M(z/L_*)}, \tag{2.1.21}$$

where κ is von Kármán constant, $u(z)$ is the wind velocity function, L_* is the Obukhov length, and ψ_M is the integral form of the stability function ϕ_M for momentum. The stability functions $\psi_{M,H}$ and $\phi_{M,H}$ for momentum and heat are detailed in Section 2.1.2, and the derivation of the Obukhov length is given in Appendix B. We can rewrite the above equation for the friction velocity (2.1.21) by differentiating the right hand side:

$$u_* = \frac{\ell_m}{\phi_M(\zeta)} \frac{\partial u}{\partial z}, \tag{2.1.22}$$

where $\ell_m = \kappa z$ is the mixing length and $\zeta = z/L_*$ corresponds to a reparametrisation of the height variable z. Similarly, we can write the sensible and latent heats in terms of the stability functions for heat:

$$\begin{aligned} H &= -\varrho c_p \frac{u_* \ell_m}{\phi_H(\zeta)} \partial\theta z, 3 \\ E &= -\varrho \frac{u_* \ell_m}{\phi_H(\zeta)} \frac{\partial q}{\partial z}, \end{aligned} \tag{2.1.23}$$

where the minus sign is used to counter the negativity of $\partial\theta/\partial z$ and $\partial q/\partial z$. Introducing the eddy viscosities for momentum and heat, ε_M and ε_H, respectively as:

$$\begin{aligned} \varepsilon_M &= \frac{\ell_m^2}{\phi_M^2} \left| \frac{\partial u}{\partial z} \right|, \\ \varepsilon_H &= \varepsilon_M \frac{\phi_M}{\phi_H}, \end{aligned} \tag{2.1.24}$$

yields the momentum flux, the sensible heat, and the latent heat respectively as

$$\begin{aligned} \tau &= \varrho \varepsilon \frac{\partial u}{\partial z}, \\ H &= -\varrho c_p \varepsilon_H \frac{\partial \theta}{\partial z}, \\ E &= -\varrho \varepsilon_H \frac{\partial q}{\partial z}. \end{aligned} \tag{2.1.25}$$

It is important to note that, in order to obtain an accurate model of the fluxes, we require a realistic formulation of the mixing length, which was so far defined as $\ell_m = \kappa z$, where $\kappa \approx 0.4$ is the von Kármán constant. This is the simplest formulation of the mixing length, which is in reality only accurate when close to the surface. Thus, it is only really used when computing the first height level in the single-layer model, which is detailed in the following section. For higher heights and in the presence of vegetation, Klaassen introduced the *adjusted mixing length* ℓ_{ma}. This adjusted length takes into account the fact that within vegetation the flow of air around obstacles can create small-scale eddies. The length can be computed using the following equation derived by Klaassen (Klaassen, 1992, Section 2.4):

$$u \frac{\partial \ell_m}{\partial x} + w \frac{\partial \ell_m}{\partial z} = u C_\ell \left(1 - \frac{\ell_m}{\ell_{ma}} \right), \tag{2.1.26}$$

where C_ℓ is the *rate of adjustment* constant. Both the rate of adjustment and the adjusted mixing length depend on the type of model used: single- or multi-layer, detailed in the next sections.

For single-layer, the adjusted mixing length is computed using Blackadar's formula (2.2.5).

2.1.2 Stability functions

As seen in the equations for sensible and latent heats, and for the eddy viscosities for momentum and heat, we require some stability functions for our models. The integral form of those stability functions for momentum and heat, $\psi_{M,H}$, used by Klaassen, are the ones given by Garratt & Pielke (1989):

$$\psi(\zeta) = \int (1 - \phi(\zeta)) d(\ln \zeta), \tag{2.1.27}$$

where $\zeta = z/L_*$ and ϕ is the differentiated form of the stability function. The stability functions $\phi_{M,H}$ for momentum and heat are given respectively by

$$\begin{aligned} \phi_M &= \begin{cases} (1 - \gamma_1 \zeta)^{-1/4}, & \text{if } \zeta \leq 0, \\ 1 + \gamma_3 \zeta, & \text{if } \zeta > 0, \end{cases} \\ \phi_H &= \begin{cases} Pr(1 - \gamma_2 \zeta)^{-1/2}, & \text{if } \zeta \leq 0, \\ Pr + \gamma_4 \zeta, & \text{if } \zeta > 0, \end{cases} \end{aligned} \tag{2.1.28}$$

where Pr is a neutral turbulent Prandtl's number, and $\{\gamma_i\}_{i=1,\dots,4}$, are constants. However, one can note that these stability functions yield two major problems: the free convection limit and the matching of the profiles at the top of the surface layers (Delage & Girard, 1991). In their paper, Delage and Girard review these two problems, and offer solutions for the heat and momentum stability functions. We do not extend further into the problems, nor the solutions in this paper. The new stability functions $\phi_{M,H}$ are thus given by:

$$\begin{aligned} \phi_M &= \begin{cases} (1 - \gamma_1 \zeta)^{-1/6}, & \text{if } \zeta \leq 0, \\ 1 + \gamma_3 \zeta, & \text{if } \zeta > 0, \end{cases} \\ \phi_H &= \begin{cases} Pr(1 - \gamma_2 \zeta)^{-1/3}, & \text{if } \zeta \leq 0, \\ Pr + \gamma_4 \zeta, & \text{if } \zeta > 0, \end{cases} \end{aligned} \tag{2.1.29}$$

where $\zeta = z/L_*$, and L_* is the Obukhov length. In the code by Luppes (1993), the stability function for momentum ϕ_M for $L_* \leq 0$, is given by:

$$\begin{aligned} \phi_M &= \exp\left\{ -\frac{1}{6} \ln\left(1 - 40 \frac{z}{L_*} \right) \right\} \\ &= \exp\left\{ \ln\left(1 - 40 \frac{z}{L_*} \right)^{-1/6} \right\} \\ &= \left(1 - 40 \frac{z}{L_*} \right)^{-1/6}, \end{aligned} \tag{2.1.30}$$

where we can thus read that $\gamma_1 = 40$. Similarly, for $L_* \geq 0$, the code gives the stability function for momentum as:

$$\phi_M = 1 + 5.2 \frac{z}{L_*}, \tag{2.1.31}$$

from which we obtain $\gamma_3 = 5.2$. The stability function for heat is given in the code as

$$\begin{aligned} L_* \geq 0: &\quad \phi_H = \left(1 - 40 \frac{z}{L_*} \right)^{-1/3}, \\ L_* \leq 0: &\quad \phi_H = 1 + 5.2 \frac{z}{L_*}. \end{aligned} \tag{2.1.32}$$

Hence, $\gamma_2 = 40$ and $\gamma_4 = 5.2$. Therefore, the stability functions $\phi_{M,H}$ for momentum and heat used for the simulations follow those given by Delage and Girard, with known constants

for $\{\gamma_i\}_{i=1,\dots,4}$, as presented above.

We have thus detailed the general equations underlining both approaches for heterogeneous vegetated terrains. In the following two sections, we look at the specific equations, and the initial profiles corresponding to each particular model.

2.2 Single-layer model

In this section, we interest ourselves to the single-layer model. In this model, we consider the surfaces of both homogeneous vegetated zones to be represented by single layers, each with a constant *roughness length* z_0 and constant *stomatal resistance* r_s. We also suppose that two adjacent zones vary widely in roughness and/or in vegetation height. For instance, a zone of grassland adjacent to a zone of forest. In the single-layer model, fluxes from the canopy can be computed using the standard flux profile relations to the first height-level of the atmosphere z_1. The initial profiles are given by Klaassen (1992) and Luppes (1993):

$$\begin{aligned} \tau_0 &= \varrho u_{*0} \mathrm{sgn}\left(\frac{\partial u}{\partial z}\right), \\ u_{*_0} &= \left|\frac{u(z_1)\kappa}{\ln(z_1/z_0)+\psi_m}\right|, \\ H_0 &= \varrho c_p \frac{T_s - T_a}{r_a}, \\ E_0 &= 0.622 \frac{\varrho}{p} \frac{e_s^* - e_a}{r_a + r_s}, \end{aligned} \tag{2.2.1}$$

where z_0 is the roughness length of the canopy, ψ_m is the integrated form of the stability function ϕ_m as in (2.1.28) or (2.1.29), T is the absolute temperature, e is the water vapour pressure, e^* denotes the *saturated* water vapour pressure, and r is the resistance. The subscripts s, a designate the surface and the air at height z_1 respectively, and we call r_s the *stomatal resistance*. The absolute temperate and the water vapour pressure of the air at height z_1 can be computed using

$$\begin{aligned} T_a &= \theta_1 - \Gamma z_1, \\ e_a &= \frac{q(z_1)p}{0.622}, \end{aligned} \tag{2.2.2}$$

where Γ is the adiabatic lapse rate, that is, the rate at which the temperature changes under compression or expansion associated with elevation change, in an adiabatic process.

We consider the roughness length and the stomatal resistance to be constant in the horizontal direction, and they serve as surface characteristics. The initial conditions τ_0, H_0, and E_0 are used as implicit boundary layer conditions on u, θ, and q, respectively. These surface fluxes are related to each other by:

$$\begin{aligned} A_{\varepsilon_0} &= \lambda E_0 + H_0, \\ A_{\varepsilon_0} &= (1 - \mathrm{groco}) R_{n_0}, \\ R_{n_0} &= (1-\alpha)R_s + \varepsilon(R_\ell - \sigma T_s^4), \\ r_a &= \frac{\ln(z_1/z_{0_h}) + \psi_H}{\kappa u_{*_0}}, \end{aligned} \tag{2.2.3}$$

where A_{ε_0} is the available energy at the surface, λ is the latent heat of vaporisation, groco is the ground heat constant, R_{n_0} is the net radiation of the surface, R_s (R_ℓ) is the short (long) wave radiation, α is the albedo, ε is the emissivity of the surface, σ is the Stephan-Boltzman constant, ψ_H is the integrated form of the stability function ϕ_H (2.1.28), and $z_{0_h} = z_0 e^{-2}$ is the roughness length for heat. The albedo is the fraction of light that is reflected by the surface. The

emissivity is the ratio of the radiant energy emitted by a surface to that emitted by a 'perfect emitter' at the same temperature.

We also consider the ground heat constant, the albedo, and the emissivity as constant surface characteristics. Furthermore, in the single-layer model, the source terms from the model in equation (2.1.18) are considered to be zero:

$$F_d = F_{cg} = H_s = E_s = 0. \tag{2.2.4}$$

The reason behind this is that we do not have leaf area in the single-layer model, hence we do not have enough information to compute the drag force and the countergradient force. They are thus implicitly included in the roughness length z_0. Similarly, for the surface latent and sensible heats, we only consider heights $z \geq 0$, we thus have no heat 'leaking' into the ground.

The adjusted mixing length, which is found after an infinite fetch over a homogeneous single layer canopy, is given by Blackadar's formula:

$$\ell_{ma} = \frac{\kappa z}{1 + (\kappa z/\ell_{mm})}, \tag{2.2.5}$$

where ℓ_{mm} is the maximum mixing length,

$$\ell_{mm} = \max_z\{\ell_m\} = \max_z\{\kappa z\}. \tag{2.2.6}$$

The above equations together with the equations given in Section 2.1 completely describe single-layer models. In the next section, we look at the equations that are particular for multi-layer models.

2.3 Multi-layer model

In multi-layer model, we consider the surface of the smoother zone to still be represented by a single layer, but the rougher zone is instead represented by a multi-layer vegetation model with horizontally constant leaf area density and stomatal resistance. This model describes the exchange between a horizontal layer of the canopy and the surrounding air, which yields the source terms F_d, F_{cd}, H_s, E_s as in (2.1.18). For the lowest layer corresponding to the surface level, the surface flux calculations from the previous section are still valid, since the first layer can be modelled using a single-layer approach.

Above the lower layer, the multi-layer model comes into importance. The drag force and the counter gradient force are respectively given by (Klaassen, 1992, Section 2.3),(Luppes, 1993, Section 2.4):

$$\begin{aligned} F_d &= 0.08 A_\ell \, |u(z)| \, u(z), \\ F_{cg} &= \frac{0.04 \, (u(h_c) - u(z)) \, z}{1 + 0.8 A_{\ell_r} h_c}, \end{aligned} \tag{2.3.1}$$

where

$$A_{\ell_r} = \begin{cases} \max\{A_\ell\}, & \text{if } z \leq h_{\max}, \\ A_\ell, & \text{if } z > h_{\max}, \end{cases} \tag{2.3.2}$$

and where A_ℓ is the leaf area density of the layer, A_{ℓ_r} is a reference value for A_ℓ, h_c is the canopy height, and $h_{\max}$ is the height at which the maximum value of A_ℓ is attained. Klaassen introduced the factor of 0.08 instead of 0.16, which was the factor that was initially used, because the leaf area perpendicular to the flow is only half of the total leaf area. The original factor 0.16 is present to take into account the shelter effect of clustered leaves (Klaassen, 1992, Section 2.3).

The net radiation of the layer, which corresponds to the balance between incoming and outcoming radiant energy, is given by

$$R_n(z) = R_n(z + \Delta z) \exp\{-K_R A_\ell \Delta z\}, \tag{2.3.3}$$

where $R_n(z + \Delta z)$ is the net radiation of the layer that is above the one considered, K_R is the extinction coefficient for net radiation, and Δz is the thickness of the layer. The term $A_\ell \Delta z$ may be sometimes referred to as the leaf area index.

For the top layer, the net radiation is computed using the radiation balance given in the third equation of (2.2.3), with the potential temperature θ of the second highest layer (i.e. the layer below) instead of T_s. In other words, the net radiation for the highest level is given by

$$R_n(h_c) = (1 - \alpha)R_s + \varepsilon\left(R_\ell - \sigma\theta^4\right), \tag{2.3.4}$$

where R_s (R_ℓ) is the short (long) wave radiation, α is the albedo, ε is the emissivity, σ is the Stephan-Boltzmann constant, and θ is the potential temperature at the layer $h_c - \Delta z$.

The available energy in a layer is computed by

$$A_\varepsilon(z) = R_n(z) - R_n(z - \Delta z), \tag{2.3.5}$$

where $R_n(z - \Delta z)$ is the net radiation of the layer below the one considered. In the multi-layer model, the atmospheric resistance is defined to be the resistance between the leaves and the surrounding air, and is given by:

$$r_a = \frac{90}{A_\ell \Delta z}\left(\frac{\ell_w}{u(z)}\right)^{0.5}, \tag{2.3.6}$$

where ℓ_w is the leaf width. The factor of 90 takes into account leaf shading. The stomatal resistance in multi-layer model increases with the depth of the canopy, and is considered to be inversely proportional to the net radiation at that level, that is:

$$r_s = \frac{r_{to} R_n(h_c)}{A_\ell \Delta z R_n(z)}, \tag{2.3.7}$$

where r_{to} is the free parameter corresponding to the overall level of transpiration. To compute the source terms H_s and E_s, we can use the Penman equation (which estimates the evaporation) and the energy balance (Luppes, 1993, Section 2.4):

$$\begin{aligned} \lambda E_s &= \frac{s A_\varepsilon + \varrho c_p \left(\frac{e_a^* - e_a}{r_a}\right)}{s + \nu\left(\frac{r_a + r_s}{r_a}\right)}, \\ A_\varepsilon &= H_s + \lambda E_s, \end{aligned} \tag{2.3.8}$$

where s is the slope of the saturated vapour pressure function, e_a^* is the saturated vapour pressure at the temperature of the layer, e_a is the vapour pressure in the layer given by

$$e_a = \frac{q_a p}{0.622}, \tag{2.3.9}$$

with q_a the specific humidity of the layer, and ν is the psychrometer constant defined by

$$\nu = \frac{p c_p}{0.622\lambda}, \tag{2.3.10}$$

where λ is the latent heat of vaporisation. The surface resistance is calculated using

$$r_{s_0} = r_{to} \exp\left\{K_r \sum_{\text{layers}} A_\ell \Delta z\right\}. \tag{2.3.11}$$

This equation is derived using equations (2.3.3) and (2.3.7) as follows:

$$\begin{aligned}
r_{s_0} &= \frac{r_{to} R_n(h_c)}{A_{\ell 0} \Delta z R_n(z_0)} \\
&= \frac{r_{to} R_n(h_c)}{A_{\ell 0} \Delta z} \frac{\exp\{K_R A_{\ell 0} \Delta z\}}{R_n(z_1)} \\
&= \frac{r_{to} R_n(h_c)}{A_{\ell 0} \Delta z} \exp\{K_R A_{\ell 0} \Delta z\} \frac{\exp\{K_R A_{\ell 1} \Delta z\}}{R_n(z_2)} \\
&\vdots \\
&= \frac{r_{to} R_n(h_c)}{A_{\ell 0} \Delta z} \exp\{K_R A_{\ell 0} \Delta z\} \exp\{K_R A_{\ell 1} \Delta z\} \ldots \frac{\exp\{K_R A_{\ell h_c - \Delta z} \Delta z\}}{R_n(h_c)} \\
&= \frac{r_{to}}{A_{\ell_0} \Delta z} \exp\left\{K_R \sum_{\text{layers}} A_\ell \Delta z\right\} \\
&= r_{to} \exp\left\{K_r \sum_{\text{layers}} A_\ell \Delta z\right\},
\end{aligned} \tag{2.3.12}$$

where we set $A_{\ell_0} \Delta z = 1$, so that it doesn't block radiations coming down from the first height level to the surface level, as the surface level behaves in similar way to the single-layer model.

Similarly to the single-layer model, the available energy at the surface is given by

$$A_{\varepsilon_0} = (1 - \text{groco}) R_{n_0}, \tag{2.3.13}$$

where R_{n_0} is net radiation at the lowest level, and groco is the ground heat constant of the ground surface. The adjusted mixing length for multi-layer model is given by (Klaassen, 1992, Section 2.4):

$$\ell_{ma}(z) = \ell_{ma}(z - \Delta z) \exp\{-K_\ell A_\ell \Delta z\}, \tag{2.3.14}$$

where $\ell_{ma}(z - \Delta z)$ is the adjusted mixing length of the layer below the one considered, and K_ℓ is the reduction coefficient for mixing length by leaves, estimated from the roughness length and the zero-plane displacement. K_ℓ determines the adjusted mixing length within and just above tall vegetation. For the surface level, we use $\ell_{ma} = \kappa z$ as a boundary condition for the adjusted mixing length.

All the equations detailed in this section, together with the equations from Section 2.2 for the first layer, and from Section 2.1 for the general atmospheric flow, completely describe the multi-layer model. In the next section, we look at the boundary conditions that hold for both single-layer and multi-layer models.

2.4 Boundary conditions

In this section, we look at the boundary conditions needed to solve the atmospheric flow equations given in (2.1.18). For the velocity, the lower boundary conditions are

$$\begin{aligned}
u &= 0, \quad \text{at } z = z_0, \\
w &= 0, \quad \text{at } z = z_0,
\end{aligned} \tag{2.4.1}$$

where z_0 denotes the roughness length which varies for each homogeneous vegetated zone. The value of τ_0 is used in the discretised momentum equation, which appears in the simulation code.

The upper boundary condition for the horizontal velocity is given by the *interaction law* (Veldman, 2009, Section 7.1 and 7.2). We divide the flow field into two parts, the boundary layer and the external flow. Then, the velocity along the edge of the boundary layer u_e and the displacement thickness δ^* are related by

$$\begin{aligned} \text{external flow} \quad & u_e = E[\delta^*], \\ \text{boundary-layer flow} \quad & u_e = B[\delta^*], \end{aligned} \tag{2.4.2}$$

where E and B denote 'external' and 'boundary-layer' flow respectively. We assume that after discretisation, both equations of (2.4.2) have a unique solution. The form in which the second equation, for the boundary-layer flow, is written allows that for any δ^*, we can find a u_e. However, the reverse does not necessarily hold. To solve the above equation (2.4.2), one can use the following iteration method:

$$\begin{cases} u_e^{(n)} = E[\delta^{*(n-1)}], \\ \delta^{*(n)} = B^{-1}[u_e^{(n)}]. \end{cases} \tag{2.4.3}$$

This is called the classical or *direct* method. However, problems may arise since B^{-1} may not always exist. To counter that we can reverse the iteration process, yielding the *inverse* method,

$$\begin{cases} \delta^{*(n)} = E^{-1}[u_e^{(n-1)}], \\ u_e^{(n)} = B[\delta^{*(n)}]. \end{cases} \tag{2.4.4}$$

In practice, the operator E^{-1} does not create further problems. However, we also want to avoid an iterative treatment as much as possible, and we do this by introducing an approximation I of the external operator E, which is so simple that it can be used as a boundary condition for the boundary-layer equation. I is then called the *interaction law*, as it describes an approximation of the interaction between the boundary-layer and the external flows. This creates the following iterative process, called *quasi-simultaneous*:

$$\begin{cases} u_e^{(n)} - I[\delta^{*(n)}] = E[\delta^{*(n-1)}] - I[\delta^{*(n-1)}], \\ u_e^{(n)} - B[\delta^{*(n)}] = 0. \end{cases} \tag{2.4.5}$$

In this method, the approximation I of E is solved simultaneously with B. In what follows, we consider the x-axis, between some x_0 and x_{N+1}, as presented in Figure 2.

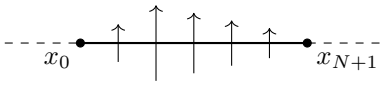

Figure 2. Sketch of the x-axis and the vertical velocity on $[x_0, x_{N+1}]$.

Consider the vertical velocity between x_0 and x_{N+1} to be given by $w(x, 0)$, and suppose that for $x < x_0$ and $x > X_{N+1}$, we have $w(x, 0) \equiv 0$. A potential flow satisfying these boundary conditions has (along the x-axis) a velocity given by, up to a constant,

$$u(x, 0) = \frac{1}{\pi} \int_{x_0}^{x_{N+1}} \frac{w(\xi, 0)}{x - \xi} d\xi. \tag{2.4.6}$$

We can write the value u_e of the external flow as

$$u_e(x) = u_{e_0}(x) + u_{e_{\delta^*}}(x), \tag{2.4.7}$$

where u_{e_0} is the solution past the 'clean' profile, i.e. outside of $[x_0, x_{N+1}]$, and $u_{e_{\delta^*}}$ represents the effect of the boundary layer. We then obtain the model given by:

$$u_e(x) = u_{e_0}(x) + \frac{1}{\pi}\int_{x_0}^{x_{N+1}} \frac{w(\xi,0)}{x-\xi} d\xi. \tag{2.4.8}$$

Since we want the boundary-layer flow to match smoothly with the external flow, we can write:

$$w(\xi,0) = \frac{d}{d\xi}(u_e\delta^*). \tag{2.4.9}$$

For convenience, we introduce $\hat{\delta} := u_e\delta^*$. Plugging this into (2.4.8) yields

$$u_e(x) = u_{e_0}(x) + \frac{1}{\pi}\int \frac{d\hat{\delta}}{d\xi}\frac{d\xi}{x-\xi}. \tag{2.4.10}$$

This integral has to be evaluated over the entire region where we simulate the atmospheric flow. Another way to write $\hat{\delta} = u_e\delta^*$ is as:

$$\hat{\delta} = y_e u_e - \int_0^{y_e} u \; dy, \tag{2.4.11}$$

where y_e is the height of the upper edge (Luppes, 1993, Section 2.5).

An alternative upper boundary condition on u is by considering the friction velocity. This upper boundary condition is called the *matched load*, and is used by Klaassen (Klaassen, 1992, Section 3.1). It is described by

$$u_*(x+\Delta x, y_e) = \frac{u_*(x,y_e) + u_*(x, y_e - \Delta z)}{2}. \tag{2.4.12}$$

In other words, the upper friction velocity u_* at the next horizontal point of calculation $(x+\Delta x)$ is equal to the mean of the two upper values of u_* of the current layer. This mathematical description in equation (2.4.12) is difficult to rewrite in terms of u, rather than keeping it as a formulation of the friction velocity u_*.

We may note that it is more advantageous to use the interaction law instead of the matched load. That is because the calculations of the velocity and pressure will react to downstream values. On the other hand, under the matched load condition, calculations will only react to upstream values, as if the atmospheric flow was unable to 'see' its direction. Therefore, when using the interaction law, the effect of vegetation ahead is already witnessed, which is not accounted for in the matched load condition. Furthermore, the interaction law takes into account the inviscid outer flow that is above the viscous boundary layer when producing the horizontal velocity. The matched load condition only uses the boundary layer itself, and hence acts as if there was no atmosphere above it.

With all of that in mind, we therefore use the interaction law as our upper boundary layer condition for the horizontal velocity.

The lower boundary conditions for the potential temperature and the specific humidity are given by, respectively,

$$\begin{aligned} &\text{at } z = 0, \quad \theta = T_s, \\ &\text{at } z = 0, \quad q = \frac{0.622 e_s^*}{p}, \end{aligned} \tag{2.4.13}$$

where T_s is the absolute temperature at the surface, e_s^* is the saturated vapour pressure at temperature T_s, and p is the pressure of the air. These conditions are coherent with the initial profiles for the singe-layer model given in equation (2.2.1).

The values of H_0 and E_0 are used in the discretised forms of the heat and humidity equations at height z_1, as seen in the simulation code. The upper boundary conditions for the potential temperature and specific humidity are given by the matched load condition, in terms of the atmospheric fluxes H and E, respectively sensible and latent heat,

$$\begin{aligned} H(x+\Delta x, y_e) &= \frac{H(x,y_e)+H(x,y_e-\Delta z)}{2}, \\ E(x+\Delta x, y_e) &= \frac{E(x,y_e)+E(x,y_e-\Delta z)}{2}. \end{aligned} \tag{2.4.14}$$

For the mixing length equation, we only require one boundary condition, given by

$$\ell_m = \kappa z, \quad \text{at } z = y_0, \tag{2.4.15}$$

where y_0 is the lowest intermediate height level, which then lays above z_0. The lower boundary condition on the adjusted mixing length ℓ_{ma} is the same as the one given above, for both the single-layer and the multi-layer models.

The final conditions necessary to solve the atmospheric flow equations (2.1.18) are the initial conditions. We require initial profiles for u, θ, q, and ℓ_m since these variables occur in the flow equations with derivatives along the horizontal direction. The pressure is assumed to be constant with regard to height, so it is thus treated differently. Under the assumption that the atmospheric flow is 'adjusted' at $x = 0$, and with vertically constant atmospheric fluxes in the surface layer, the initial profiles can be computed from the following system of equations:

$$\begin{aligned} &\text{at } x = 0, \\ &\qquad \ell_m = \ell_{ma}, \\ &\qquad w = 0, \\ &\qquad u_* = u_{*0}, \\ &\qquad H = H_0, \\ &\qquad E = E_0, \end{aligned} \tag{2.4.16}$$

where ℓ_{ma} is given by Blackadar's formula (2.2.5), and u_{*0}, H_0, and E_0 follow from calculations under the single-layer model. The flow is called *adjusted* at $x = 0$, if we suppose an infinitely long smooth surface to the left of the z-axis, in order to have a standard logarithmic profile at the start of the terrain considered.

We have thus detailed all equations underlining both the single-layer and the multi-layer model, as well as the system of equations describing the atmospheric flow, and the boundary conditions needed to solve (2.1.18). In the following section, we focus on the roughness length z_0, and particularly on the *effective* roughness length z_0^{eff}.

3 Theoretical effective roughness length

The equations given for the above model types, single- and multi-layer, describe the wind profile rather accurately under the assumption that the local conditions are spatially homogeneous or if we only consider surfaces sufficiently close to the bottom boundary layer. When the surface becomes inhomogeneous or we attempt to apply the theory to higher levels, i.e. outside of the surface layer, the roughness length that was used thus far needs to be increased from its local value to the *effective roughness length* (ERL) z_0^{eff}. The ERL then represents the inhomogeneous terrain when looking at larger-scale meteorological simulations, where we may not know the individual properties of each terrain. In this section, we look at three different ways of computing this effective roughness length, and the different properties that the formulas yield, following the papers written by André & Blondin (1986), Taylor (1987), and de Vries et al. (2003).

3.1 André and Blondin (1986)

In their 1986 paper, André & Blondin (1986) derive an equation for the effective roughness length, under a few important assumptions. Furthermore, they show the dependence of this ERL on the first height level z_1. In this section, we detail the motivations and the computations made. However, our model is only considered for two dimensions, so the equations given here are thus slightly different from the ones they give, adapted to our model.

For simplicity, we assume that the atmosphere, or at least the boundary layer, is neutrally stratified. This means that the Richardson number satisfies $R_i = 0$, and that the existence or formation of distinct layers in the atmosphere does not influence the development of turbulence. This also implies that the distribution of temperature with height is adiabatic: there is no transfer of heat and the change in internal energy is only due to work. More on the Richardson number and the stratification of the atmosphere can be found in Appendix B.

We also assume that the roughness length and the logarithmic wind profile are of physical significance at the local or micro-meteorological scale, i.e. at a scale that is smaller than the grid size of the two-dimensional simulations. In other words, we suppose that z_0 and u are continuous functions on the grid. Finally, we assume that the grid of such a model consists of a patchwork of individual elements, each with a local roughness length $z_0(x)$, dependent on the horizontal coordinate x, at height $z = 0$.

In the two-dimensional model, only some kind of averaged wind over the grid is known, e.g. its value U_1 at the lowest available level z_1. For parametrisation purposes, we suppose that below z_1, the wind profile behaves according to the *universal law of the wall*:

$$U_1 = \frac{u_*^{\text{eff}}}{\kappa} \ln\left(\frac{z_1}{z_0^{\text{eff}}}\right), \tag{3.1.1}$$

where κ is the von Kármán constant, u_*^{eff} is the effective friction velocity, which is proportional to the square root of the momentum flux averaged over the grid square, and z_0^{eff} is the effective roughness length one would like to find in order to parametrise the surface fluxes. Under our above hypothesis, along the x-axis and for altitudes lower than z_1, the wind profile follows the *logarithmic law*:

$$\tilde{u}(x, z) = \frac{\tilde{u}_*(x)}{\kappa} \ln\left(\frac{z}{z_0(x)}\right). \tag{3.1.2}$$

In order to make the two above equations (3.1.1) and (3.1.2) compatible, we may require that all local profiles described in (3.1.2) give the same value for $z = z_1$. Namely, we want that at height $z = z_1$, the logarithmic law yields U_1. In other words, we require that the following relationship

$$U_1 = \frac{\tilde{u}_*(x)}{\kappa} \ln\left(\frac{z_1}{z_0(x)}\right) \tag{3.1.3}$$

between the small-scale friction velocity $\tilde{u}_*$ and the roughness length $z_0(x)$ exists. Using the local relation (3.1.3), we can get rid of the local friction velocity $\tilde{u}_*(x)$ in order to rewrite the logarithmic law (3.1.2) into

$$\begin{aligned} \tilde{u}_*(x) &= \frac{U_1 \kappa}{\ln(z_1) - \ln(z_0(x))} \\ \implies \tilde{u}(x,z) &= U_1 \frac{\ln(z) - \ln(z_0(x))}{\ln(z_1) - \ln(z_0(x))}. \end{aligned} \tag{3.1.4}$$

Since we want to compute the effective roughness length, we interest ourselves at values of $z \leq z_1$. We can thus average out the above equation over the grid size, denoted by Δ, which gives the '*numerical integral average*':

$$\begin{aligned} \overline{u}(z) &= \frac{1}{\mu(\Delta)} \int_\Delta \tilde{u}(x,z) dx \\ &= \frac{U_1}{\mu(\Delta)} \int_\Delta \frac{\ln(z) - \ln(z_0(x))}{\ln(z_1) - \ln(z_0(x))} \, dx, \end{aligned} \tag{3.1.5}$$

where $\mu(\Delta)$ corresponds to the Lebesgue measure of Δ, which is the volume if Δ is three-dimensional, the area if Δ is two-dimensional, and the length if Δ is one-dimensional. Here, Δ is one-dimensional, so we divide by its length. U_1 is given by the universal law of the wall (3.1.1), so it is independent of x and hence can be taken out of the integral.

From this equation, we see that the average wind profile $\overline{u}(z)$ follows a logarithmic law. Furthermore, since we consider the *average* wind profile, we can extract the effective friction velocity u_*^{eff}, by considering equation (3.1.2), and taking the grid-square average, where we set $\tilde{u}_*(x) = u_*^{\text{eff}}$, which is thus independent of x and can be moved out of the integral. This yields:

$$\begin{aligned} \overline{u}(z) &= \frac{u_*^{\text{eff}}}{\kappa} \int_\Delta \ln\left(\frac{z}{z_0(x)}\right) dx \\ \implies u_*^{\text{eff}} &= \kappa \overline{u}(z) \int_\Delta \frac{dx}{\ln(z) - \ln(z_0(x))} \\ &= \frac{\kappa U_1}{\mu(\Delta)} \int_\Delta \frac{dx}{\ln(z_1) - \ln(z_0(x))}. \end{aligned} \tag{3.1.6}$$

Comparing with the local relationship between the small-scale friction velocity and the roughness length given in (3.1.3), we obtain the following equation for the effective friction velocity

$$u_*^{\text{eff}} = \frac{1}{\mu(\Delta)} \int_\Delta \tilde{u}_*(x) dx. \tag{3.1.7}$$

This result allows us to write the effective roughness length by looking at the universal law of the wall (3.1.1), which states that

$$\begin{aligned} \ln\left(\frac{z_0^{\text{eff}}}{z_1}\right) &= -\frac{U_1 \kappa}{u_*^{\text{eff}}} \\ &= -\frac{\mu(\Delta)}{\displaystyle\int_\Delta \frac{dx}{\ln(z_1) - \ln(z_0(x))}} \\ &= \frac{1}{\dfrac{1}{\mu(\Delta)} \displaystyle\int_\Delta \frac{dx}{\ln(z_0(x)) - \ln(z_1)}}. \end{aligned} \tag{3.1.8}$$

We have thus found an equation for the effective roughness length z_0^{eff}. It is clear that the height z_1 of the lowest level in the large-scale model influences the ERL. Adding $\ln(z_1)$ on both

sides yields:

$$\ln(z_0^{\text{eff}}) = \frac{1}{\dfrac{1}{\mu(\Delta)}\displaystyle\int_\Delta \frac{dx}{\ln(z_0(x)) - \ln(z_1)}} + \ln(z_1). \tag{3.1.9}$$

Before detailing more of the properties of this ERL, we need to note that under the simplified assumptions given above, we obtain an effective friction velocity that corresponds to the grid-square average of the local friction velocity $\tilde{u}_*$, as written in equation (3.1.7). However, physically, we would expect the effective friction velocity to be the square root of the local kinematic momentum flux, that is, we would instead expect

$$u_*^{\text{eff}} = \sqrt{\frac{\tilde{\tau}}{\varrho}}, \tag{3.1.10}$$

where ϱ is the density of the air and $\tilde{\tau}$ is the local momentum flux. This difference needs to be kept in mind when computing the effective roughness length using the formula given above, as it may lead to approximation errors.

Looking at the formula for the ERL, (3.1.9), we see that it depends more on large values of $z_0(x)$ than on smaller values, which is as expected from a physical point of view. To see this more clearly, consider the following example, where the local roughness is given by:

$$z_0(x) = \begin{cases} \delta/a, & \text{if } x \in \dfrac{a}{1+a}\Delta, \\[2ex] a\delta, & \text{if } x \in \dfrac{1}{1+a}\Delta, \end{cases} \tag{3.1.11}$$

where $a > 0$ is some parameter and Δ is the interval on the x-axis of the heterogeneous vegetated terrain considered. We then have that the arithmetic for $z_0(x)$ is given by:

$$\overline{z_0(x)} = \frac{\delta}{a}\frac{a}{1+a}\Delta + a\delta\frac{1}{1+a}\Delta = \delta, \tag{3.1.12}$$

which is thus independent on the parameter a. However, on the other hand, as a increases, the rougher zone becomes rougher and decreases in size compared to the smoother (i.e. less rough) one. As a decreases, the rougher zone becomes smoother. To compute the effective roughness length, we apply equation (3.1.8) to the above distribution (3.1.11), where we suppose that the interval $\Delta = [\Delta_0, \Delta_1]$,

$$\begin{aligned}
\ln\left(\frac{z_0^{\text{eff}}}{z_1}\right) &= \frac{\mu(\Delta)}{\displaystyle\int_{\frac{a}{1+a}\Delta} \frac{dx}{\ln(\delta/a) - \ln(z_1)} + \int_{\frac{1}{1+a}\Delta} \frac{dx}{\ln(a\delta) - \ln(z_1)}} \\
&= \frac{\Delta_1 - \Delta_0}{\dfrac{1}{\ln(\delta/a) - \ln(z_1)}\displaystyle\int_{\frac{a}{1+a}\Delta_0}^{\frac{a}{1+a}\Delta_1} dx + \frac{1}{\ln(a\delta) - \ln(z_1)}\int_{\frac{1}{1+a}\Delta_0}^{\frac{1}{1+a}\Delta_1} dx} \\
&= \frac{\Delta_1 - \Delta_0}{\dfrac{1}{\ln(\delta/a) - \ln(z_1)}\dfrac{a}{1+a}(\Delta_1 - \Delta_0) + \dfrac{1}{\ln(a\delta) - \ln(z_1)}\dfrac{1}{1+a}(\Delta_1 - \Delta_0)} \\
&= \left(\frac{a}{1+a}\frac{1}{\ln(\delta/a) - \ln(z_1)} + \frac{1}{1+a}\frac{1}{\ln(a\delta) - \ln(z_1)}\right)^{-1} \\
&= \frac{(1+a)(\ln(\delta/a) - \ln(z_1))(\ln(a\delta) - \ln(z_1)}{a(\ln(a\delta) - \ln(z_1)) + \ln(\delta/a) - \ln(z_1)} \\
&= \frac{(1+a)\left(\ln^2(\delta/z_1) - \ln^2(a)\right)}{(1+a)\ln(\delta/z_1) - (1-a)\ln(a)}.
\end{aligned} \tag{3.1.13}$$

This function is plotted in Figure 3 for different values of a, and where the ratio $\delta/z_1 \leq 1$. This ratio must remain large enough such that the lowest level z_1 still lies in the logarithmic surface layer. On the other hand, it must also not become too large. z_1 should not approach a value close to the largest roughness length $a\delta$ present in our example model, since then equation (3.1.13) would diverge.

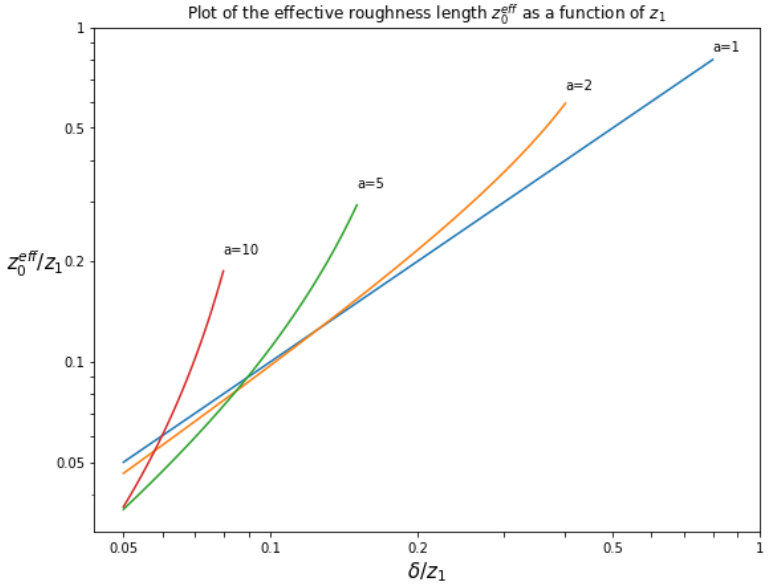

Figure 3. Plot of the effective roughness length z_0^{eff} as a function of the first level z_1, as given in equation (3.1.13), for the roughness distribution example (3.1.11).

As shown in Figure 3, the effective roughness length increases with a for a given value δ/z_1. This illustrates the initial guess that the effective roughness length depends on the largest local roughness length. Furthermore, we can note from this figure that for given a and δ, the effective roughness length increases when the height of the lowest level z_1 approaches the ground level. To see this more clearly, we can differentiate equation (3.1.8) with respect to z_1:

$$
\begin{aligned}
\frac{\partial}{\partial z_1} \ln\left(\frac{z_0^{\text{eff}}}{z_1}\right) &= \frac{\partial}{\partial z_1}\left(\frac{1}{\mu(\Delta)}\int_\Delta \frac{dx}{\ln(z_0(x)) - \ln(z_1)}\right)^{-1} \\
\implies \frac{\partial}{\partial z_1}\ln(z_0^{\text{eff}}) - \frac{\partial}{\partial z_1}\ln(z_1) &= \mu(\Delta)\frac{-\frac{\partial}{\partial z_1}\int_\Delta \frac{dx}{\ln(z_0(x))-\ln(z_1)}}{\left(\int_\Delta \frac{dx}{\ln(z_0(x))-\ln(z_1)}\right)^2} \\
\implies \frac{\partial z_0^{\text{eff}}}{\partial z_1}\frac{1}{z_0^{\text{eff}}} - \frac{1}{z_1} &= -\mu(\Delta)\frac{\int_\Delta \frac{\partial}{\partial z_1}\frac{dx}{\ln(z_0(x))-\ln(z_1)}}{\left(\int_\Delta \frac{dx}{\ln(z_0(x))-\ln(z_1)}\right)^2} \\
\implies \frac{\partial z_0^{\text{eff}}}{\partial z_1}\frac{1}{z_0^{\text{eff}}} - \frac{1}{z_1} &= -\mu(\Delta)\frac{\int_\Delta \frac{1}{z_1}\frac{dx}{\ln^2(z_0(x)/z_1)}}{\left(\int_\Delta \frac{dx}{\ln(z_0(x)/z_1)}\right)^2} \\
\implies \frac{\partial z_0^{\text{eff}}}{\partial z_1}\frac{1}{z_0^{\text{eff}}} &= \frac{1}{z_1} - \frac{1}{z_1}\frac{\mu(\Delta)\int_\Delta \frac{dx}{\ln^2(z_0(x)/z_1)}}{\left(\int_\Delta \frac{dx}{\ln(z_0(x)/z_1)}\right)^2} \\
\implies \frac{\partial z_0^{\text{eff}}}{\partial z_1} &= \frac{z_0^{\text{eff}}}{z_1}\left\{1 - \frac{\mu(\Delta)\int_\Delta \frac{dx}{\ln^2(z_0(x)/z_1)}}{\left(\int_\Delta \frac{dx}{\ln(z_0(x)/z_1)}\right)^2}\right\}.
\end{aligned}
\tag{3.1.14}
$$

Using Schwarz's inequality, which says $\left(\int f(x)dx\right)^2 \leq \int f^2(x)dx$, we obtain:

$$\frac{\mu(\Delta)\int_\Delta \frac{dx}{\ln^2(z_0(x)/z_1)}}{\left(\int_\Delta \frac{dx}{\ln(z_0(x)/z_1)}\right)^2} \geq \frac{\mu(\Delta)\int_\Delta \frac{dx}{\ln^2(z_0(x)/z_1)}}{\int_\Delta \frac{dx}{\ln^2(z_0(x)/z_1)}} \geq 1 \implies \frac{\partial z_0^{\text{eff}}}{\partial z_1} \leq 0, \tag{3.1.15}$$

which in other words tells us that the effective roughness length in a two-dimensional model becomes larger as the lowest height level approaches the ground. This effect results in an increase of the effective drag coefficient, which is defined as

$$C_d = \left(\frac{\kappa}{\ln(z_1/z_0^{\text{eff}})}\right)^2. \tag{3.1.16}$$

To conclude, we have found one formula for the effective roughness length, namely

$$\ln\left(\frac{z_0^{\text{eff}}}{z_1}\right) = \frac{1}{\frac{1}{\mu(\Delta)}\int_\Delta \frac{dx}{\ln(z_0(x)) - \ln(z_1)}}. \tag{3.1.17}$$

This ERL is dependent on the first height level z_1, and requires an effective friction velocity to be equal to the grid-square average of the local friction velocity, which does not necessarily correspond to reality. In the next section, we analyse the problems that may occur using such an ERL, before finding an alternative formula.

3.2 Taylor (1987)

In his paper, Taylor (1987) reviews the effective length given by André and Blondin, and explains why this formula is not correct. He also gives two formulas for an an effective length that are supposedly more accurate. In this section, we explore the reasons given by Taylor on why the formula for the ERL (3.1.17) is incorrect, and we detail the derivation for the ERL proposed.

One can first note that the effective roughness length given by André and Blondin depends on the first height level z_1. Moreover, it is significantly different from the value obtained by simply taking a spatial average of (the logarithm of) the local micrometeorological roughness lengths. Indeed, Taylor suggests that the effective roughness length of a terrain can simply be found by the grid-square average:

$$z_0^{\text{eff}} \approx z_0^m, \quad \text{where} \quad \ln(z_0^m) = \langle \ln(z_0) \rangle, \tag{3.2.1}$$

where z_0^{eff} denotes Taylor's effective roughness length, and z_0 is the local roughness length. Considering a terrain with length Δ on the x-axis, we obtain the grid-square average as:

$$\langle \ln(z_0) \rangle = \frac{1}{\mu(\Delta)} \int_\Delta \ln(z_0(x))dx, \tag{3.2.2}$$

where $\mu(\Delta)$ is the measure of Δ. Since our model is two-dimensional and thus Δ is one-dimensional, $\mu(\Delta)$ corresponds to the length of the interval over which we integrate. Clearly Taylor suggests that the effective roughness length does not depend upon the first height level z_1.

Taylor begins his paper by assuming the same profile as André and Blondin. In other words, we only consider neutral stratifications, and we suppose that z_1 is sufficiently close to the ground, in order for the local velocity profiles to be of the logarithmic form

$$u = \frac{u_*}{\kappa}(\ln(z) - \ln(z_0)). \tag{3.2.3}$$

Furthermore, we assume that the heterogeneous grid consists of patchwork areas of different roughness lengths. Then, although the local roughness length z_0 depends on x (i.e. $z_0 = z_0(x)$),

the local profiles will indeed be of the form (3.2.3) except in the narrow transition areas between the different regions. According to Taylor, these areas should only have a small contribution to the average. Alternatively, one may want to assume slow spatial variation in z_0 (i.e. we consider z_0 to be a continuous function), so that the profiles are always in approximate local equilibrium. Then, averaging equation (3.2.3) over the grid square yields

$$\langle u(z) \rangle = \frac{1}{\kappa} \left(\langle u_* \rangle \ln z - \langle u_* \ln z_0 \rangle \right), \tag{3.2.4}$$

where the notation $\langle \cdot \rangle$ corresponds to the numerical integral average, as in equation (3.2.2). This average profile is indeed logarithmic in z, but we find ourselves with two main problems:

i. the apparent friction velocity $\langle u_* \rangle$ is not necessarily equal to the square root of the average stress $\langle u_*^2 \rangle$ (which was an issue pointed out in the previous section);

ii. the apparent roughness length is not only related to the local roughness length distribution, but it also depends on the distribution of the friction velocity. In other words, denoting the *apparent roughness length* z_0^a, we would need to obtain

$$\ln(z_0^a) = \frac{\langle u_* \ln z_0 \rangle}{\langle u_* \rangle}, \tag{3.2.5}$$

in order for the following to hold:

$$\langle u(z) \rangle = \frac{\langle u_* \rangle}{\kappa} \ln \left(\frac{z}{z_0^a} \right), \tag{3.2.6}$$

which would then be in a more similar form to (3.2.3) than (3.2.4) is.

Taylor suggests to set $z_0^{\text{eff}} = z_0^a$. We however need to distinguish between the two in order to properly establish Taylor's reasoning. To this end, let us consider a simple case: a 'half and half' grid square, where the first half corresponds to a smooth zone with $z_0(x) = z_{0s}$, and the second half is a rougher zone, with $z_0(x) = z_{0r}$.

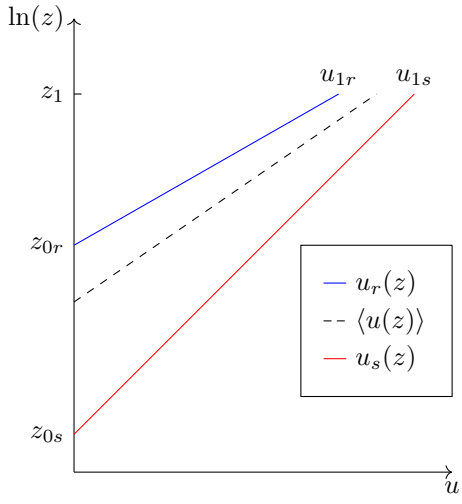

Figure 4. Schematic diagram of velocity profiles for a 'half and half' grid square, where u_1 corresponds to the velocity at height z_1. The subscripts r, s denote the rougher and the smoother regions, respectively.,

Figure 4 shows a schematic diagram of the velocity profiles against $\ln(z)$. In this sketch, we do not know the relationship between the smooth and rougher wind profiles u_s and u_r, but we do know that since they are generated by the same driving force, we would expect $u_s(z) > u_r(z)$ for all z. Two key questions that one may ask are

1. What should be considered as the driving force?

2. Is it uniform over the grid?

To answer these questions, Taylor looks at the assumptions made by André and Blondin. Namely, they assume that u is fixed, and it is equal to U_1 at $z = z_1$, as given by equation (3.1.1). In the 'half and half' grid square, this assumption would mean that $u_{1s} = u_{1r}$. This is a correct approximation for large values of z_1, say of the order $\mathcal{O}(200\text{m})$, where hence the first height level is much higher than the canopy height. However, for smaller values of z_1, say of order $\mathcal{O}(10\text{m})$, this is not an appropriate approximation. Indeed, at heights below or sufficiently close to the canopy level in a forest, we know that wind is slowed down. In general, over rougher surfaces, we have that for heights $z_1 \sim 10\text{m}$, the wind flow is significantly reduced.

Hence, in the example considered here, is is inappropriate to consider the wind speed at some height within the surface layer as being the driving mechanism for the boundary-layer flow near the surface, since it will not be uniform over the grid square. This shows that the effective roughness length *should not* depend on the first height level z_1, contradicting André and Blondin's reasoning.

For surface boundary-layer flow above a heterogeneous vegetated terrain, where the upstream or unperturbed flow is a constant stress layer, the appropriate driving force corresponds to a constantly applied shear stress. Taylor points out that this force is not strictly appropriate here, but it does lead to equilibrium profiles above different terrains with different roughness lengths, over which the value of friction velocity u_* is constant. Hence, in this case, the apparent roughness length z_0^a is given by

$$\ln(z_0^a) = \frac{\langle u_* \ln z_0 \rangle}{\langle u_* \rangle} = \langle \ln(z_0) \rangle = \ln(z_0^m). \tag{3.2.7}$$

Therefore, under this driving force and for this model, we have $z_0^a = z_0^m$. Thus, this yields the effective roughness length $\ln(z_0^{\text{eff}}) = \langle \ln(z_0) \rangle$.

For global climate models (GCMs) and regional scale numerical weather prediction (NWP) models, the horizontal pressure gradients will vary only slowly across a grid square and will be relatively unaffected by sub-grid scale variations in surface properties. The sub-grid scale problem consists of representing the average planetary boundary layer (PBL) over a heterogeneous terrain. The driving force becomes the pressure gradient. In this model, we assume that the transition zones of the PBL (e.g. the transition in the topography of the boundary layer) is small compared to the size of individual areas in our grid square. Under the assumption that the surface stress adjusts rather rapidly to changes in z_0, we can estimate the relationship between u_* and $\ln(z_0)$ needed in equation (3.2.5) from models for the planetary boundary layer over homogeneous terrain.

We define $\mathbf{u}_g$ to be the geostrophic flow, that is the theoretical wind resulting from an exact balance between the Coriolis force and the pressure gradient force. The Coriolis force is an inertial force which acts on objects in motion, within a reference frame rotating with respect to some inertial frame. We also denote $V_g = |\mathbf{u}_g|$ the length of the geostrophic wind. The Rossby number is defined by:

$$Ro = \frac{V_g}{f z_0}, \tag{3.2.8}$$

where f is the Coriolis parameter, corresponding to twice the component of the Earth's angular velocity about the local vertical. In other words,

$$f = 2\omega \sin \varphi, \tag{3.2.9}$$

where ω is the angular speed of the Earth, and φ is the latitude. Then, planetary boundary layer similarity tells us that the relationship between surface friction velocity u_* and the roughness

Rossby number is

$$\ln\left(\frac{u_*}{V_g}Ro\right) = B + \left(\frac{\kappa^2}{(u_*/V_g)^2} - A^2\right)^{1/2}, \tag{3.2.10}$$

where κ is the von Kármán constant, and A and B are constants for neutral stratification. They can also be considered functions of the stability parameter $(\kappa u_*)/(fL_*)$, where L_* is the Obukhov length, for non-neutral stratification. Taylor uses in his paper $A = 4$ and $B = 2$ as 'typical' values for all computations.

Differentiating the left hand side of (3.2.10) with respect to $\ln(z_0)$ yields:

$$\begin{aligned}\frac{d}{d\ln(z_0)}\ln\left(\frac{u_*}{V_g}Ro\right) &= \frac{d}{d\ln(z_0)}\ln\left(\frac{u_*}{fz_0}\right)\\ &= \frac{1}{u_*}\frac{du_*}{d\ln(z_0)} - \frac{1}{z_0}\frac{d(z_0)}{d\ln(z_0)}\\ &= \frac{1}{u_*}\frac{du_*}{d\ln(z_0)} - \frac{1}{z_0}\frac{de^{\ln(z_0)}}{d\ln(z_0)}\\ &= \frac{1}{u_*}\frac{du_*}{d\ln(z_0)} - 1.\end{aligned} \tag{3.2.11}$$

Similarly, differentiating the right hand side with respect to $\ln(z_0)$ yields, for neutral stratification where we thus consider A and B constant:

$$\frac{d}{d\ln(z_0)}\left(B + \sqrt{\frac{\kappa^2}{(u_*/V_g)^2} - A^2}\right) = \frac{\frac{d}{d\ln(z_0)}\left(\kappa^2 V_g^2/u_*^2\right)}{2\sqrt{\kappa^2 V_g^2/u_*^2 - A^2}} = \frac{-\kappa^2 V_g^2 \frac{du_*}{d\ln(z_0)}}{u_*^3\sqrt{\kappa^2 V_g^2/u_*^2 - A^2}} \tag{3.2.12}$$

Setting

$$F = \ln\left(\frac{u_*}{V_g}\right) - B + \ln\left(\frac{V_g}{fz_0}\right) \tag{3.2.13}$$

yields:

$$\frac{d}{d\ln(z_0)}\left(B + \sqrt{\frac{\kappa^2}{(u_*/V_g)^2} - A^2}\right) = -\frac{1}{u_*}\frac{du_*}{d\ln(z_0)}\frac{\kappa^2}{(u_*/V_g)^2 F} \tag{3.2.14}$$

.

Putting the left hand side and the right hand side together gives

$$\begin{aligned}\frac{1}{u_*}\frac{du_*}{d\ln(z_0)} - 1 &= -\frac{1}{u_*}\frac{du_*}{d\ln(z_0)}\frac{\kappa^2}{(u_*/V_g)^2 F}\\ \implies u_*\left(\frac{du_*}{d\ln(z_0)}\right)^{-1} &= \frac{\kappa^2 + (u_*/V_g)^2 F}{(u_*/V_g)^2 F}\\ \implies \frac{1}{u_*}\frac{du_*}{d\ln(z_0)} &= \frac{(u_*/V_g)^2 F}{\kappa^2 + (u_*/V_g)^2 F}\\ &= \frac{F}{\kappa^2 V_g^2/u_*^2 + F} =: a_1.\end{aligned} \tag{3.2.15}$$

The above equation only holds for neutral stratification, i.e. when A and B are constant. If the stability parameter depends on $\ln(z_0)$ there would be additional terms involving $dA/d\ln(z_0)$ and $dB/d\ln(z_0)$,

Continuing with establishing a relationship between u_* and $\ln(z_0)$, we first need to note that u_* varies relatively slowly with z_0. When reasonably restricting the ranges of the model, u_* can be approximated as varying linearly with $\ln(z_0)$, as can be seen by equation (3.2.15). Considering V_g and f to be fixed, i.e. we consider a fixed latitude for the model, we obtain an

approximation of u_* using z_0^m as given in (3.2.1), where $\ln(z_0^m)$ corresponds to the grid square average of $\ln(z_0(x))$,

$$u_* = u_*^m \left[1 + a_1 \left(\ln(z_0) - \ln(z_0^m)\right)\right]. \tag{3.2.16}$$

Here, a_1 is as given above in (3.2.15), and u_*^m is the value of u_* corresponding to $\ln(z_0) = \ln(z_0^m)$. Since we have a linear relationship between u_* and $\ln(z_0)$, we see that u_*^m corresponds to the grid square average $\langle u_* \rangle$. Substituting (3.2.16) into (3.2.5), assuming that $u_*^m = \langle u_* \rangle$ yields

$$\begin{aligned} \ln(z_0^a) &= \frac{\langle u_* \ln(z_0) \rangle}{\langle u_* \rangle} \\ &= \langle [1 + a_1 \left(\ln(z_0) - \ln(z_0^m)\right)] \ln(z_0) \rangle \\ &= \langle \ln(z_0) \rangle + a_1 \left(\langle \ln^2(z_0) \rangle - \langle \ln(z_0) \rangle^2 \right). \end{aligned} \tag{3.2.17}$$

Since $a_1 > 0$, we will always have $\ln(z_0^a) \geq \langle \ln(z_0) \rangle$, and in many cases they will be close to each other. The second ERL given by Taylor is thus $\ln(z_0^{\text{eff}}) = \ln(z_0^a)$, as in equation (3.2.17). In the analysis done here, we do not have any dependency on the first height level z_1, which is the main difference with André and Blondin André & Blondin (1986).

3.3 De Vries et al. (2003)

In their 2003 paper, de Vries et al. (2003) look at estimating the effective roughness length (as well as the displacement height, which we look into further in Section 5.5.). For bluff-rough surfaces, where only sparse objects (e.g. trees) influence the roughness, they review an equation proposed by Lettau (1969):

$$z_0 = CH\lambda, \tag{3.3.1}$$

where H is the average obstacle height and λ is the density of the roughness elements, which can be approximated by A/S, where A is the average silhouette area of the roughness elements in a horizontal area S. Note that the silhouette area is similar to the leaf area A_ℓ. For two dimensional models, and thus two dimensional obstacles, the calculation of A/S can be simplified to H/L, where L is the distance between two obstacles. C is supposed to be a constant, taken by Lettau as $C = 0.5$ for $A/S < 0.1$.

On the other hand, Wooding et al. (1973) suggest that C is a factor of shape, based on wind tunnel data:

$$C = 2.05 \left(\frac{H}{S}\right)^{\kappa}, \tag{3.3.2}$$

where $\kappa \approx 0.40$ is the von Kármán constant. An alternative to Lettau's equation to compute the roughness length is given by Kustas & Brutsaert (1986):

$$\frac{z_0}{H} = \lambda \left(\frac{H}{S}\right)^{\kappa}, \tag{3.3.3}$$

where S is the average horizontal dimension of the roughness element. In this equation, we do not take into account the shape of the individual obstacle. All above equations do account for the form drag, which is caused by large scale roughness elements, but neglect the shear stress contributed by the small scale elements like vegetation. By definition, the total drag F_t consists of both the form drag F_f and the shear stress F_s,

$$F_t = F_f + F_s. \tag{3.3.4}$$

Form drag is the drag created by the roughness elements per unit horizontal area, and depends more upon the larger obstacles than the smaller ones. Shear stress represents the friction stress due to the smaller scale elements, and depends on the surface area. De Vries et al. give the

following equation for the form drag:

$$F_f = 0.5\varrho C_d A u^2(H/2), \tag{3.3.5}$$

where C_d is the drag coefficient, ϱ is the density of air, A is the average silhouette area of the roughness element, and $u(H/2)$ is the horizontal wind speed at height $H/2$, where H is the average obstacle height. In their study, de Vries et al. use a constant $C_d = 0.3$. Using the roughness length attributed to flat terrain, denoted by z_{01} and estimated to being $z_{01} = 0.01$m, the contribution from the shear stress is computed by:

$$F_s = \frac{\kappa^2}{\ln^2(H/2z_{01})}\varrho u^2(H/2)S. \tag{3.3.6}$$

Since shear stress is due to the surface area, de Vries et al. argue that the total drag is related to the effective roughness length, using the above equation for shear stress,

$$F_t = \frac{\kappa^2}{\ln^2(H/2z_0^{\text{eff}})}\varrho u^2(H/2)S. \tag{3.3.7}$$

Then, extracting the effective roughness length from (3.3.7), and using the above equations, yields

$$\begin{aligned}
\left(\ln(H) - \ln(2z_0^{\text{eff}})\right)^2 &= \frac{\kappa^2\varrho u^2(H/2)S}{F_t} \\
\implies \ln(2z_0^{\text{eff}}) &= \ln(H) - \sqrt{\frac{\kappa^2\varrho u^2(H/2)S}{F_t}} \\
\implies 2z_0^{\text{eff}} &= \exp\left\{\ln(H) - \sqrt{\frac{\kappa^2\varrho u^2(H/2)S}{F_t}}\right\} \\
\implies z_0^{\text{eff}} &= \frac{H}{2}\exp\left\{-\sqrt{\frac{\kappa^2\varrho u^2(H/2)S}{F_t}}\right\} \\
&= \frac{H}{2}\exp\left\{-\left[\frac{\kappa^2 S}{0.5C_dA + \frac{\kappa^2}{\ln^2(H/2z_{01})}S}\right]^{1/2}\right\} \\
&= \frac{H}{2}\exp\left\{-\frac{\kappa}{\left[0.5C_d\lambda + \frac{\kappa^2}{\ln^2(H/2z_{01})}\right]^{1/2}}\right\}.
\end{aligned} \tag{3.3.8}$$

In this model, as de Vries et al. point out, the shadowing effects of the roughness elements are ignored, and it is a valid model for obstacle slopes satisfying $\tan\theta > 0.2$. On the other hand, for slopes satisfying $\tan\theta < 0.1$, the effect of the obstacle drag on the roughness length can be neglected, and for slopes with $0.1 < \tan\theta < 0.2$, it is suggested that the effective roughness length is parametrised based on linear theory, i.e.

$$\ln\left(\frac{z_0}{z_{01}}\right) = \frac{1}{\kappa^2}\ln(1 + 63 \times 6.4\tan\theta^2). \tag{3.3.9}$$

Note that, in this thesis, we only interest ourselves to models consisting of trees and grass. Trees are generally perpendicular to the ground, hence the obstacle slope is $\theta = \pi/2$, but then $\tan\theta$ is not defined. To this end, let us consider the obstacle slope to be $\theta = \pi/2 - \varepsilon$, for some $\varepsilon > 0$ sufficiently small. This then allows us to check that indeed $\tan\theta > 0.2$, and hence the equation given by de Vries et al. can be used for our models. In conclusion, we have a third equation for

the effective roughness length, namely:

$$z_0^{\text{eff}} = \frac{H}{2} \exp\left\{ -\frac{\kappa}{\left[0.5 C_d \lambda + \frac{\kappa^2}{\ln^2(H/2z_{01})}\right]^{1/2}} \right\}, \tag{3.3.10}$$

where H is the average obstacle height, C_d is the drag coefficient, here set to be $C_d = 0.3$, and $\lambda \approx H/L$ is the density of the roughness elements, for L the distance between two obstacles. Here, z_{01} is the is the roughness length attributed to flat terrain ($z_{01} = 0.03$m in our case), and κ is the von Kármám constant, $\kappa \approx 0.40$.

We have thus found three different methods of computing the effective roughness length for a heterogeneous vegetated terrain. These methods are compared in Section 5.

4 Simulations

Throughout this section, we consider two distinct homogeneous terrains: grass and forest. The properties and conditions for each zone are taken from (Klaassen, 1992, Table 1). All simulations are done using the final code by Slump (2021), which is a grid-refined version of the code by Luppes (1993).

We first run the simulation for a 900 m long terrain, with three distinct homogeneous zones: grass, forest, grass, as given in Figure 5a. Then, we suppose that instead of having a single region of 300m of forest, we have two regions, one of 100m and another of 200m. For this model, we still suppose that the entire terrain has a length of 900 m. For example, we may suppose that the terrain is given by Figure 5b. We also interchange the two forest regions to see the effect it has on the final wind profile, as in Figure 5c.

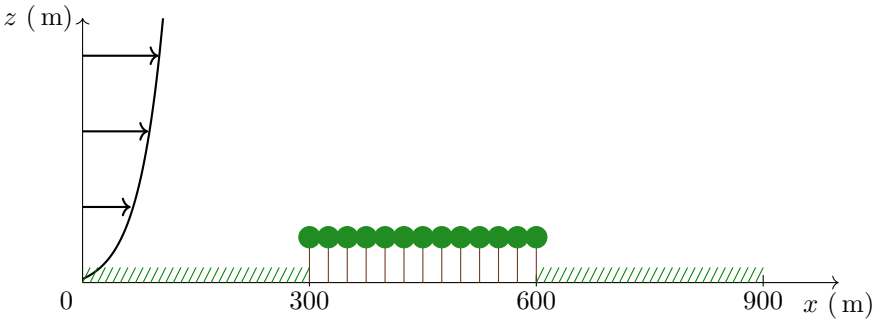

(a) Sketch of three homogeneous regions, model 3.

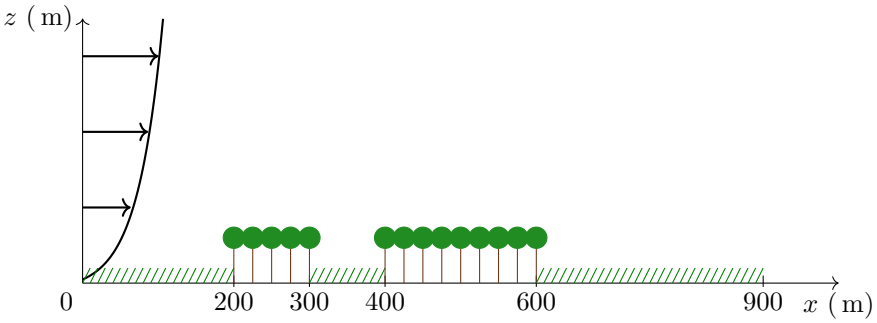

(b) Sketch of five homogeneous regions, model 5.1.

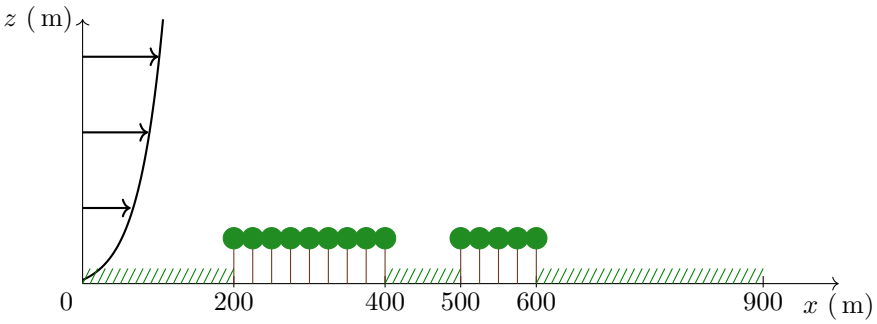

(c) Sketch of five homogeneous regions, model 5.2.

Figure 5. Sketches of the three types of models considered in this paper.

In what follows, the 3 regions terrain is referred to as *model 3*, while the 5 regions terrains are called *model 5.1* and *model 5.2*. For all simulations, we first run the single-layer model, then the multi-layer model. In the next section, we compare all models together, but first we analyse them separately. To distinguish between the three models, under single- and multi-layer approach, we denote by s and m the surface type considered for each simulation.

4.1 Three regions, single-layer model (3s)

In this section, we run simulations for three homogeneous zones, as illustrated in Figure 5a. We consider all regions to be of equal length (300m each), and all regions are modelled by a single-layer profile. Furthermore, since we want to look at the effect of the vortices on the velocity, we select a few x locations to compare the velocity at those points. We choose $x \in \{900, 800, 700, 650\}$, since the forest region stops at 600m, and we should avoid values too close to that boundary. Otherwise, we would directly be under the influence of the vortices which may yield a biased result. After running the simulations, we obtain the velocity profiles as given in Figure 6.

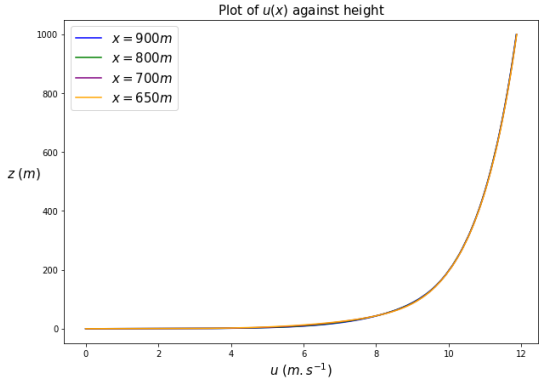

Figure 6. Plot of the velocity against the height for model 3s.

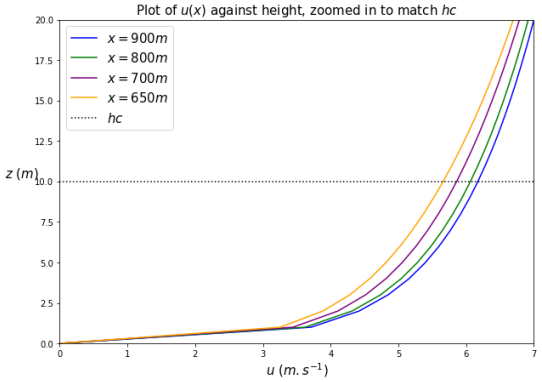

Figure 7. Zoomed plot of the velocity against the height for model 3s, to indicate the canopy layer $h_c = 10\,\text{m}$.

Note that all Figure 6 tells us is that the curves are indeed logarithmic, without providing further information regarding the difference in velocity for various locations of x. Hence, from this point onward, we only look at the zoomed-in version of those plots, as in Figure 7. The canopy height is given by $h_c = 10\,\text{m}$, so we only consider height values of $z \leq 20\,\text{m}$. From this, we conclude that for three homogeneous single-layer regions, the vortices probably slow down the atmospheric flow when closer to the boundary of the rougher zone. This result is coherent with what we know from real-life observations. More precisely, when plotting the difference between $x = 900\,\text{m}$ and $x = 650\,\text{m}$ as given in Figure 8, we see that at the canopy height of 10m, the difference is $0.493\,\text{m/s}$, which corresponds to 7.8% of the wind flow at the end of the model (i.e. at 900m) for the same height.

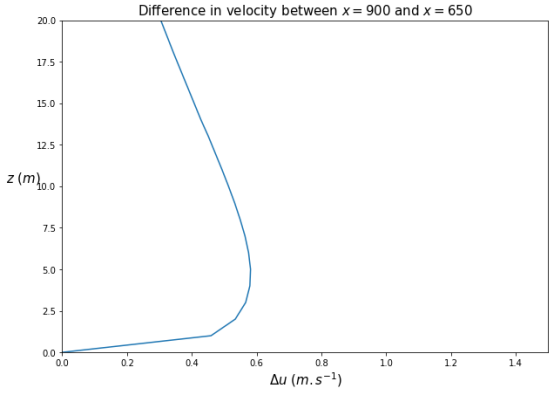

Figure 8. Difference in velocity between $x = 900\,\text{m}$ and $x = 650\,\text{m}$ for model 3s.

Hence, for a simulation with three homogeneous single-layer regions, the vortices slow down the wind flow at the canopy height by 7.8%. We note that in reality, we do not have a 'block' of trees, but rather different layers with different characteristics.

4.2 Three regions, multi-layer model (3m)

In this section, we still consider three regions as illustrated in Figure 5a, but the forest is now modelled using a multi-layer approach. To make the model more accurate, we suppose that at the bottom of the forest there is a layer of grass, which means that the first layer of the multi-layer model has properties corresponding to grass. Similar to the single-layer model above, we find that the wind profile is logarithmic, as given in Figure 9. Furthermore, by zooming in, we again see that the velocity for $x = 650\,\text{m}$ is smaller than the velocity at $x = 900\,\text{m}$.

Plotting the difference in velocity between $x = 650\,\text{m}$ and $x = 900\,\text{m}$, as in Figure 10, shows us that the vortices slow down the atmospheric flow at the canopy height by 9.2% of the speed at $x = 900\,\text{m}$.

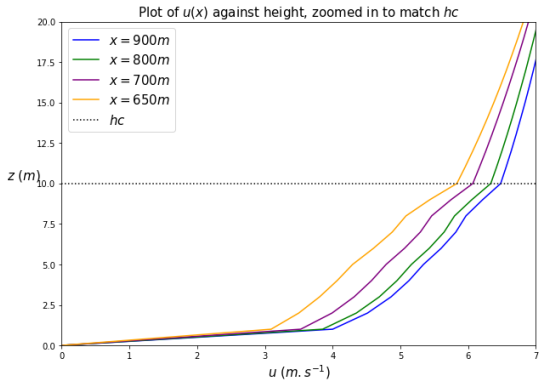

Figure 9. Zoomed plot of the velocity against the height for model 3m.

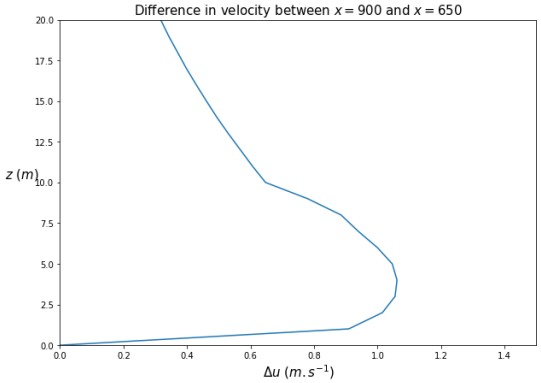

Figure 10. Difference in velocity between $x = 900\,\text{m}$ and $x = 650\,\text{m}$ for model 3m.

We note that in the multi-layer model, the effect of the vortices is stronger than for the single-layer model, since in the multi-layer model the wind flow is slowed down by 9.2%, compared to only 7.8% for the single-layer. Moreover, as plotted in Figure 11, we read that the velocity for $x = 650\,\text{m}$ in the multi-layer model is less than that in the single-layer, for heights $z \leq 10\,\text{m}$, which corresponds to the canopy level.

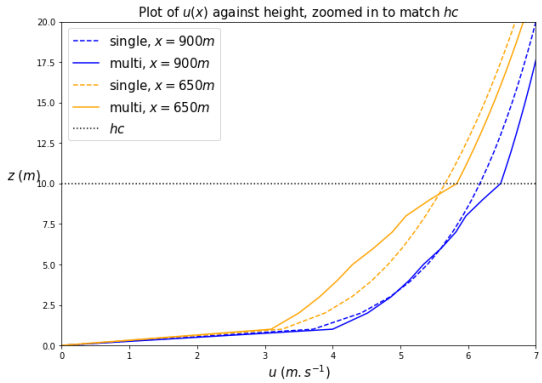

Figure 11. Comparison of single- and multi-layer models for three regions.

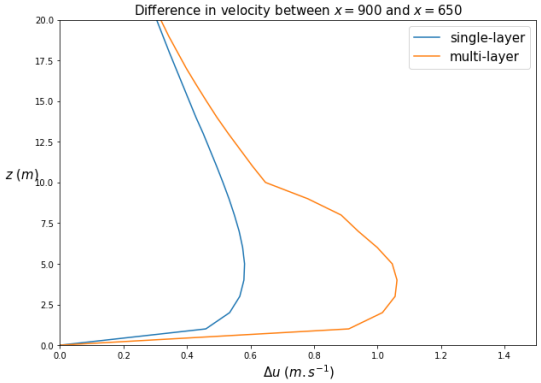

Figure 12. Comparison of the differences in velocity (between $x = 900$ and $x = 650$) between models 3s and 3m.

On the other hand, for $x = 900\,\text{m}$, the curve for the single-layer model is similar to that for the multi-layer model. This can be explained by the fact that at this distance we are far enough from the boundary between the rougher and the smoother regions, and hence the effect of the vortices is diminished. Furthermore, we must note that as seen in Section 2.3, the multi-layer approach takes into account some extra parameters, which are not present in single-layer.

Namely, we note the presence of two forces, the drag force F_d and the countergradient force F_{cg}. These forces act on the wind velocity directly, which explains why the wind is slowed down more in multi-layer than in the single-layer approach. In other words, it is not only the effect of the vortices that influence the wind velocity.

Plotting the difference in velocity between $x = 900$ and $x = 650$ for single-layer and multi-layer in Figure 12 shows us that the difference in velocity in the multi-layer model is greater than for the single-layer. Hence, the effect of vortices (and the presence of the drag and countergradient forces) for the multi-layer model is greater than that for the single-layer model. In the single-layer model we consider the forest region to be equivalent to a single 'block' with constant roughness length. Thus, as we do not consider the leaf area density in this model, and the wind does not flow in between the trees and the leaves, the single-layer model yields less vortices than the multi-layer approach. Therefore, the velocity is slowed down more in the latter.

Since the multi-layer model is a more accurate description of reality, we conclude that the vortices slow down the atmospheric flow by 9.2%, rather than by 7.8%, at the canopy height. We then may ask ourselves what happens when considering two separate rough zones instead of a single one. This is discussed in the following subsections.

4.3 Five regions, single-layer model (5.1s)

In this section, we consider a terrain of total length of 900m consisting of five distinct homogeneous regions, as illustrated in Figure 5b. We suppose that the first forest-type region has length 100m and the second has length 200m. Starting with the first model, we obtain that the wind flow for the same x locations as above is also following a logarithmic profile, as shown in Figure 13.

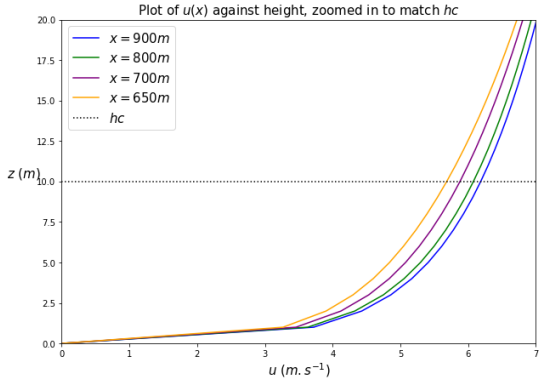

Figure 13. Zoomed plot of the velocity against the height for model 5.1s.

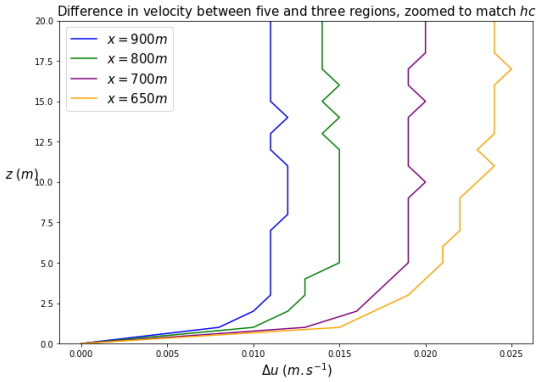

Figure 14. Comparison of the velocity for three and five regions, models 3s and 5.1s.

Looking at Figure 13 and comparing it with the plot for model 3s in Figure 7, we notice that they are very similar. The plot showing the difference between the two is given in Figure 14, and we see that the difference is less than 0.025 m/s. This corresponds to about 0.4% of the velocity for three terrains in single-layer model at distance $x = 650$ m.

Hence, we can conclude that for model 5.1s, the vortices that appear at the end of the first rough zone do not influence the output wind profile. The final wind flow is however still impacted by the vortices of the second rough zone. Furthermore, we can compute that the velocity at $x = 650$ is 7.6% slower than at $x = 900$, which is close to the 7.8% we obtained for the three regions in single-layer model, at the canopy height h_c. However, this result is not coherent with real-life expectations. Indeed, we would expect that the vortices apeparing at the end of the first rough region propagate and slow the wind down after the second region.

4.4 Five regions, multi-layer model (5.1m)

Under the first model and using multi-layer modelling of the rough zones, we obtain a logarithmic wind profile for certain x locations, as given in Figure 15.

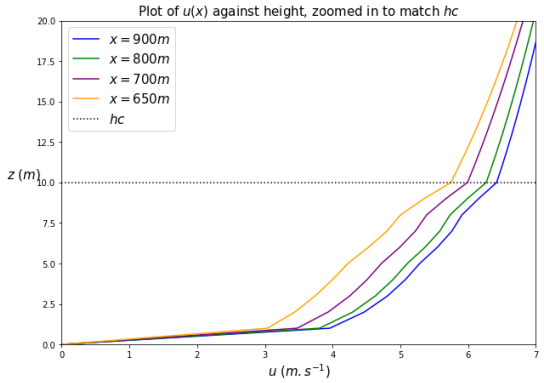

Figure 15. Zoomed plot of the velocity against the height for model 5.1m.

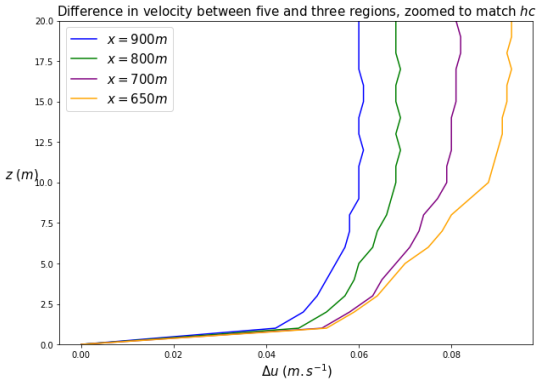

Figure 16. Comparison of the velocity for three and five regions, models 3m and 5.1m.

Comparing Figure 15 with the plot of the velocity against height for three multi-layer regions as in Figure 9, we obtain an error of 0.09 m/s, which corresponds to about 1% of the velocity in model 3m at the canopy height height for $x = 650$. Hence, for the first model, the vortices of the first rough zone reduce the velocity at the end of the terrain by 1%.

4.5 Five regions, single-layer model (5.2s)

The second model is similar to the model described above, with the exception that the first and second rougher zones are interchanged. In other words, instead of having a terrain that is divided as in Figure 5b, it is now divided as presented in Figure 5c, with the first rough region being 200m long, and the second 100m, with 100m of smoother zone in between. Using this model, the output wind flow is once again logarithmic, as can be seen from Figure 17. Furthermore, comparing Figure 17 with Figure 7, corresponding to the velocity versus height for three single-layer regions, yields Figure 18.

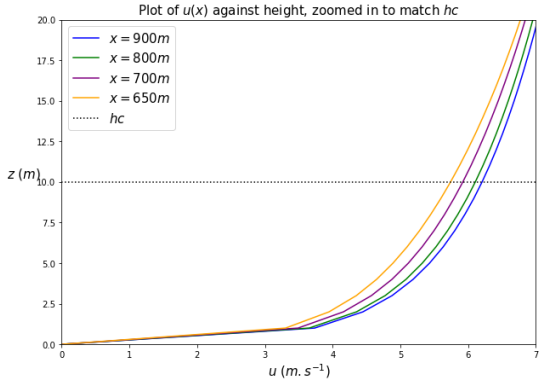

Figure 17. Zoomed plot of the velocity against the height for model 5.2s.

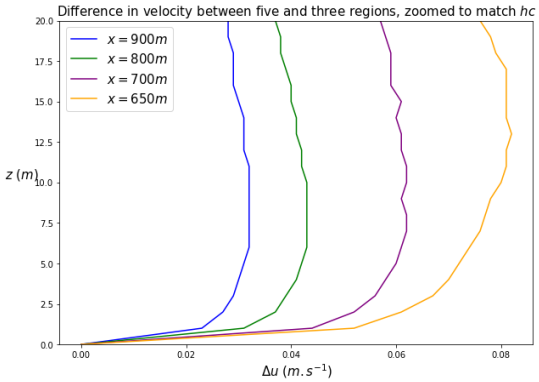

Figure 18. Comparison of the velocity for three and five regions, model 3s and 5.2s.

We then see that the curves are similar, and their difference is of about 1% of the velocity at $x = 900\,\text{m}$ at the canopy height $h_c = 10\,\text{m}$. Moreover, the velocity at $x = 650$ is 7% slower at the canopy height than the velocity at $x = 900$, which is smaller than the 7.6% we obtained previously. Therefore, we have a stronger effect of the vortices that appear after the first rough region on the final output in the first model of five regions than in the second, under single-layer models. This can be explained by the fact that in the first model, there is a smaller region of rougher terrain to begin with than in the second model.

4.6 Five regions, multi-layer model (5.2m)

Using this model, we obtain a logarithmic wind profile for certain x locations as plotted in Figure 19.

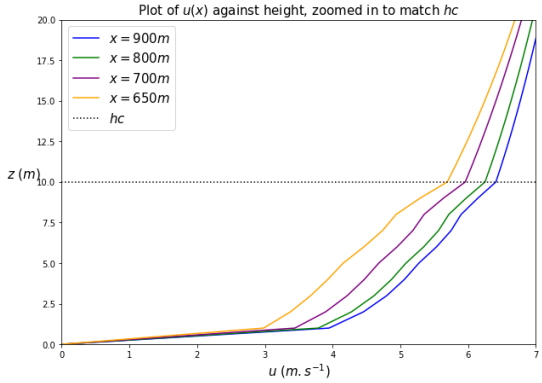

Figure 19. Zoomed plot of the velocity against the height for model 5.2m.

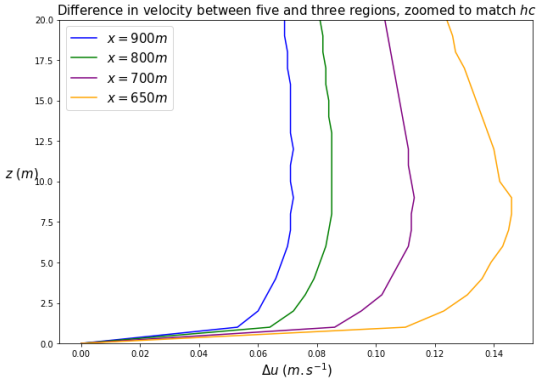

Figure 20. Comparison of the velocity for three and five regions, models 3m and 5.2m

Comparing Figure 19 with the plot for three multi-layer regions in Figure 9, as given in Figure 20, tells us that at the canopy level for $x = 650\,\text{m}$, the error is of $0.14\,\text{m/s}$, which corresponds to about 2% of the velocity in model 3m at $x = 900\,\text{m}$, at that height h_c. Hence, for a multi-layer model of the terrain considered in model 5.2, the vortices appearing after the first rough zone influence the final velocity by 2% of the velocity at the canopy height at $x = 650\,\text{m}$.

4.7 Comparison of all models

Plotting all the curves together at location $x = 650\,\text{m}$, we obtain Figure 21a. We choose this location since we then find ourselves sufficiently close to the boundary between the rougher and smoother zone (at 600m) to analyse and compare the effect of the vortices. At the same time, this location is sufficiently far to not directly be in the zone in which the vortices appear, as that may yield biased results.

Figure 21a shows us that for all three heterogeneous vegetated terrains considered, the multi-layer model always yields lower velocity at $x = 650\,\text{m}$ for heights $z \leq 10\,\text{m}$, compared to the single-layer approach for the same values of x and z. Figure 21b shows the percentage at which the velocity decreases per model. This tells us that in the multi-layer models, the velocity is decreased by a much higher factor than for single-layer models. Furthermore, when comparing models 5.1 and 5.2 with the terrain of three regions, model 3, we see that for single layer models the velocity is increased, whereas for multi-layer models it is decreased. The fact that the velocity is lower for five regions than for three under multi-layer can be explained by noting that in five regions we have two rough regions, which both produce vortices. Hence, the vortices accumulate and thus the velocity is decreased more in this case.

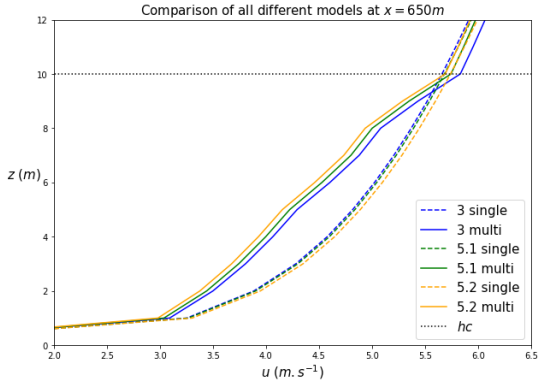

(a) Comparison of the velocity at $x = 650$.

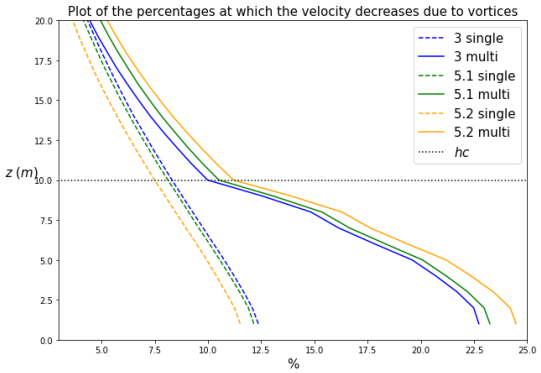

(b) Percentage of decrease in velocity.

Figure 21. Comparison of the velocity at $x = 650\,\text{m}$ and of the decrease in velocity due to the vortices between all the regions. The decrease in velocity due to the vortices is given as a percentage of the velocity at $x = 900\,\text{m}$.

This allows us to conclude two things, namely that the vortices render the terrain 'rougher', since the velocity is slowed down, and that when considering five regions the velocity is slower than for three. However, this difference is rather small. Indeed, by looking at Table 1, which presents the maximum difference in velocity between three and five regions at distance $x = 650\,\text{m}$, we see that this difference is not big enough to be of significance.

Models	3, 5.1 single	3, 5.1 multi	3, 5.2 single	3, 5.2 multi
Difference (m/s)	0.025	0.093	0.082	0.146

Table 1. Maximum difference in m/s of the output velocity at distance $x = 650\,\text{m}$ between three and five regions. This table is obtained by taking the absolute difference between the curves in Figure 21a, for single- and multi-layer simulations respectively, and extracting the maximum value over height.

We can see from Table 1 that for both of the 5 regions model, the single-layer approach yields a velocity that is closer to the 3 regions model. In other words, under multi-layer simulations, the vortices and the presence of the drag and countergradient forces (F_d, F_{cg}) propagate from the first rough region to the second. This then slows the wind flow more than in single-layer, where $F_d = F_{cg} = 0$.

5 Measured effective roughness length

In this section, we apply the methods for computing the effective roughness length, detailed in Section 3, in chronological order. For each method, we compare the output wind profile with that of the original heterogeneous terrain. We do so by considering a 1100m long terrain with roughness length corresponding to the ERL computed with the method in question.

The reason behind this extension of the terrain is that if we were to compare the output velocity of the effective terrain with the output of the original 900m long terrain, as sketched in Figure 22, we would find ourselves in a tricky situation. Indeed, the ERL is meant to be used in larger scale meteorological situations, and hence, at 900m we are 'too close' to the effective model (i.e. the model consisting of a single region with $z_0 = z_0^{\text{eff}}$) to properly compare it with the corresponding original simulation. Too close at the end of the heterogeneous vegetated terrain may yield biased results, since at $x = 900\,\text{m}$ the effective model is assumed to be rougher than the original one.

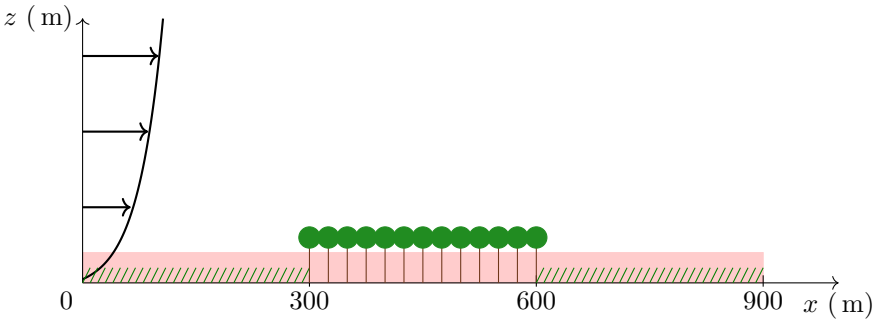

Figure 22. Sketch of the three region model and the corresponding effective model in red.

A sketch of the terrain with effective roughness length under extension is given in Figure 23, where the red block corresponds to the effective region, and the blue blocks correspond to the extensions. The extension must have a roughness length as low as possible, so as to not disturb the result. Note that the extension at the start of the terrain is for computational purposes, in order to allow the wind to properly flow over the region with roughness length corresponding to the ERL.

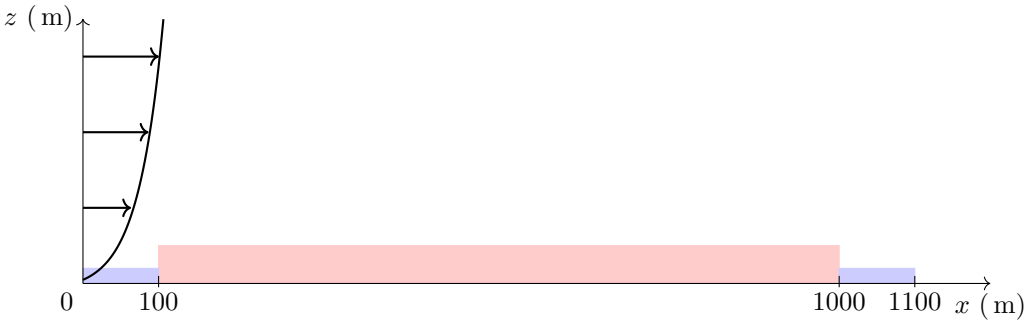

Figure 23. Sketch of the extended effective model.

We proceed similarly for the 'original' models, i.e. we extend the terrains by adding 100m at the start and at the end, each with roughness length $z_0 = 0.01\,\text{m}$. In all the figures presented in the following sections, we measure the output velocity at location $x = 1100\,\text{m}$ for both the original and the effective models.

5.1 André and Blondin's method

As detailed in Section 3.1, André and Blondin suggest that the effective roughness length depends on the first height level considered, and is given by:

$$\ln(z_0^{\text{eff}}) = \frac{\mu(\Delta)}{\int_\Delta \frac{dx}{\ln(z_0(x))-\ln(z_1)}} + \ln(z_1), \tag{5.1.1}$$

where Δ is the terrain considered, and $\mu(\Delta)$ is its length, z_1 is the first height level, and z_0 is the roughness length corresponding to each region. Recall that all our different models have the same proportion of grass and forest, namely 600m of grass and 300m of forest. Furthermore, by looking at the code, we see that the first height level is $z_1 = 1\,\text{m}$. This yields the effective roughness for all models:

$$\ln(z_0^{\text{eff}}) = \frac{900}{\frac{600}{\ln(0.03)} + \frac{300}{\ln(0.9)}} \implies z_0^{\text{eff}} = 0.742\,\text{m}. \tag{5.1.2}$$

However, as seen in Section 3.2, the dependency of the ERL on z_1 is not appropriate. Upon grid refinement, we would obtain different values of the first height level. Grid-refinement is further explained in Section 5.6.

z_1 (m)	1	1/2	1/4	1/8
z_0^{eff} (m)	0.742	10.339	$2.427 \cdot 10^{-9}$	0.004

Table 2. Effective roughness length per height level, following André and Blondin (5.1.1).

Table 2 shows different values of z_0^{eff} per height level z_1. From this table, we can first confirm that the dependencyof the effective roughness length on the first height level can yield inaccurate results, namely for $z_1 = 1/2$ and $z_1 = 1/4$, the effective roughness length resulting is either too big, or too small to be an accurate representation for any of our models. The results obtained at height levels $z_1 = 1$ and $z_1 = 1/8$ are in the range of what is expected, and hence these are the ones that we will focus on for verifying the accuracy of this ERL.

Comparing the original heterogeneous terrains with the two extended averaged models corresponding to the André-Blondin's formulas, taking $z_1 = 1$ or $z_1 = 1/8$, yields the plots in Figure 24.

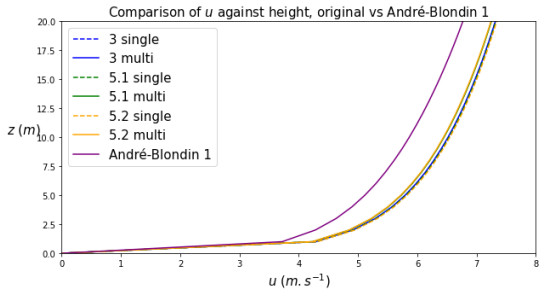

(a) Comparison between original and André-Blondin, for the first height level $z_1 = 1\,\text{m}$.

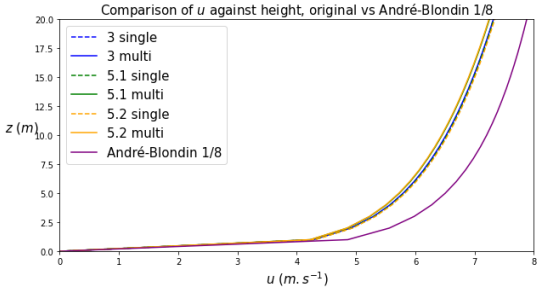

(b) Comparison between original and André-Blondin for the first height level $z_1 = 1/8\,\text{m}$.

Figure 24. Comparison of the output velocity, at $x = 1100\,\text{m}$, using the ERL of André and Blondin methods, with the velocity of each of the other models.

We see from this figure that for $z_1 = 1$ and for $z_1 = 1/8$, there is quite a large difference between the velocity output of the effective model, and that of the original model. To see this more clearly, we can plot the difference between the effective model and the original, as in Figure 25. The maximum error per method and per model is provided in Table 3.

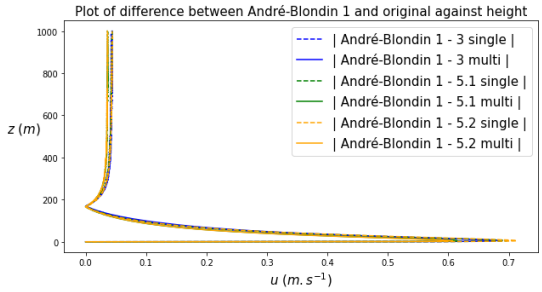

(a) Absolute difference between André-Blondin 1 and the original models.

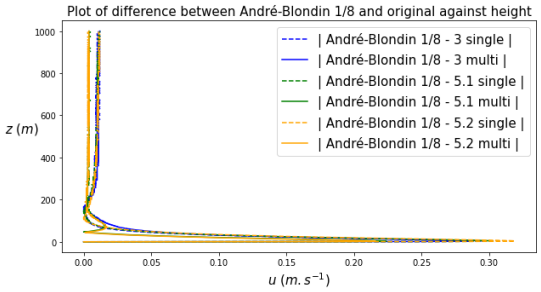

(b) Absolute difference between André-Blondin 1/8 and the original models.

Figure 25. Difference in velocity (in absolute value) between André-Blondin's formulas for the first height level $z_1 = \{1, 1/8\}$, and the original models, when considering the extended terrain, at $x = 1100\,\text{m}$.

Method \ Model	3 single	3 multi	5.1 single	5.1 multi	5.2 single	5.2 multi
AB 1	0.689	0.679	0.697	0.615	0.713	0.607
AB 1/8	0.703	0.712	0.694	0.777	0.678	0.786

Table 3. Maximum error in m/s of the output velocity between the effective and the original models, using André and Blondin's method, for two values of grid-refinement: 1 and 1/8.

5.2 Taylor's two methods

As detailed in Section 3.2, Taylor first suggests that the effective roughness length satisfies:

$$z_0^{\text{eff}} \approx z_0^m, \quad \text{where} \quad \ln(z_0^m) = \langle \ln(z_0) \rangle \,. \tag{5.2.1}$$

Hence, according to Taylor, this would mean that for all the different models studied here, we obtain the same effective roughness length, namely,

$$\ln(z_0^{\text{eff}}) = -2.37 \implies z_0^{\text{eff}} = 0.093\text{m}. \tag{5.2.2}$$

This result then corresponds to Taylor's first method for the effective roughness length. Taylor's second suggestion is that the ERL satisfies: $z_0^{\text{eff}} \approx z_0^a$, where

$$\ln(z_0^a) = \langle \ln(z_0) \rangle + a_1 \left(\langle \ln^2(z_0) \rangle - \langle \ln(z_0) \rangle^2 \right), \tag{5.2.3}$$

and

$$a_1 = \frac{F}{\kappa^2 V_g^2 / u_*^2 + F}, \qquad F = \ln\left(\frac{u_*}{V_g}\right) - B + \ln\left(\frac{V_g}{f z_0}\right). \tag{5.2.4}$$

In his paper, Taylor uses constant values for B, V_g and f given by:

$$V_g = 10\text{m/s}, \qquad f = 10^{-4}\text{s}^{-1}, \qquad B = 2. \tag{5.2.5}$$

We shall use the same values for our computations, and furthermore, $\kappa \approx 0.4$ is the von Kármán constant. Then, for model 3m we obtain the plot for the apparent roughness length z_0^a from equation (5.2.3) as given in Figure 26a. However, this figure is rather difficult to read. We note that all the different coloured lines correspond to different heights z and to different corresponding values of friction velocity u_*. In order to obtain a more readable graph, we take the 'running vertical average' of z_0^a from Figure 26a. This is plotted in Figure 26b. The running average is computed by summing all vertical over height and dividing by the number of vertical values.

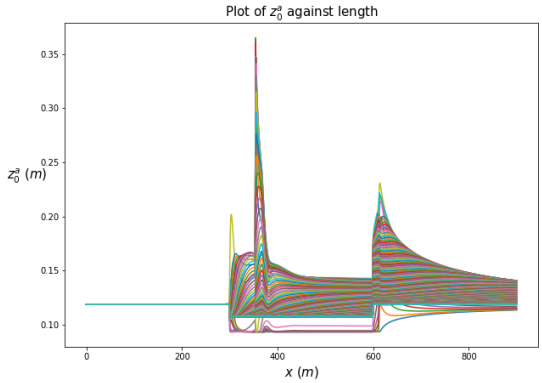

(a) Plot of z_0^a against x.

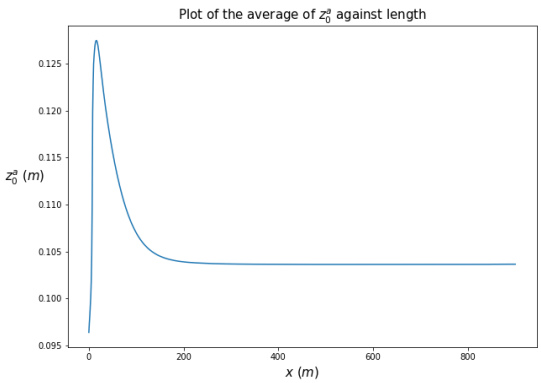

(b) Plot of the vertical average of Figure 3.

Figure 26. Plot of z_0^a and its vertical average over the length of the terrain, for model 3m.

Looking at Figure 26b, we see that after $x = 200$m, the apparent roughness length is approximatively constant, and equals $z_0^a = 0.104$. Proceeding similarly for all models, we obtain the values given in Table 4, where we note that the values given are rounded to 3 digits.

Model	3 single	3 multi	5.1 single	5.1 multi	5.2 single	5.2 multi
z_0^a (m)	0.104	0.104	0.104	0.104	0.104	0.104

Table 4. Values for the apparent roughness length z_0^a per model, rounded to three digits. This corresponds to Taylor's second method for the ERL, since $z_0^{\text{eff}} \approx z_0^a$.

Similarly as to what is done in the previous section, we verify the accuracy of Taylor's effective roughness length. This is shown in Figure 27.

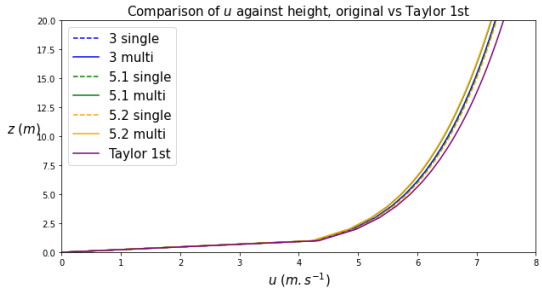

(a) Comparison between original models and Taylor 1st.

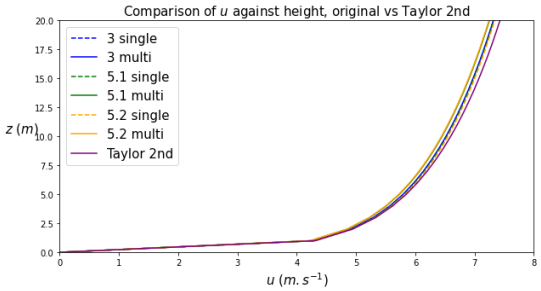

(b) Comparison between original models and Taylor 2nd.

Figure 27. Comparison of the output velocity of Taylor's 1st and 2nd methods with the velocity of each of the other models, at $x = 1100$m.

As can be seen from Figure 27, the effective model corresponding to Taylor 1st and 2nd methods yields an output velocity that is very close to the output velocity corresponding to our original models (with 100m extension). The plots representing the difference between Taylor's models and each original model are given in Figure 28. The maximum error in the plots are given in Table 5.

Comparing with Table 3, which displays the maximum error using André and Blondin's methods, we see that Taylor's effective roughness lengths always yield a smaller error. Hence, Taylor's ERL is indeed more accurate than the ERL of André and Blondin. To further check the quality of Taylor's effective roughness length, we study the ERL derived by de Vries et al in the next section.

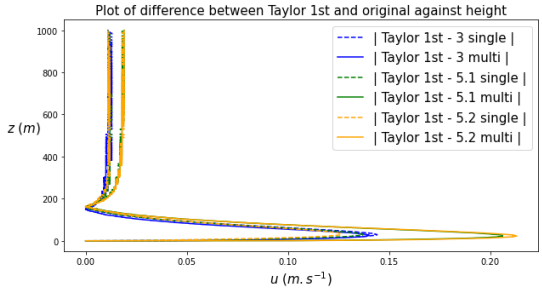

(a) Absolute difference between Taylor 1st and the original models.

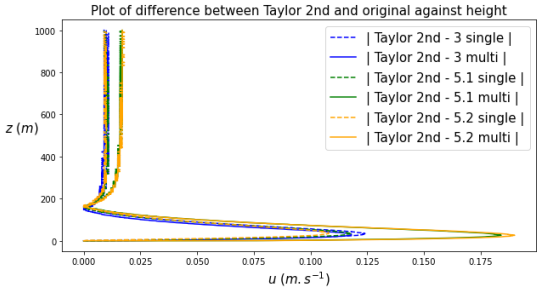

(b) Absolute difference between Taylor 2nd and the original models.

Figure 28. Difference in absolute value between Taylor's 1st and 2nd methods and each original models, when considering the extended terrain, at $x = 1100$m.

Method \ Model	3 single	3 multi	5.1 single	5.1 multi	5.2 single	5.2 multi
Taylor 1st	0.144	0.140	0.137	0.206	0.126	0.213
Taylor 2nd	0.124	0.118	0.118	0.184	0.108	0.190

Table 5. Maximum error in m/s of the output velocity between the effective and the original models, using Taylor's methods.

5.3 De Vries et al.'s method

From Section 3.3, we have a formula for the effective roughness length given by de Vries et al.:

$$z_0^{\text{eff}} = \frac{H}{2} \exp\left\{ -\frac{\kappa}{\left[0.5 C_d \lambda + \frac{\kappa^2}{\ln^2(H/2z_{01})}\right]^{1/2}} \right\}. \tag{5.3.1}$$

To find the average obstacle height, we recall that the canopy height was given to be $h_c = 10\,\text{m}$, and thus,

$$H = 10\,\text{m}. \tag{5.3.2}$$

We use the same value for the drag coefficient as de Vries et al., which is $C_d = 0.3$. However, for the roughness length of the smoothest region, z_{01}, we do not use the same value. In fact, we use $z_{01} = 0.03\,\text{m}$, which corresponds to the roughness length for the smoothest region in our models. λ corresponds to the density of the roughness elements, and for two dimensional models it can be approximated via $\lambda \approx H/L$, and $\kappa \approx 0.4$ is the von Kármán constant.

In their paper, de Vries et al. consider the distance L between the middle of two obstacles. Note that, for the three regions model, we only have a single obstacle, which would yield $L = 0$. To overcome this, we write L as a function of δ, where δ denotes the space in between the two forests in the five regions model. Then, for the three regions model, we can take the limit $\delta \to 0$ to find L. Looking at how the five regions model is defined, we see that setting δ as the distance between the to forests gives:

$$L(\delta) = 150 + \delta, \tag{5.3.3}$$

and so, for $\delta = 100\,\text{m}$, we obtain $L(100) = 250\,\text{m}$, which thus corresponds to the distance between the two obstacles for both of the five regions models. For the tree regions model, we take the limit $\delta \to 0$, which yields $L(0) = 150\,\text{m}$.

Using all of this, we can compute the effective roughness length for the various heterogeneous vegetated terrains we have. The results per model are given in Table 6.

We see that this method yields the same effective roughness length for both of the five regions models, while slightly different for the three regions one. This is due to the fact that in the five

Model	model 3	model 5.1	model 5.2
z_0^{eff} (m)	0.214	0.132	0.132

Table 6. Effective roughness length per model, following de Vries et al.'s method.

region model we have a larger distance between the two obstacles than in the three region model.

Comparing the effective model resulting from this ERL with the original models yields Figure 29.

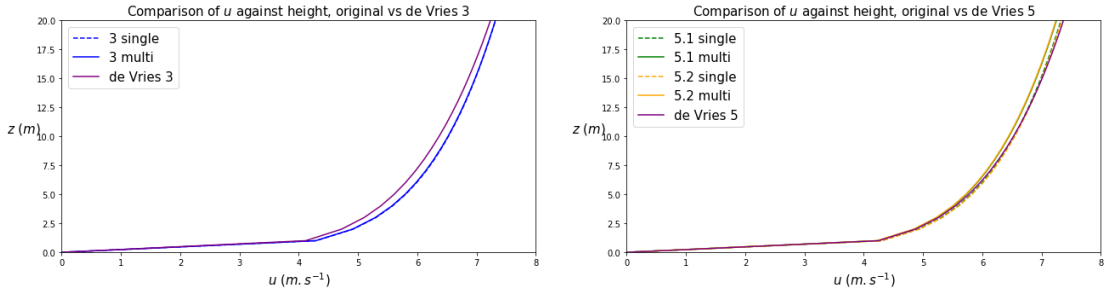

(a) Comparison between original models and de Vries, for 3 regions.

(b) Comparison between original models and de Vries, for 5 regions.

Figure 29. Comparison of the output velocity of de Vries et al.'s method with each of the original models, for three and five regions, at $x = 1100\,\text{m}$.

From these plots, we notice that the effective model from de Vries et. al yields an output velocity that is very similar to that of our original models. To see this more clearly, the error is plotted in Figure 30, and the maximum error per model is given in Table 7.

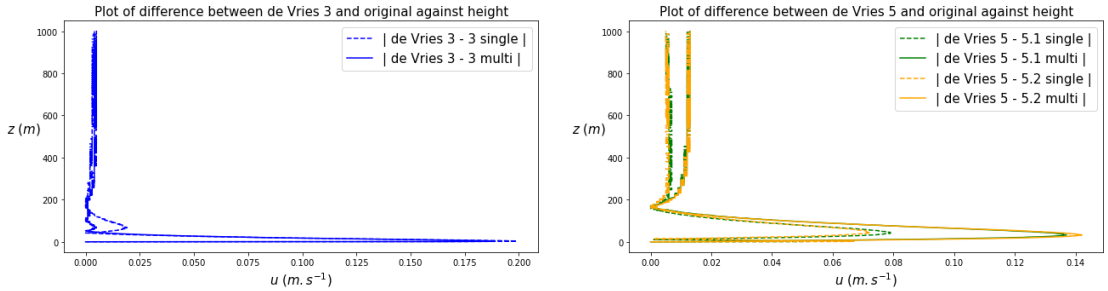

(a) Absolute difference between original models and de Vries, for 3 regions.

(b) Absolute difference between original models and de Vries, for 5 regions.

Figure 30. Plots of the difference in absolute value between de Vries et al.'s method and each original model, when considering the extended terrain, at $x = 1100\,\text{m}$.

Comparing the errors for the ERL of de Vries et al. with that of André and Blondin and Taylor, we can conclude that the former yields the best results for five regions, and rather good results for three regions. The fact that this method is less accurate for three regions could be expected, since their research was more focused on the influence of multiple rough regions on the effective roughness length. This also follows from the fact that the distance L between two obstacles is not well defined for 3 regions.

We have computed the output velocity for three methods of effective roughness length, and compared them with each of the original model. The ERLs used thus far were given in existing papers and relied, one way or another, on the logarithmic wind profile. However, none of the methods extracted the roughness length from this logarithmic equation directly. Therefore, this is the approach considered in the following section.

Model	3 single	3 multi	5.1 single	5. multi	5.2 single	5.2 multi
Error (m/s)	0.199	0.189	0.079	0.137	0.072	0.142

Table 7. Maximum error in $m \cdot s^{-1}$ of the output velocity between the effective and the original models, using de Vries et al.'s method.

5.4 'Averaged' ERL using the logarithmic law

To compute the average roughness length by taking into account the effect of the vortices, we turn to the logarithmic law (given in equation (1.1.1)). This law relies on the horizontal velocity u and the friction velocity u_*, which both depend on vortices. Using the logarithmic law, we can extract the roughness length z_0. Namely,

$$u = \frac{u_*}{\kappa}(\ln z - \ln z_0) \implies z_0 = \exp\left\{\ln z - \frac{u\kappa}{u_*}\right\}. \tag{5.4.1}$$

In particular, when considering height values $z = 2$ and $z = 15$, we obtain the plots given in Figure 31.

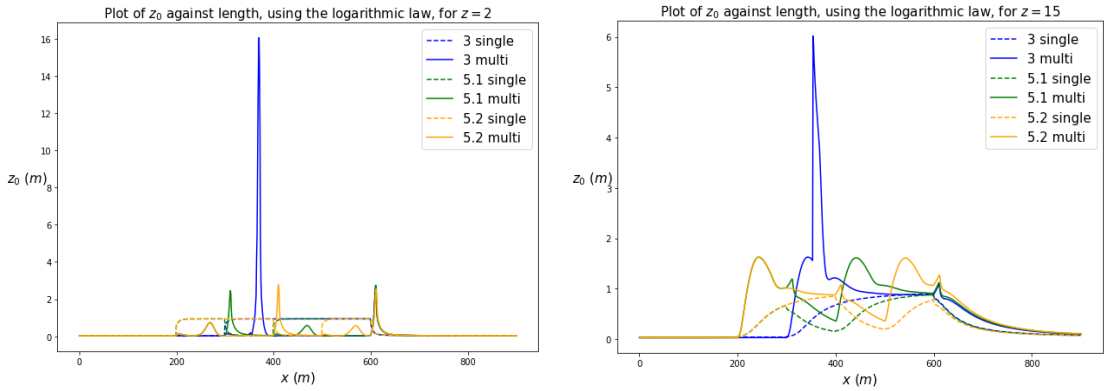

(a) When considering $z = 2\,\text{m}$.

(b) When considering $z = 15\,\text{m}$.

Figure 31. Plot of z_0 against the location in the terrain for the different models, considering heights $z = 2\,\text{m}$ and $z = 15\,\text{m}$ in the logarithmic law (5.4.1).

In both cases, for $z = 2$ and $z = 15$, all the single-layer models display roughness lengths corresponding to the initial z_0 that was set, i.e. 0.03 for smoother regions and 0.9 for the rougher ones. This can be explained by recalling that in single-layer modelling we simply suppose that both the rough and the smooth regions are modeled by a single layer, and that, as seen above in Figure 21b, the influence of the vortices on the velocity was much lower for single-layer than for multi-layer models. Thus, using the logarithmic law to extract z_0 yields values that are close to those that were the initial input of the code.

Furthermore, we can see spikes in the values of z_0 in particular at $x = 600$ for all the multi-layer models (the blue line is 'hidden' by the green and the yellow ones in the plot for $z = 2$, but it is indeed there), and at $x = 300$ for the first model of 5 multi-layer regions, and at $x = 400$ for the second ones. Those spikes can probably be explained by the presence of the vortices that appear after the rougher regions, as the above values of x correspond to the end of the forest. The bumps can be explained by the fact that the wind enters the forest, leading to a decrease in velocity and thus an increase in surface roughness.

In the results for $z = 15$, we note the presence of 'bumps', which correspond do the start of the rougher zones. These bumps can be explained by the fact that the wind enters the forest, leading to a decrease in velocity and thus an increase in surface roughness. The spikes mentioned previously are still present, at the positions at which the forest ends. This is consistent with real-life observations.

We also have a spike for the 3 multi-layer regions model at $x = 369$, which seems to appear in the middle of a forest region. This may be due to the grid size. To check this, we apply grid refinement to our simulations, for model 3m, which is further detailed in Section 5.6. Figure 32 shows an example of grid refinement for three regions, for height values of $z = 2\,\text{m}$ and $z = 15\,\text{m}$.

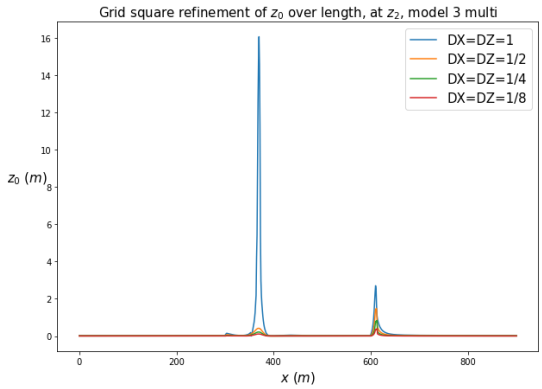

(a) Refining the grid-square by a half, a quarter, and an eighth, at $z = 2$.

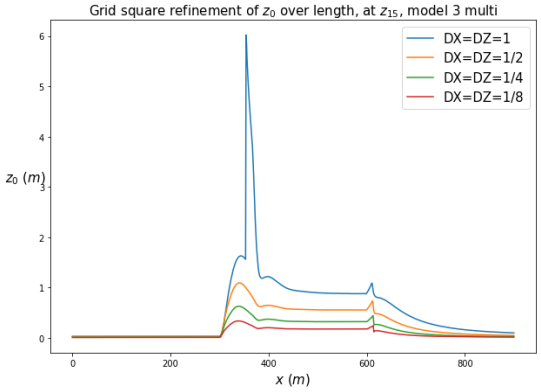

(b) Refining the grid-square by a half, a quarter, and an eighth, at $z = 15$.

Figure 32. Grid refinement done by dividing the grid size by 2,4, and 8, for the model 3m case, also discussed in Figure 31.

Using the grid-refinement for model 3m, we can compute the average roughness length per model, by summing all the values and dividing by the number of them, which is given in Table 8. For the other models, we simply use the original grid, without refinement, to save computation time.

Model / z (m)	3 single	3 multi	5.1 single	5.1 multi	5.2 single	5.2 multi
$z = 2$	0.340	0.079	0.343	0.120	0.343	0.120
$z = 3$	0.346	0.082	0.349	0.132	0.349	0.133
$z = 4$	0.348	0.107	0.352	0.169	0.352	0.171
$z = 5$	0.349	0.338	0.352	0.367	0.352	0.369
$z = 6$	0.348	0.618	0.350	0.621	0.351	0.624
$z = 7$	0.346	0.857	0.348	0.906	0.348	0.908
$z = 8$	0.343	1.018	0.344	1.137	0.344	1.139
$z = 9$	0.340	0.661	0.338	0.800	0.339	0.802
$z = 10$	0.336	0.472	0.333	0.594	0.334	0.596
$z = 11$	0.332	0.492	0.327	0.593	0.329	0.595
$z = 12$	0.327	0.510	0.321	0.589	0.323	0.592
$z = 13$	0.322	0.525	0.315	0.585	0.317	0.587
$z = 14$	0.317	0.538	0.309	0.579	0.311	0.581
$z = 15$	0.312	0.545	0.303	0.571	0.305	0.574
$z = 16$	0.306	0.560	0.296	0.563	0.298	0.566
$z = 17$	0.301	0.569	0.290	0.554	0.292	0.557
$z = 18$	0.295	0.576	0.284	0.544	0.286	0547
$z = 19$	0.290	0.582	0.278	0.534	0.280	0.537
$z = 20$	0.284	0.587	0.272	0.523	0.274	0.526
Average	0.325	0.511	0.322	0.504	0.323	0.534

Table 8. Average roughness length per model, using the logarithmic law, for different height values z, where the averaged value for model 3m is computed under grid refinement. Computing the average of each column yields the last row of the table.

Note that for height values above $z = 10$, we find ourselves above the canopy height h_c. At the top of the trees, there is still friction present, and the vortices still have influence on the wind

flow. Looking at Figure 21b, we see that the velocity decreases due to the presence of vortices (and of forces F_d, F_{cg} for the multi-layer approach) for heights up to about $z = 20\,\text{m}$. Hence, in Table 8, we only interest ourselves to values of $2 \leq z \leq 20$. Note that we do not consider the first height level, i.e. z_1 or $z = 1$, since this level is directly dependent on the lower boundary conditions, which themselves depend on a system of seven equations in seven unknowns. This would yield inaccurate results, as we obtain a peak for the first height level, as detailed in Section 5.6 on grid refinement.

The comparison between the effective model obtained using the last row of Table 8 and the original models is given in Figure 33. We notice a rather considerable difference between the velocity output for the effective model and that of the corresponding original model. The error corresponding to each graph is plotted in Figure 34, and the maximum error per model is provided in Table 9.

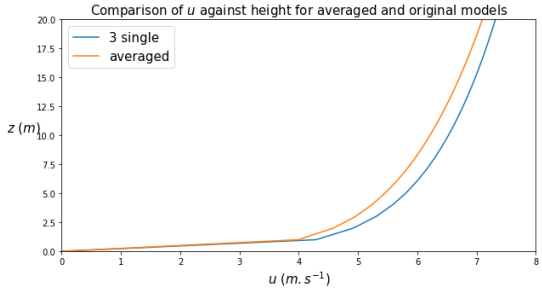

(a) Comparison between averaged model and model 3s.

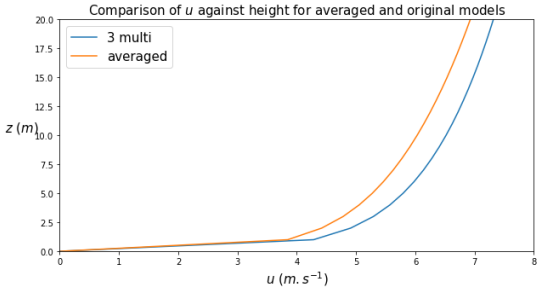

(b) Comparison between averaged model and model 3m.

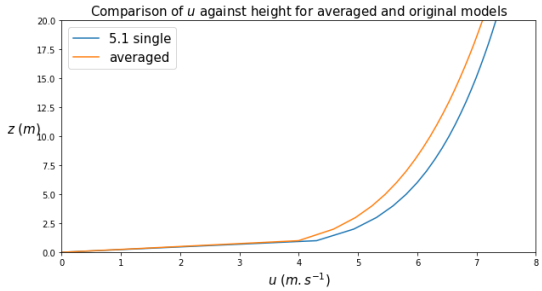

(c) Comparison between averaged model and model 5.1s.

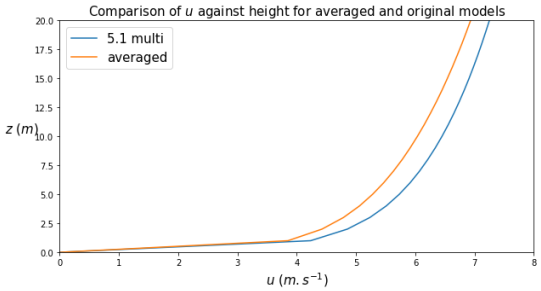

(d) Comparison between averaged model and model 5.1m.

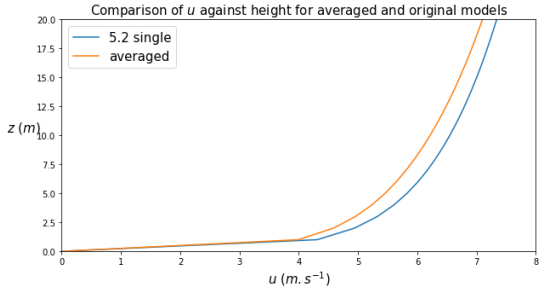

(e) Comparison between averaged model and model 5.2s.

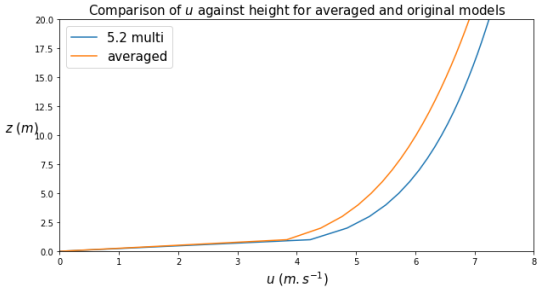

(f) Comparison between averaged model and model 5.2m.

Figure 33. Comparison between the averaged model and each corresponding model, for the extended terrains, at $x = 1100\,\text{m}$, zoomed to match the canopy height $h_c = 10\,\text{m}$.

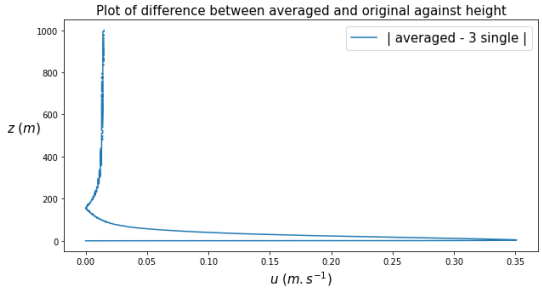

(a) Absolute difference between averaged model and model 3s.

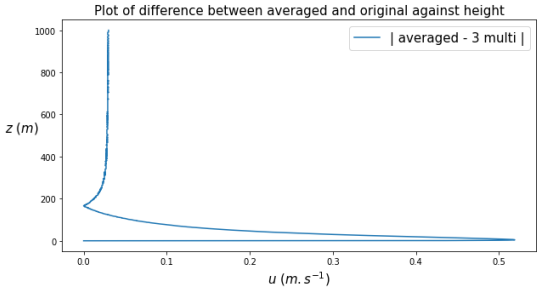

(b) Absolute difference between averaged model and model 3m.

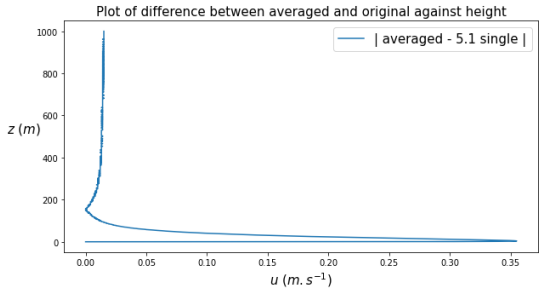

(c) Absolute difference between averaged model and model 5.1s.

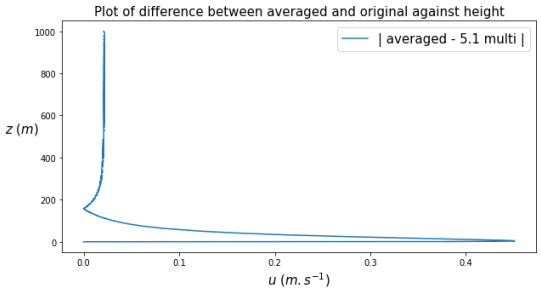

(d) Absolute difference between averaged model and model 5.1m.

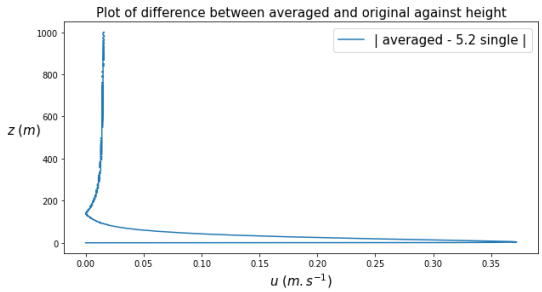

(e) Absolute difference between averaged model and model 5.2s.

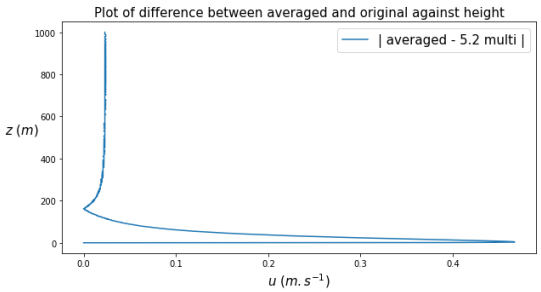

(f) Absolute difference between averaged model and model 5.2m.

Figure 34. Plots of the difference in absolute value between the averaged model and each corresponding model, for the extended terrains, at $x = 1100\,\mathrm{m}$.

Model	3 single	3 multi	5.1 single	5.1 multi	5.2 single	5.2 multi
Error (m/s)	0.351	0.519	0.355	0.451	0.372	0.467

Table 9. Maximum error in m/s of the output velocity between the effective and the original models, using the 'averaged' method.

From this, we note that the averaged method also yields rather inaccurate results, since the error is still much greater than for Taylor's method. To this end, we may ask ourselves if this method can be improved. And the answer to that question is yes; one can indeed improve the accuracy of the effective roughness length extracted from the logarithmic law. This is further explained below.

5.5 Improvement of the 'averaged' ERL

In the previous section, we extract an 'averaged' roughness length from the logarithmic law, i.e.,

$$u(z) = \frac{u_*}{\kappa} \ln\left(\frac{z}{z_0}\right), \tag{5.5.1}$$

where u_* is the friction velocity, κ is the von Kármán constant. We computed the average for various height levels z, where $2 \leq z \leq 20$. Through the years, there have been quite a few different equations for the logarithmic wind profile, e.g. (5.5.1), or

$$u(z) = \frac{u_*}{\kappa} \ln\left(\frac{z - d_0}{z_0}\right), \tag{5.5.2}$$

where d_0 is the displacement height. This formula is used by de Vries et al. (2003) when computing the ERL. The displacement height is the height at which the wind begins to behave in a logarithmic manner. It can be related to the density of the roughness obstacles via the following:

$$d_0 = d\lambda^e H, \tag{5.5.3}$$

where H is the average obstacle height and λ is the density of the roughness elements. We can approximate $\lambda \approx A/S$, where A is the average silhouette area of the roughness elements in a horizontal area S. For two-dimensional obstacles, A/S can be simplified to H/L, where L is the distance between obstacles. d and e are constants, given by $d = 1.09$ and $e = 0.29$, and we require λ to be in the range $0.09 < \lambda < 0.18$.

Recall from Section 5.3, the average obstacle height for our models is $H = 5\,\text{m}$, and the distance between two obstacles is given by:

$$L = \begin{cases} 150\,\text{m}, & \text{for three regions,} \\ 250\,\text{m}, & \text{for five regions.} \end{cases} \tag{5.5.4}$$

Then, for three regions we obtain the displacement height of $d_0 = 2.033\,\text{m}$. Similarly, for five regions we obtain: $d_0 = 1.753\,\text{m}$. Extracting the roughness length from the logarithmic law by de Vries et al. (5.5.2) yields

$$\ln(z_0) = \ln(z - d_0) - \frac{u(z)\kappa}{u_*}. \tag{5.5.5}$$

The plots of z_0 against the location in the terrain are given in Figure 35 for heights $z = \{3, 15\}$. Note that, due to the presence of the displacement height, we cannot consider heights $z \leq 2$.

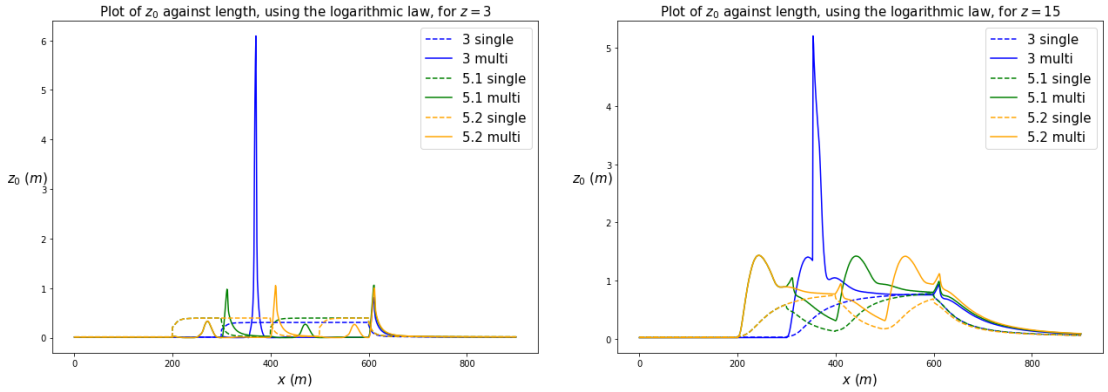

(a) When considering $z = 3\,\text{m}$.

(b) When considering $z = 15\,\text{m}$.

Figure 35. Plot of z_0 against the location in the terrain for the different models, considering heights $z = 3\,\text{m}$ and $z = 15\,\text{m}$ in the logarithmic law (5.5.5).

Again, similar to the roughness length extracted from the logarithmic law *without* the dis-

placement height in Figure 31, there is an unwanted peak for the three regions multi-layer model. To make the curve smoother and get rid of the peak, we apply grid-refinement, as detailed in Section 5.6. This yields the average of z_0 for heights $3 \leq z \leq 20$ for the various models as given in Table 10.

Model / z (m)	3 single	3 multi	5.1 single	5.1 multi	5.2 single	5.2 multi
$z = 3$	0.111	0.062	0.145	0.055	0.145	0.055
$z = 4$	0.171	0.099	0.198	0.095	0.198	0.096
$z = 5$	0.207	0.242	0.229	0.238	0.229	0.24
$z = 6$	0.23	0.403	0.248	0.44	0.248	0.442
$z = 7$	0.245	0.602	0.26	0.679	0.261	0.681
$z = 8$	0.256	0.776	0.268	0.888	0.269	0.889
$z = 9$	0.263	0.571	0.273	0.644	0.273	0.646
$z = 10$	0.268	0.434	0.275	0.49	0.275	0.492
$z = 11$	0.27	0.443	0.275	0.498	0.276	0.5
$z = 12$	0.272	0.45	0.274	0.503	0.276	0.505
$z = 13$	0.272	0.454	0.273	0.506	0.274	0.508
$z = 14$	0.271	0.457	0.27	0.506	0.272	0.509
$z = 15$	0.27	0.457	0.267	0.505	0.269	0.507
$z = 16$	0.268	0.455	0.264	0.501	0.266	0.504
$z = 17$	0.265	0.451	0.26	0.497	0.262	0.499
$z = 18$	0.262	0.446	0.256	0.491	0.258	0.494
$z = 19$	0.259	0.44	0.252	0.484	0.254	0.487
$z = 20$	0.255	0.432	0.248	0.477	0.25	0.48
Average	0.245	0.426	0.252	0.471	0.238	0.522

Table 10. Average roughness length per model, using the logarithmic law (5.5.5), for different height values z, where the averaged value for 3 multi-layer regions is computed under grid refinement. Computing the average of each column yields the last row of the table.

Using the values given in the last row of the table, i.e. the 'averaged' values, we can compare the output wind profile for that model with the one for the original model. Figure 36 shows the comparison between each original model and the two corresponding averaged models. Note that the orange line corresponds to the 'first' averaged method, and the green line to the 'second', where the second is computed using the logarithmic law which includes the displacement height d_0 (5.5.5).

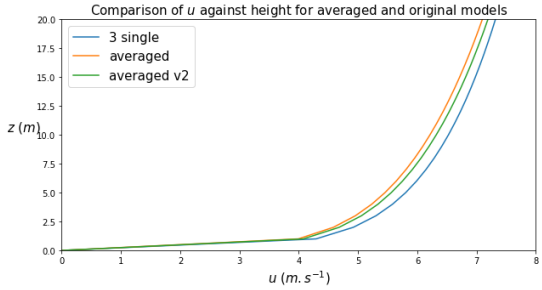

(a) Comparison between averaged models and model 3s.

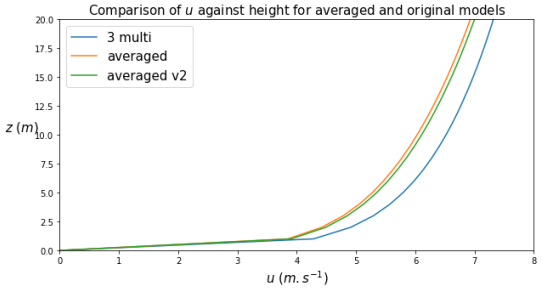

(b) Comparison between averaged models and model 3m.

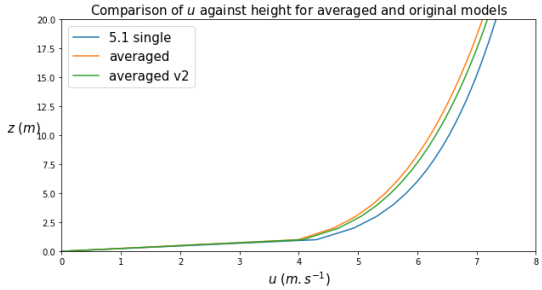

(c) Comparison between averaged models and model 5.1s.

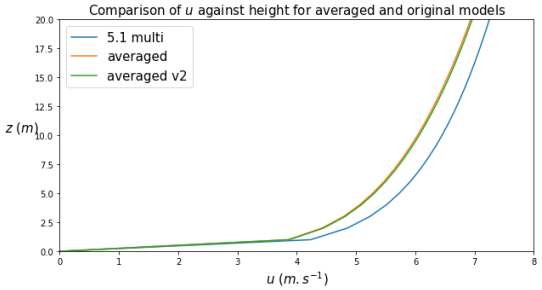

(d) Comparison between averaged models and model 5.1m.

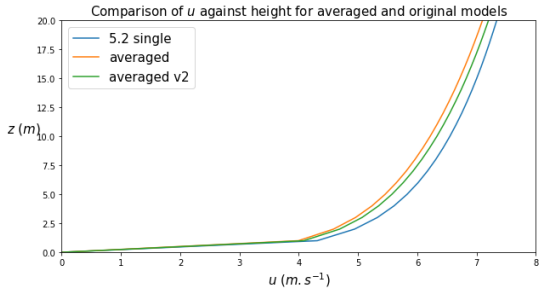

(e) Comparison between averaged models and model 5.2s.

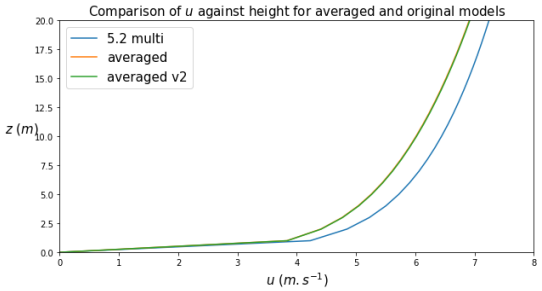

(f) Comparison between averaged models and model 5.2m.

Figure 36. Comparison between the first and the second averaged model, which takes into account the displacement height d_0, for the extended terrains, at $x = 1100\,\mathrm{m}$.

We see from these plots that for most of the models, namely three regions (both single- and multi-layer) and for five regions in single-layer (regardless of which region of forest is first), the roughness length extracted from the logarithmic law with displacement height yields more accurate results than without. However, for five regions in multi-layer, the results are the same. Plotting the error between the averaged models and the original models yields Figure 37. The maximum error per model and per method, where we compare the two 'averaged' methods, is given in Table 11.

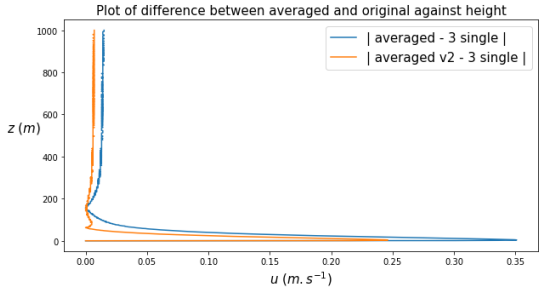

(a) Absolute difference between averaged models and model 3s.

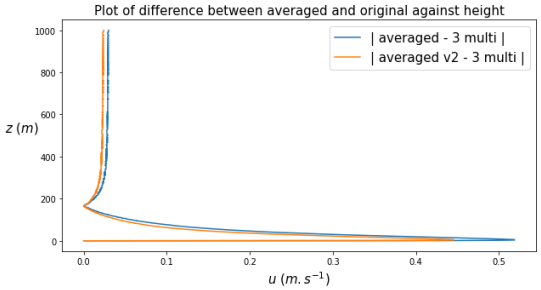

(b) Absolute difference between averaged models and model 3m.

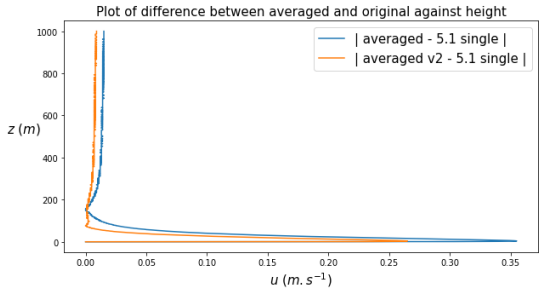

(c) Absolute difference between averaged models and model 5.1s.

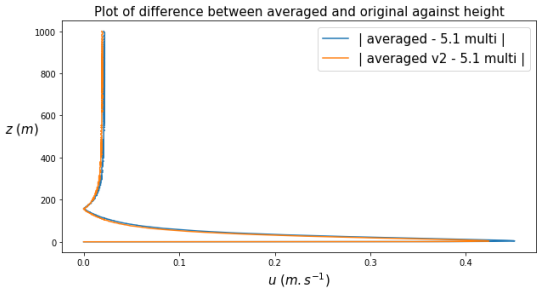

(d) Absolute difference between averaged models and model 5.1m.

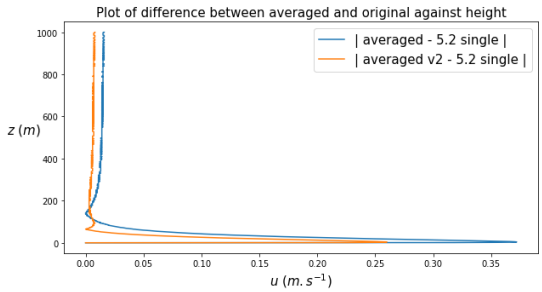

(e) Absolute difference between averaged models and model 5.2s.

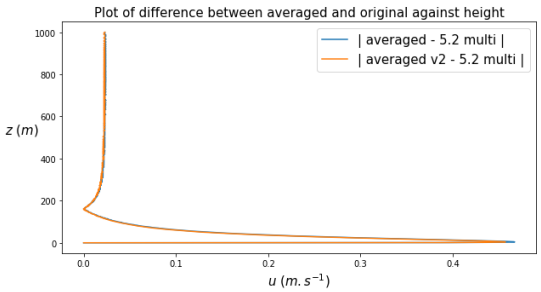

(f) Absolute difference between averaged models and model 5.2m.

Figure 37. Plots of the difference in absolute value between the first averaged model and the second, which includes the displacement height d_0, for the extended terrains, at $x = 1100$ m.

Method \ Model	3 single	3 multi	5.1 single	5.1 multi	5.2 single	5.2 multi
Averaged 1	0.351	0.519	0.355	0.451	0.372	0.467
Averaged 2	0.246	0.445	0.265	0.424	0.260	0.457

Table 11. Maximum error in m/s of the output velocity between the first and second averaged models and the original model, when considering the extended terrain, per model and per method of effective roughness length.

Including the displacement height d_0 in the logarithmic law clearly yields more accurate results. However, when comparing with the maximum error for Taylor's second method as given in Table 5, we see that the latter still yields more accurate results. Hence, our 'improved averaged' roughness length using the logarithmic law and including the displacement height is not the most representative for any of our terrains.

5.6 Grid-refinement

In this section, we look at refining the grid considered for all six original models. We first look at grid-refinement for the three regions multi-layer model, specifically used to overcome the pike appearing when extracting the roughness length from the logarithmic law, as discussed in Section 5.4. Grid refinement is a tool used in simulations to yield more accurate and precise results. This method consists in reducing the size of each grid-cell in the Cartesian plane, until we see no difference in the output between two consecutive refinements.

The initial grid is defined by $DX = DZ = 1$, and we begin by dividing it in two, i.e. we set $DX = DZ = 0.5$. This means that we thus have to double the total number of gridpoints. We may also change the initial parameters for the leaf area density in the multi layer model. The result is provided in Figure 38 for three height levels of z. Note that we consider the ERL extracted from the logarithmic law without displacement height (5.4.1).

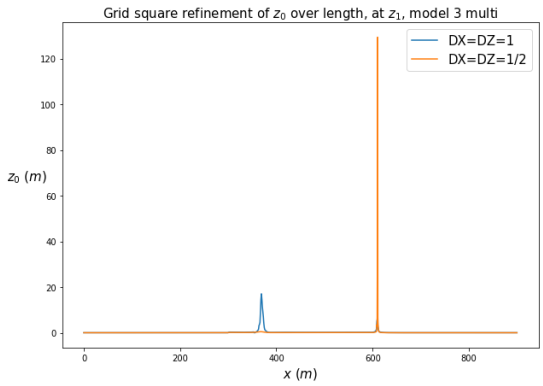

(a) Refining the grid-size by a half, at the first height level.

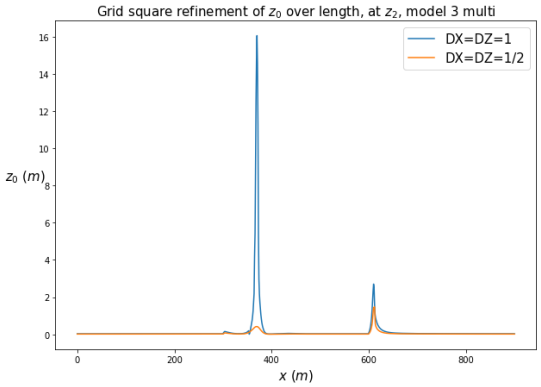

(b) Refining the grid-cell by a half, at the second height level.

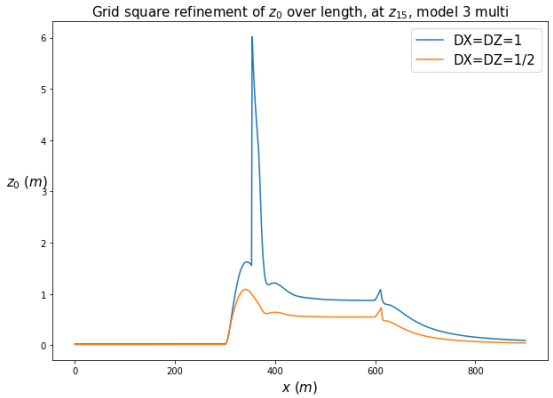

(c) Refining the grid-size by a half, at the fifteenth height level.

Figure 38. Grid refinement done by dividing the grid-size by 2 for model 3m from Figure 31, for various height levels z.

Under the grid refinement, we notice that the peak at $x = 369$ vanishes. However, for $z_1 = 1/2$ the first height level, we note the presence of another peak in the grid-refined curve at $x = 610$. This peak is coherent with the presence of vortices, but its magnitude is unexpected. The peak for the first height level z_1 disappears in the second height level z_2, which is due to the lower boundary conditions dependent on a system of seven equations with seven unknowns (Luppes, 1993, Chapter 3), which directly affect the first level. For the second level, the results depends on the Navier-Stokes equations, and are only indirectly influenced by the lower boundary conditions. Thus, from this point onward, we do not consider the first height level z_1 anymore.

On the plots for $z = 2$ and $z = 15$ we do not have any surprising peaks, and the bump signalling the start of the rough zone is indeed present. Furthermore, we note a quite significant difference between the original grid and the refined grid for a half. Hence we require further grid refinement. In other words, we set $DX = DZ = 0.25$, which gives the plot in Figure 39.

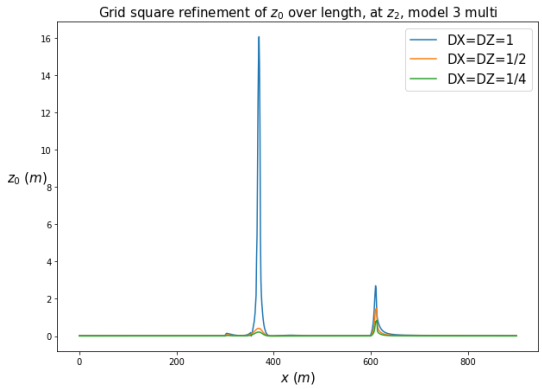

(a) Refining the grid-size by a quarter, at the second height level.

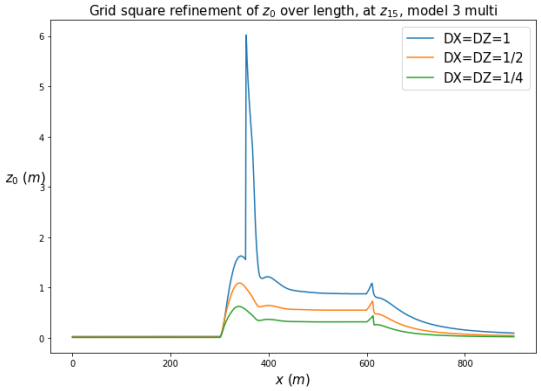

(b) Refining the grid-size by a quarter, at the fifteenth height level.

Figure 39. Grid refinement done by dividing the original grid-size by 4 for model 3m from Figure 31, for the second and the fifteenth height levels.

From this additional grid-refinement, we note that there is still a difference between the curve for half grid-cell refinement, and quarter grid-cell refinement. Therefore, we half the grid-cell size once again which is provided in Figure 40.

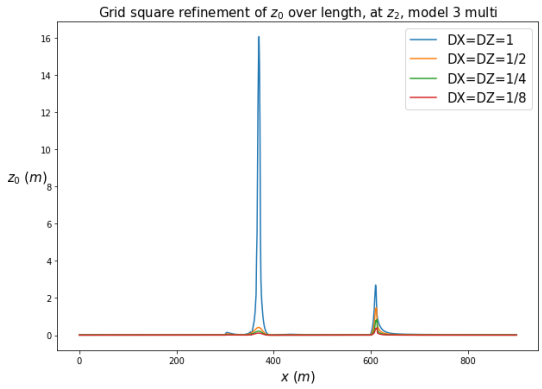

(a) Refining the grid-size by an eighth, at the second level.

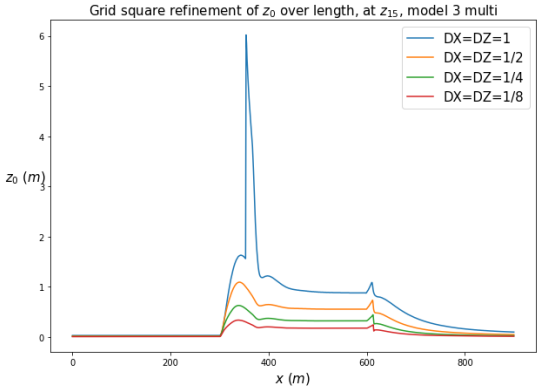

(b) Refining the grid-size by an eighth, at the fifteenth level.

Figure 40. Grid refinement done by dividing the original grid-size by 8 for model 3m from Figure 31, for the second and the fifteenth height levels.

The curve for the 1/8 grid is similar to that for 1/4, but we still note a slight difference. Hence, we aim to further apply grid refinement to 1/16. However, such a grid refinement requires a large memory capacity, thus it is not done here and left as a recommendation.

5.7 Most accurate effective roughness length

We have studied five methods for computing an effective roughness length, given by:

- *André and Blondin*:
$$\ln(z_0^{\text{eff}}) = \frac{\mu(\Delta)}{\int_\Delta \frac{dx}{\ln(z_0)-\ln(z_1)}} - \ln(z_1); \tag{5.7.1}$$

- *Taylor*:
$$\ln(z_0^{\text{eff}}) = \langle \ln(z_0) \rangle \,, \tag{5.7.2}$$
$$\ln(z_0^{\text{eff}}) = \langle \ln(z_0) \rangle + a_1 \left(\langle \ln^2(z_0) \rangle - \langle \ln(z_0) \rangle^2 \right), \tag{5.7.3}$$
where $a_1 = \frac{F}{\kappa^2 V_g^2/u_*^2+F}$ and $F = \ln(u_*/V_g) - B + \ln(V_g/f z_0)$;

- *de Vries et al.*:
$$z_0^{\text{eff}} = \frac{H}{2} \exp\left\{ - \left[\frac{2\kappa}{C_d \lambda + \frac{\kappa^2}{\ln^2(H/2z_{01}}} \right] \right\}; \tag{5.7.4}$$

- *averaged*:
$$z_0^{\text{eff}} = \left\langle (z-d_0) \exp\left\{ -\frac{u(z)\kappa}{u_*} \right\} \right\rangle. \tag{5.7.5}$$

These methods give the ERL per model as in Table 12.

Method \ Model	3 single	3 multi	5.1 single	5.1 multi	5.2 single	5.2 multi
AB 1	0.742	0.742	0.742	0.742	0.742	0.742
AB 1/8	0.004	0.004	0.004	0.004	0.004	0.004
Taylor, 1st	0.093	0.093	0.093	0.093	0.093	0.093
Taylor, 2nd	0.104	0.104	0.104	0.104	0.104	0.104
de Vries	0.03	0.03	0.01	0.01	0.01	0.01
Averaged	0.325	0.511	0.322	0.504	0.323	0.534

Table 12. Recapitulation of all effective roughness lengths z_0^{eff} (m) obtained, per model and per method.

For each method, we compared the output velocity with that of the original model, and computed the maximum error. A recapitulation of those errors per model and per method is given in Table 13.

Method \ Model	3 single	3 multi	5.1 single	5.1 multi	5.2 single	5.2 multi
AB 1	0.689	0.679	0.697	0.615	0.713	0.607
AB 1/8	0.703	0.712	0.694	0.777	0.678	0.786
Taylor 1st	0.144	0.140	0.137	0.206	0.126	0.213
Taylor 2nd	0.124	0.118	0.118	0.184	0.108	0.190
de Vries	0.199	0.189	0.079	0.137	0.072	0.142
Averaged	0.351	0.519	0.355	0.451	0.372	0.467

Table 13. Maximum error in m/s of the output velocity between the effective model and the original model, when considering the extended terrain, per model and per method.

This table allows us to conclude that the most accurate ERL for the three regions models is the one given by Taylor (5.7.3). On the other hand, for five regions models, and thus models with multiple rough terrains, the most accurate ERL is the one given by de Vries et al. (5.7.4).

6 Conclusions and recommendations

We began this thesis by looking at the equations modelling two-dimensional atmospheric flow, namely the Navier-Stokes equations for stationary, two dimensional, incompressible, viscous flow. We then detailed the equations specific to each of the two surface types described by Klaassen (1992): single- and multi-layer, and finally we gave the boundary conditions for our model, following the system of seven equations in seven unknowns given by Luppes (1993).

After deriving the equations underlining our model, we looked at the main problem of this thesis: finding an average roughness length. We reviewed three already existing methods: André & Blondin (1986), Taylor (1987), and de Vries et al. (2003), where we derived the equations for the effective roughness length z_0^{eff} detailed in each paper. This lead to comparison in order to determine which was the most accurate method for three given terrain types.

In this thesis we have looked at two homogeneous regions: grassland and forest. To study these regions, we considered 300m of forest and 600m of grass, under three dispositions. In this way, we created a 3 regions model and two 5 regions models, where we alternated 100m and 200m of forest for the first rough region. These three dispositions are thus the three given terrain types considered throughout this study. We ran simulations for each of the models, under both single- and multi- layer surface type, to compare the effect of the vortices appearing after each rough region on the output wind velocity at the end of the terrain.

From this we concluded that the vortices (and the presence of drag and countergradient force, in the multi-layer approach) did slow down the velocity, but the wind velocity for three or for five regions did not present any major differences. Indeed, the wind flow was slowed down more in the five regions terrain, but only by less than 2%. Hence, such a difference is hardly significant enough to be taken into account.

We also concluded that the vortices (and the forces) slowed down the velocity more under multi-layer than under single-layer. This can be explained by the fact that in the multi-layer surface type, the rough region consists of multiple layers, where each layer has a horizontally constant leaf area density. This allows for the wind to flow between the 'leaves' of the forest. On the other hand, for the single-layer surface type, the vegetation is considered to be a single 'block', with a constant roughness length z_0, where hence wind does not pass through.

After looking at the effect of the vortices for three and five regions, we proceeded to the main goal of this paper; which is to find a way to compute an average, or effective roughness length (ERL). We compared four methods to each another, and for six different models corresponding to all three given terrains under both single- and multi-layer surface types. The methods were the ones designed by André & Blondin (1986), Taylor (1987), and de Vries et al. (2003). The fourth method is new, derived in this study by extracting the roughness length from the logarithmic law, and averaging over height to obtain the ERL. To check which method was the most accurate one, we considered an extension of the terrain for all original six models, and we compared the velocity output at the end of the new terrain for all models and all ERL methods.

We confirmed Taylor's suggestion that the dependency on the first height level in André and Blondin's method was inaccurate. Indeed, for all of the six models considered, Taylor's method for the effective roughness yielded much better results. We also concluded that Taylor's method is the most accurate one for the three regions model, while for five regions de Vries et al.'s method gives the better results.

The use of the effective roughness length is to make larger-scale meteorological simulations easier by considering a heterogeneous terrain as a single 'block'. To this end, in real life, the ERL is used to represent heterogeneous terrains containing more than one single rough region. Therefore, it is advised to consider de Vries et al.'s method to compute the ERL, as it yields the best results for terrains with two (or more) rough regions.

Further research can be done by looking into improving the 'averaged' method, by comparing the different equations for logarithmic law. We note that the logarithmic law used by André and Blondin is the most 'basic' one, while de Vries et al. use a slightly more advanced version by adding a displacement term d_0 into the logarithm. Another alternative is the logarithmic law used by Klaassen and Luppes, which depends on a stability function in terms of the the Monin-Obukhov length. The stability function improves the accuracy of the logarithmic law, but it is more complicated to work with from an algebraic point of view.

One may also look into refining the grid further than 1/8, which is as far as we went in this thesis due to limited memory storage. As seen in the section dedicated to grid refinement, the curve for the roughness length became smoother, hence further refinement would perhaps yield even more accurate results for the 'averaged' method.

Another aspect to look into is the number of regions. As seen with de Vries et al.'s method, it is more accurate for two distinct rough regions than for a single one. Hence, one may increase the number of rough regions, or change their properties. We may wonder if having two rough regions with different roughness length would yield different results regarding the accuracy of this method.

Finally, further research could be done into the impact of vortices on global scale meteorological simulations. For instance, in de Vries et al.'s method, the impact of local vortices between the two different five regions models is not taken into account. This could have some repercussions on the larger-scale simulation.

References

André, J.-C. & Blondin, C. (1986). On the effective roughness length for use in numerical three-dimensional models. *Boundary-Layer Meteorology*, 35, 231–245. https://doi.org/10.1007/BF00123642.

Delage, Y. & Girard, C. (1991). Stability functions correct at the free convection limit and consistent for for both the surface and ekman layers. *Boundary-Layer Meteoroglogy*, 58, 19–31. https://doi.org/10.1007/BF00120749.

Garratt, J. R. & Pielke, R. A. (1989). On the sensitivity of mesoscale models to surface-layer parameterization constants. *Boundary-Layer Meteorology*, 48, 377–387. https://doi.org/10.1007/BF00123060.

Klaassen, W. (1992). Average fluxes from heterogeneous vegetated regions. *Boundary-Layer Meteorology*, 58(4), 329–354. https://doi.org/10.1007/BF00120236.

Kustas, W. P. & Brutsaert, W. (1986). Wind profile constants in a neutral atmospheric boundary layer over complex terrain. *Boundary-Layer Meteorology*, 34. https://doi.org/10.1007/BF00120907.

Lettau, H. (1969). Note on Aerodynamic Roughness-Parameter Estimation on the Basis of Roughness-Element Description . *Journal of Applied Meteorology*, 8. https://doi.org/10.1175/1520-0450(1969)008<0828:NOARPE>2.0.CO;2.

Luppes, R. (1993). Atmospheric Flow In Heterogeneous Vegetated Regions. Rijksuniversiteit Groningen.

Monin, A. & Obukhov, A. (1954). Basic laws of turbulent mixing in the surface layer of the atmosphere. *Proceedings of the USSR Academy of Sciences*, 24, 163–187. https://gibbs.science/efd/handouts/monin_obukhov_1954.pdf.

Obukhov, A. M. (1971). Turbulence in an atmosphere with a non-uniform temperature. *Boundary-Layer Meteorology*, 2, 7–29. https://doi.org/10.1007/BF00718085.

Slump, W. A. H. (2021). Application of Grid Refinement to Improve 2D Atmospheric Boundary Layer Software. Rijksuniversiteit Groningen.

Stull, R. B. (2013). *An Introduction to Boundary Layer Meteorology* (4 ed.). Oxford : Academic Press. https://doi.org/10.1007/978-94-009-3027-8.

Taylor, P. A. (1987). Comments and further analysis on effective roughness lengths for use in numerical three-dimensional models. *Boundary-Layer Meteorology*, 39, 403–418. https://doi.org/10.1007/BF00125144.

Veldman, A. (2009). *Boundary Layers in Fluid Dynamics*. University of Groningen.

de Vries, A., Kustas, W., Ritchie, J., Klaassen, W., Menenti, M., Rango, A., & Prueger, J. (2003). Effective aerodynamic roughness estimated from airborne laser altimeter measurements of surface features. *International Journal of Remote Sensing*, 24(3), 1545–1558. https://doi.org/10.1080/01431160110115997.

Wooding, R., Bradley, E., & Marshall, J. (1973). Drag due to regular arrays of roughness elements of varying geometry. *Boundary-Layer Meteorology*, 5. https://doi.org/10.1007/BF00155238.

A Background on fluid dynamics

This section provides some background into three main topics that are considered in this thesis: the Navier-Stokes equations, the equations of state for ideal gases, and the principle of Reynolds averaging. This section follows the lecture notes written by Veldman (2009).

A.1 The Navier-Stokes equations

Conservation of mass is given by

$$\partial_t \varrho + \textstyle\sum_i \partial_i(\varrho u_i) = 0, \tag{A.1.1}$$

where ϱ is the density of air and u_i is the i-th component of the velocity. This equation is called the *continuity equation*. Conservation of energy is given by:

$$\partial_t(\varrho E) + \textstyle\sum_i \partial_i(\varrho E u_i) = \varrho F_i u_i + \sum_j \partial_j(u_i \sigma_{ij}) + \sum_i \partial_i q_i. \tag{A.1.2}$$

This equation is called the *energy equation* For many fluids, the heat flux q_i is proportional to the temperature gradient: $q_i = -k\partial_i T$, where k is the heat conduction constant.

We can write the stress tensor as

$$\sigma_{ij} = -p\delta_{ij} + \tau_{ij}, \tag{A.1.3}$$

where p is the pressure, δ_{ij} is the Kronecker δ, that is and τ_{ij} is the viscous shear stress tensor for two dimensions, given by $\tau_{ij} = 2\mu e_{ij}$. Here, μ is the dynamical viscosity and

$$e_{ij} = \frac{1}{2}\left(\frac{\partial u_i}{\partial j} + \frac{\partial u_j}{\partial i}\right), \tag{A.1.4}$$

where u_i, u_j are the i, j components of the velocity vector $\mathbf{u}$, respectively. Conservation of momentum can thus be written component wise as:

$$\partial_t(\varrho u_i) + \textstyle\sum_j \partial_j(\varrho u_i u_j) = \varrho F_i + \sum_j \partial_j \sigma_{ij}, \tag{A.1.5}$$

where F_i is the i-th component of the body force per unit of mass and volume. This equation is called the *balance of momentum*.

The Navier-Stokes equations, which model the motion of every fluid flow, are a set of equations presented by Navier and Stokes independently. Factually, these equations are the equation of balance of momentum (A.1.5), together with the stress tensor, as defined in (A.1.3) and (A.1.4):

$$\partial_t(\varrho u_i) + \textstyle\sum_j \partial_j(\varrho u_i u_j) = \varrho F_i + \sum_j \partial_j \sigma_{ij}. \tag{A.1.6}$$

In common day practice, however, the Navier-Stokes equations also cover the continuity equation (A.1.1) and the energy equation (A.1.2):

$$\begin{aligned} \partial_t \varrho + \textstyle\sum_i \partial_i(\varrho u_i) &= 0, \\ \partial_t(\varrho E) + \textstyle\sum_i \partial_i(\varrho E u_i) &= \varrho F_i u_i + \sum_j \partial_j(u_i \sigma_{ij}) + \sum_i \partial_i q_i. \end{aligned} \tag{A.1.7}$$

In this thesis, we consider the atmospheric flow to be incompressible (see Section 2.1), which means that the density ϱ is considered constant. Under this assumption, we can simplify the equations of motion. Namely, the continuity and momentum equations become

$$\begin{aligned} \textstyle\sum_i \partial_i u_i &= 0, \\ \partial_t(u_i) + \textstyle\sum_j \partial_j(u_i u_j) &= F_i + \dfrac{1}{\varrho}\sum_j \partial_j \sigma_{ij}. \end{aligned} \tag{A.1.8}$$

Finally, by expanding the stress tensor in the newly obtained balance of momentum above, one obtains the Navier-Stokes equations for an incompressible fluid as

$$\begin{aligned} \operatorname{div} \mathbf{u} &= 0 \\ \frac{\partial \mathbf{u}}{\partial t} + (\mathbf{u} \cdot \nabla)\mathbf{u} &= \mathbf{F} - \frac{1}{\varrho}\nabla p + \nu \operatorname{div} \operatorname{grad} \mathbf{u}, \end{aligned} \tag{A.1.9}$$

where $\nu = \mu/p$ is the kinematic viscosity and $\mathbf{u}$ is the velocity vector. These equations, as well as accurate boundary conditions for the model studied in this paper are explored further in Section 2.1.

A.2 Equations of state

An ideal fluid is a theoretical fluid that is incompressible and has zero viscosity. For ideal gases, in particular, we have two thermodynamic equations of state:

$$\begin{aligned} p &= \varrho R_s T, \quad R_s = c_p - c_v, \\ e &= c_v T, \end{aligned} \tag{A.2.1}$$

where c_p, c_v are the specific heats at constant pressure and constant volume respectively, e is the internal energy of the fluid, and T is the temperature. R_s is the specific gas constant, defined by $R_s = R/M$, where R is the gas constant and M is the molar mass, i.e. the molecular weight of a particle.

A.3 Reynolds averaging

The surface layer-model, which is studied in Section 2, is a turbulence model, which can still be described using the equations of motion (A.1.6) and (A.1.7). However, since turbulent flows require very fine computations with very small time steps, we require all variables to be averaged, following the process of Reynolds averaging (Veldman, 2009, Section 2.2). To this end, we divide all the variables into a mean value and a fluctuation. For instance, for the velocity vector $\mathbf{u}$ and the pressure p, we obtain

$$\mathbf{u} = \overline{\mathbf{u}} + \mathbf{u}', \quad p = \overline{p} + p', \tag{A.3.1}$$

where $\overline{\mathbf{u}}$ denotes the mean value of $\mathbf{u}$ over a time interval T that is small with respect to the global time scale, but large with respect to the turbulent time scale. That is,

$$\overline{\mathbf{u}}(\mathbf{x}, t) = \frac{1}{T}\int_t^{t+T} \mathbf{u}(\mathbf{x}, \tau) d\tau. \tag{A.3.2}$$

We proceed similarly for $\overline{p}$. For the incompressible case, we can detail this equation further. Namely, by substituting (A.3.1) into the equation of motion for incompressible flow (A.1.8),

$$\begin{aligned} \textstyle\sum_i \partial_i u_i &= \textstyle\sum_i \partial_i(\overline{u}_i + u_i') = 0, \\ \partial_t u_i + \textstyle\sum_j \partial_j(u_i u_j) &= \partial_t(\overline{u}_i + u_i') + \textstyle\sum_j \partial_j((\overline{u}_i + u_i')(\overline{u}_j + u_j')) = F_i + \textstyle\sum_j \frac{1}{\varrho}\partial_j \sigma_{ij}. \end{aligned} \tag{A.3.3}$$

Then, since by definition of the mean value $\overline{\mathbf{u}}$ as in equation (A.3.2), we get $\int_t^{t+T} \mathbf{u}'(\mathbf{x}, \tau) d\tau \approx 0$, and similarly for p', this means that the linear terms in $\mathbf{u}$ and p do not obtain a contribution from the fluctuations $\mathbf{u}'$ and p'. By integrating both above equations (A.3.3), between t and $t + T$ we obtain for the continuity equation

$$\int_t^{t+T} \textstyle\sum_i \partial_i u_i d\tau = \textstyle\sum_i \partial_i \int_t^{t+T} \overline{u}_i d\tau = 0 \implies \textstyle\sum_i \partial_i \overline{u}_i = 0, \tag{A.3.4}$$

and for the balance of momentum we are left with (Veldman, 2009, Section 2.2)

$$\overline{\partial_t \overline{u}_i} + \sum_j \overline{\partial_j (\overline{u}_i \overline{u}_j)} + \partial_j R_{ij} = \overline{F}_i + \sum_j \frac{1}{\varrho} \partial_j \overline{\sigma}_{ij}, \tag{A.3.5}$$

where R_{ij} is the *Reynolds stress tensor*, defined by:

$$R_{ij} = \overline{u_i' u_j'} + \overline{u_i' \overline{u}_j} + \overline{\overline{u}_i u_j'}. \tag{A.3.6}$$

Note that the Reynolds stress tensor stems from the convective terms, but has the appearance of a stress tensor, and thus it is usually combined with the stress tensor σ_{ij}. We can also introduce some further approximations, namely that when $\overline{u}_i$ and $\overline{u}_j$ are constant over the interval between t and $t + T$, the following hold:

$$\overline{u_i' \overline{u}_j} = 0, \quad \overline{\overline{u}_i u_j'} = 0, \quad \overline{\overline{u}_i \overline{u}_j} = \overline{u}_i \overline{u}_j, \quad \text{and } \overline{\partial_t \overline{u}_i} = \partial_t \overline{u}_i. \tag{A.3.7}$$

In general, the above results only hold approximately. Substituting (A.3.7) into the continuity equation (A.3.4) and into the balance of momentum (A.3.5) yields the Reynolds-averaged Navier-Stokes equations:

$$\begin{gathered} \textstyle\sum_i \partial_i \overline{u_i} = 0, \\ \partial_t \overline{u}_i + \textstyle\sum_j \partial_j (\overline{u}_i \overline{u}_j) = \overline{F}_i + \sum_j \partial_j \left(\frac{1}{\varrho} \overline{\sigma}_{ij} + \tilde{R}_{ij} \right), \end{gathered} \tag{A.3.8}$$

where $\tilde{R}_{ij} = -\overline{u_i' u_j'}$. However, we then reach of problem in these new averaged Navier-Stokes equation: the unknowns u_i' in $\overline{R}_{ij}$, for which no equation is available in first instance. Finding such an equation for the fluctuation is called the *closure problem* and is the essence of turbulence modeling. $\tilde{R}_{ij}$ has to be expressed in known quantities, like $\overline{u}$ and $\overline{p}$.

We note that for the equations describing the atmospheric flow, the Reynolds averaging of all variables is implicitly assumed

B Derivation of the Monin-Obukhov length

The Obukhov length, first defined by Monin & Obukhov (1954), and also known as the Monin-Obukhov length, is given by

$$L_* = -\frac{u_*^3}{\kappa \frac{g}{T_0} \frac{q}{c_p \varrho}}, \tag{B.1.1}$$

where u_* is the friction velocity, κ is the von Kármán constant, g is the gravitational acceleration, T_0 is the mean temperature of the surface layer, q is the turbulent vertical heat flux, c_p is the specific heat of the air at constant pressure, and ϱ is the density of air. Here, the three parameters given by u_*, $\frac{g}{T_0}$, and $\frac{q}{c_p \varrho}$ are considered to be the definitive characteristic of the turbulence of the surface layer, that is the surface above the grass for example.

In what follows, we establish the steps leading to the Obukhov length, and we end this section by rewriting it into an easier form to work with (i.e. an equation that is independent of the friction velocity). One key element used here is the gradient Richardson number:

$$R_i = \frac{g}{T_0} \frac{\partial\theta/\partial z}{(\partial u/\partial z)^2}, \tag{B.1.2}$$

where θ is the potential temperature, g is the gravitational acceleration, $u = u(z)$ is the velocity of the wind, and $\partial u/\partial z$ is the velocity gradient. This number describes the qualitative character of the turbulence flow in the atmospheric boundary layer, and we obtain three cases:

(i) If $R_i > 0$ then the stratification is stable, which prevents the development of turbulence. If $R_i > R_{i_{cr}}$, for some critical value $R_{i_{cr}}$, then there are no turbulences. Stratification means the existence or the formation of distinct layers in a body of water of air, here the atmosphere.

(ii) If $R_i < 0$ then the stratification is unstable and the potential temperature decreases with height.

(iii) If $R_i = 0$ then the stratification is neutral, so it does not influence the development of turbulence. Then, distribution of temperature with height is adiabatic, which means that there is no transfer of heat and the change in internal energy is only due to work.

In the third case, we find ourselves in what resembles an incompressible environment with constant density.

We look at the derivation of the Obukhov length as given by Obukhov in 1971 (Obukhov, 1971, Section 4), where we assume that within the surface layer, the external forces are negligible in regards to the internal friction. Moreover, we suppose that the internal sources of heat, that is the heat of water condensation and the absorption of radiation, are absent. This then leads to a model where the momentum and heat flows are constant with regard to the height z, or, in other words,

$$\begin{aligned} \tau(z) &= \tau = \text{constant}, \\ q(z) &= q = \text{constant}, \end{aligned} \tag{B.1.3}$$

respectively. Prandtl's equation allows to describe a turbulent process in a uniform fluid such as:

$$\tau(z) = \varrho \ell_m^2 \left(\frac{\partial u}{\partial z}\right)^2, \tag{B.1.4}$$

where $\ell_m = \kappa z$ is the mixing length, also called the turbulent length scale, for $\kappa \approx 0.4$ the von Kármán constant. One can also describe turbulence with the use of the *coefficient of eddy*

viscosity A, such as $\tau = A\frac{du}{dz}$, which leads to a formulation of the eddy viscosity coefficient:

$$A = \varrho \ell_m^2 \frac{\partial u}{\partial z}. \tag{B.1.5}$$

From this, we can introduce the *coefficient of turbulence*, usually defined in terms of the coefficient of eddy viscosity:

$$K = \frac{A}{\varrho}. \tag{B.1.6}$$

The friction velocity, determined in terms of the shear stress τ and the density ϱ as $u_* = \sqrt{\tau/\varrho}$, can be used to rewrite the Prandtl's equation (B.1.4) as

$$u_*^2 = \ell_m^2 \left(\frac{\partial u}{\partial z}\right)^2 \implies \ell_m \frac{\partial u}{\partial z} = u_*, \tag{B.1.7}$$

and the coefficient of turbulence as

$$K = u_* \ell_m. \tag{B.1.8}$$

We note that the coefficient of turbulence depends on both the friction velocity u_* and on the height coordinate z, and hence it is variable. Therefore, it is more useful to use this coefficient rather than the coefficient of eddy viscosity A, as we can use Prandtl's equation (B.1.4) directly in that case.

Before continuing with the derivation of the Obukhov length, we must state three assumptions with regard to the transfer of substances:

(i) If a substance moves while unmixed with the surrounding air, then it is indestructible, i.e. its quantity remains unchanged.

(ii) The total quantity of a substance is preserved when mixing two masses of air. This property is called the continuity property.

(iii) The mixing of a substance with the environment (e.g. air) does not have an essential influence on the development of turbulences. We say that a substance is passive.

These assumptions will be implicitely supposed throughout this appendix, and this thesis.

We then look at the *coefficient of eddy diffusivity* K_s and the *coefficient of turbulent heat exchange* K_T. Eddy diffusion is a process where fluid substances mix together due to eddy motion. These two coefficients satisfy

$$K_s \approx K_T \approx K = u_* \ell_m. \tag{B.1.9}$$

We can also use the diffusion equation and the equation for turbulent heat transfer to determine K_s and K_T respectively:

$$\begin{aligned} F_s &= -K_s \varrho \frac{\partial s}{\partial z}, \\ q &= -c_p \varrho K_T \frac{\partial \theta}{\partial z}, \end{aligned} \tag{B.1.10}$$

where in the first equation, F_s is the mean flux of the substance, s is the gravimetric concentration of the substance. Gravimetric analysis is a method of determining the mass or concentration of a substance by measuring a change in mass.

In the second equation, q is the mean heat flux, c_p is the specific heat at constant pressure of the air, ϱ is the air density, and $\partial\theta/\partial z$ is the vertical gradient of potential temperature. We note that equation (B.1.9) is not strictly established, i.e. we cannot determine the exact value of K_s and K_T, only they order of magnitude. This then means that there is a dimensionless α_s

(respectively α_T) such that $K_s = \alpha_s K$ ($K_T = \alpha_T K$). This allows us to rewrite the equations given in (B.1.10):

$$\begin{aligned} F_s &= -\alpha_s \varrho \ell_m^2 \left|\frac{\partial u}{\partial z}\right| \frac{\partial s}{\partial z}, \\ q &= -\alpha_T c_p \varrho \ell_m^2 \left|\frac{\partial u}{\partial z}\right| \frac{\partial \theta}{\partial z}. \end{aligned} \tag{B.1.11}$$

In general, the coefficient α_T depends on Prandtl's number

$$Pr = \frac{\mu c_p}{\lambda}, \tag{B.1.12}$$

where μ and λ are the molecular viscosity and the molecular thermal conductivity of the environment, respectively. Since α_s and α_T are dimensionless, it can be assumed that they are definite functions of the Richardson number. In general, one may assume that all the dimensionless characteristics of a turbulent flow with a density variable, or potential temperature variable, are defined as functions of some basic dimensionless parameter.

We define K_0 to be the coefficient of turbulence under the condition of normal stratification stratification (i.e. that $R_i = 0$). This allows us to write the coefficient of turbulence K in terms of the gradient Richardson number R_i and K_0:

$$K = \phi(R_i) K_0. \tag{B.1.13}$$

Determining the dimensionless function ϕ is challenging and requires a deep study of turbulence, and thus will not be done here. However, we know some general information about it. Namely, since $\phi(R_i)$ is defined in such a way that $\phi(R_i = 0)K_0 = K_0$, we can conclude that

$$\phi(0) = 1. \tag{B.1.14}$$

Furthermore, as seen in the three cases for the Richardson number, when R_i increases the stratification of the atmosphere becomes more stable, meaning that we have less turbulence. Hence, as R_i increases, the coefficient of turbulence K decreases, and thus $\phi(R_i)$ is a monotonically decreasing function. Here, monotonicity of the function follows from the definition of $K = u_* \ell_m$, which is also monotone. We also stated that for $R_i > R_{i_{cr}}$, there was no turbulence, and hence

$$\phi(R_i) = 0 \quad \text{for } R_i > R_{i_{cr}}. \tag{B.1.15}$$

Various works have been dedicated to computing the critical Richardson number, ranging from 1/24 (as stated by Tollmien in 1935) to 1 (Richardson in 1920). In his paper, Obukhov (1971) used 1/11 for numerical calculations.

Having stated a few properties of the dimensionless function $\phi(R_i)$, we can rewrite the diffusion and heat transfer equation given in (B.1.11) into their final form, by setting $\alpha = \alpha_s/\alpha_T$ and noting that $\tau = F_s$ since the momentum flux corresponds to a diffusion equation,

$$\begin{aligned} \tau &= \phi(R_i) \varrho \ell_m^2 \left|\frac{\partial u}{\partial z}\right| \frac{\partial u}{\partial z}, \\ q &= -\alpha \phi(R_i) c_p \varrho \ell_m^2 \left|\frac{\partial u}{\partial z}\right| \frac{\partial \theta}{\partial z}, \end{aligned} \tag{B.1.16}$$

where we recall that

$$R_i = \frac{g}{T_0} \frac{\partial \theta / \partial z}{(\partial u / \partial z)^2}, \quad \ell_m = \kappa z. \tag{B.1.17}$$

This allows us to go back to the model given by Obukhov, in which we suppose that the external forces are negligible with regard to the internal friction and that the internal sources

of heat are absent. These assumptions define the concept of surface layer of the atmosphere. The momentum and heat flows are thus constant with regard to the height z, i.e. $\tau(z) = \tau_0$ and $q(z) = q_0$. Hence,

$$\begin{aligned} \tau_0 &= \phi(R_i)\varrho\ell_m^2 \left|\frac{\partial u}{\partial z}\right| \frac{\partial u}{\partial z}, \\ q_0 &= -\alpha\phi(R_i)c_p\varrho\ell_m^2 \left|\frac{\partial u}{\partial z}\right| \frac{\partial \theta}{\partial z}, \end{aligned} \tag{B.1.18}$$

For convenience, we introduce the *heat flux velocity* $v = -q/(c_p\varrho T_0)$, and together with the friction velocity $u_* = \sqrt{\tau/\varrho}$, this yields

$$\frac{v}{\alpha u_*^2} = \frac{1}{T_0}\frac{\partial \theta}{\partial z}\left(\frac{\partial u}{\partial z}\right)^{-1} = \text{constant}, \tag{B.1.19}$$

since q, τ are constant, and the changes of absolute density and temperature within the boundary layer can be considered negligible. Therefore, $v = v_0$ and $u_* = u_{*0}$ are constant. From this equation, we have the potential temperature given by

$$\frac{\partial \theta}{\partial z} = \frac{vT_0}{\alpha u_*^2}\frac{\partial u}{\partial z} \implies \theta(z) = \frac{vT_0}{\alpha u_*^2}u(z) + c, \tag{B.1.20}$$

where c is a constant. This tells us that, in the surface layer, the distribution of temperature with regard to the height is similar to the distribution of the wind. Using the friction velocity given above, we can also rewrite the momentum equation that was given in equation (B.1.11) into

$$u_* = \sqrt{\phi(R_i)}\ell_m\frac{\partial u}{\partial z}. \tag{B.1.21}$$

Recalling the equation for heat flow as given in (B.1.11), and dividing it by the cube of equation (B.1.21) yields

$$\begin{aligned} \frac{q}{u_*^3} &= \frac{-\alpha\phi(R_i)c_p\varrho\ell_m^2\left|\partial u/\partial z\right|(\partial\theta/\partial z)}{\phi(R_i)^{3/2}\ell_m^3\left(\partial u/\partial z\right)^3} \\ &= \frac{-\alpha c_p\varrho(\partial\theta/\partial z)}{\sqrt{\phi(R_i)}\ell_m\left(\partial u/\partial z\right)^2} \end{aligned}$$

Then, by recalling the definition of heat flux velocity, $v = -q/(c_p\varrho T_0)$, we have:

$$\begin{aligned} \implies \frac{q}{c_p\varrho} &= \frac{-\alpha u_*^3(\partial\theta/\partial z)}{\sqrt{\phi(R_i)}\ell_m(\partial u/\partial z)^2} \\ \implies -T_0 v &= \frac{-\alpha u_*^3(\partial\theta/\partial z)}{\sqrt{\phi(R_i)}\ell_m(\partial u/\partial z)^2} \\ \implies \frac{v}{\alpha u_*^3}\ell_m &= \frac{1}{T_0}\frac{\partial\theta/\partial z}{(\partial u/\partial z)^2}\frac{1}{\sqrt{\phi(R_i)}} \end{aligned} \tag{B.1.22}$$

Using the definition of the gradient Richardson number given in (B.1.2), we have:

$$\begin{aligned} \implies \frac{v}{\alpha u_*^3}\ell_m &= \frac{R_i}{g}\frac{1}{\sqrt{\phi(R_i)}} \\ \implies \frac{R_i}{\sqrt{\phi(R_i)}} &= \frac{g\ell_m v}{\alpha u_*^3}, \end{aligned}$$

which is another way to write the gradient Richardson number, where $\ell_m = \kappa z$. We note that this equation yields only one solution for R_i, as the left side is a monotonically increasing function.

Furthermore, when the mixing length ℓ_m is equal to zero, i.e. when the height $z = 0$, we have

$$R_i(0) = 0. \tag{B.1.23}$$

Rewriting equation (B.1.22) to have the presence of z made explicit, we obtain

$$\begin{aligned} R_i &= \frac{gv\kappa z}{\alpha u_*^3}\sqrt{\phi(R_i)} \\ \implies \frac{\partial R_i}{\partial z} &= \frac{gv\kappa}{\alpha u_*^3}\sqrt{\phi(R_i)} + \frac{gv\kappa z}{\alpha u_*^3}\frac{\partial_z \phi(R_i)}{2\sqrt{\phi(R_i)}}, \end{aligned} \tag{B.1.24}$$

since $\phi(R_i)$ is also dependent on z. Furthermore, since $\phi(0) = 1$, we obtain for $z = 0$:

$$\left(\frac{\partial R_i}{\partial z}\right)_{z=0} = \frac{gv\kappa}{\alpha u_*^3}. \tag{B.1.25}$$

Since $v = -q/(c_p \varrho T)$, it follows that the partial derivative of R_i with respect to z near $z = 0$ is negative, and hence as height decreases, the gradient Richardson number will approach zero, where at ground level $R_i(0) = 0$. The derivative of the Richardson number allows us to define the *height of the sub-layer of dynamics turbulence*, also known as the Obukhov length:

$$L_* = \frac{1}{\alpha(\partial R_i/\partial z)_{z=0}} = \frac{u_*^3}{\kappa g v}. \tag{B.1.26}$$

One can also write this length such that it does not depend on the friction velocity, using the definition of v and u_*:

$$\begin{aligned} L_* &= -\frac{u_*}{\kappa \frac{g}{T_0}\frac{q}{c_p \varrho}} \\ &= -\frac{c_p T_0 \tau^{3/2}}{\kappa g q \varrho^{1/2}}. \end{aligned} \tag{B.1.27}$$

We have thus shown the steps leading to the derivation of the Obukhov length. This characteristic length appears in Section 2, when detailing the equations underlining both surface types (single- and multi-layer).

Glossary of notation

h_c	canopy height
z_0	roughness length
$u(z)$	wind velocity at height z
u_*	friction velocity
κ	von Kármán constant ($\kappa \approx 0.40$)
z_0^{eff}	effective roughness length
ν	kinematic viscosity
p	pressure
μ	viscosity
ϱ	density
F_d	drag force
F_{cg}	countergradient force
τ	surface stress, momentum flux, turbulence
H	sensible heat
E	latent heat, total energy per unit mass of a fluid
θ	potential temperature
q	heat flux, specific humidity
T	temperature, temperature gradient
p_0	standard pressure, initial pressure
R	gas constant
c_p	specific heat capacity at constant pressure
c_v	specific heat capacity at constant volume
H_s	sensible heat at the surface
E_s	latent heat at the surface
u_e	horizontal velocity at the upper edge of the boundary layer
p_e	pressure at the upper edge of the boundary layer
T_0	mean temperature of the layer, initial absolute temperature
L_*	(Monin-)Obukhov length
$\psi_{M,H}$	integrated form of a stability function for momentum or heat
$\phi_{M,H}$	stability function for momentum or heat
ℓ_m	mixing length
ε_M	eddy viscosity for momentum
ε_H	eddy viscosity for heat
ℓ_{ma}	adjusted mixing length
C_ℓ	rate of adjustment constant
$\zeta = z/L_*$	adjusted length used in stability functions
Pr	neutral turbulent Prandtl's number
r_s	stomatal or surface resistance
τ_0	initial shear momentum
u_{*0}	initial friction velocity
H_0	initial sensible heat
T_s	absolute temperature of the surface
T_a	absolute temperature of the air
E_0	initial latent heat
e_s^*	saturated water vapour pressure of the surface
e_a	water vapour pressure of the air
r_a	air resistance
A_{ε_0}	available energy at the surface
λ	latent heat of vaporisation
groco	ground heat constant
R_{n_0}	net radiation of the surface
R_s	specific gas constant, $R_s = c_p - c_v = R/M$, short wave radiation
R_ℓ	long wave radiation
α	albedo
ε	emissivity of the surface
σ	stress tensor, Stephan-Boltzman constant
$z_{0_h} = z_0 e^{-2}$	roughness length for heat
ℓ_{mm}	maximum mixing length
A_ℓ	leaf area index
A_{ℓ_r}	reference value of the leaf area density
$R_n(z)$	net radiation at height z (or of that layer)
K_R	extinction coefficient for net radiation
Δz	height of the layer
$A_\ell \Delta z$	leaf area index
ℓ_w	leaf width
r_{to}	free parameter corresponding to the overall level of transpiration
δ^*	displacement thickness of the boundary layer
R_i	Richardson number
u_*^{eff}	effective friction velocity
Δ	length of the grid
$\mu(\Delta)$	Lebesgue measure of Δ
z_0^a	apparent roughness length
V_g	length of the geostrophic wind
Ro	Rossby number
f	Coriolis parameter
d_0	displacement height
δ_{ij}	Kronecker δ
e	internal energy of a fluid
R_{ij}	Reynolds stress tensor
g	acceleration due to gravity
A	coefficient of eddy viscosity
K	coefficient of turbulence